NUEJ

NARESUAN UNIVERSITY ENGINEERING JOURNAL

January - June 2024 Vol.19, No.1
ISSN : 2651-1568

NUEJ
Naresuan University
Engineering Journal

Editorial Team

NUEJ
Naresuan University
Engineering Journal

Editorial Board

NUEJ
Naresuan University
Engineering Journal

Editorial Board

NUEJ
Naresuan University
Engineering Journal

Research Articles

NUEJ

Naresuan University
Engineering Journal

Aims and Objectives

The primary objective of *the Naresuan University Engineering Journal (NUEJ)* is to publish high-quality research articles presenting contemporary developments in theory, design, and applications in all areas of Engineering, Science, and Technology, including research in Civil, Environmental, Mechanical, Electrical, Computer, Industrial, Chemical, and Material Engineerings. NUEJ covers all multidisciplinary research in associated areas, such as Mechatronics, Energy, Industrial and Engineering Design, Manufacturing Technology, Engineering Management, and Medical Engineering.

Journal Policies

Naresuan University Engineering Journal (NUEJ) is open access system which uses Double-blind peer review journal, According to broaden the Engineering and Technology develop the NUEJ has for Thai society and global. "No Charge policy of any publication fee", regularly published with 2 issues per year (January – June, and July – December). Submissions must be original, unpublished works, and not currently under review by other journals. NUEJ will consider only submitted works which respect research ethics, including confidentiality, consent, and the special requirements for human and animal research. All research articles dealing with human or animal subjects must attach an approval certificate from the appropriate Ethics Committee. Additionally, the research articles dealing with human subjects must provide evidence of informed consent

Editorial board of NUEJ reserves the right to decide whether the submitted manuscript should be accepted for publication. The final decision of the editorial board cannot be appealed.

The submitted manuscript has to be written in English only, and can be in Microsoft Word (doc or docx) or PDF file format. The corresponding author is required to register and submit the manuscript at https://ph01.tci-thaijo.org/index.php/nuej

Editorial board of Naresuan University Engineering Journal (NUEJ)
Faculty of Engineering, Naresuan University
Phitsanuloke, 65000 Thailand
Tel. +66(0)55 963951
Fax. +66(0)55 964000
Email: nuej@nu.ac.th

NUEJ
Naresuan University
Engineering Journal

Editor's Note

Editorial: Advancing Engineering for Entrepreneurial Society

Greetings to all our readers,

As the editor of the academic journal of the Faculty of Engineering, Naresuan University, I am delighted to present the latest issue of our journal, which serves as a vital platform for the exchange of knowledge and experiences in the ever-evolving and forward-moving field of engineering.

In this issue, we have compiled research articles that are both challenging and exciting. They reflect not only the advancements in various engineering disciplines but also the pursuit of sustainable and environmentally responsible methods. From the development of new materials to the application of advanced technologies in solving engineering problems, this issue covers a broad spectrum.

We also emphasize supporting new researchers by providing opportunities for them to publish high-quality work that presents new directions in the field of engineering. These works are not only valuable sources of information for academics but also an inspiration for the next generation of researchers.

The connection to society and industry is equally important. Hence, our journal is not just an academic forum but also a bridge linking engineering knowledge to its real-world applications.
Finally, I would like to express my gratitude to our editorial team, peer reviewers, and all members who contribute to the creation and maintenance of the quality of this journal. It is our hope that our journal will continue to be a source of high-quality knowledge and benefit the field of engineering and entrepreneurial society

With respect,

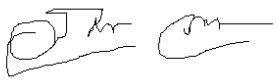

[Assist Prof. Dr. Ananchai Ukaew]
Editor, Academic Journal of the Faculty of Engineering
Naresuan University
Naresuan University Engineering Journal

NUEJ
Naresuan University
Engineering Journal

Predicting Anthropometric Dimensions Aimed at Ergonomic Design of Mounted Desktop Chairs for Thai University Students

Jirapon Promngam, Sutanit Puttapanom* and Panu Buranajarukorn

Industrial Engineering Department, Engineering Faculty, Naresuan University, Phitsanulok, Thailand

*Corresponding author e-mail: sutanitp@nu.ac.th

(Received: 29 March 2024, Revised: 24 April 2024, Accepted: 28 April 2024)

Abstract

While mounted desktop chairs have gained popularity in Thai universities for their space-saving features and affordability, many users experience discomfort and fatigue due to inconvenient adjustments or limited mobility. Addressing these concerns through improved ergonomic design can enhance user experience and make these chairs even more valuable additions to educational environments. However, achieving ergonomic design in these chairs can present challenges as acquiring accurate anthropometric measurements proves to be difficult, time-consuming, and costly. Therefore, this study applies forward stepwise regression analysis to estimate anthropometric dimensions needed for the chair design. The sample involved 857 students (430 females and 427 males) with ages ranging from 18 to 25 years old. Nineteen anthropometric measurements were collected.

The data analysis results suggest two sets of linear regression models for predicting all anthropometric measurements needed by two sets of easy to measure inputs: {Stature, Body Mass Index} and {Forearm-fingertip length, Waist circumference}. All R^2-values are greater than 70%. The predicted results obtained by proposed models were confirmed by actual anthropometry data which yielded P-values of paired sample t-tests for all outputs greater than 0.05. Moreover, new criteria determinants for some chairs' dimensions and a recommended size are proposed.

Keywords: Anthropometry, Mounted Desktop Chairs, Linear Regression, Ergonomic Design, Predicting

1. INTRODUCTION

Mounted desktop chairs are popular and widely used in Thai universities. Khanam et al. (2006), Casas S et al. (2016) and Shohel Parvez et al. (2022) indicated so many problems with this kind of chair, including discomfort and fatigue during use due to inconvenient adjustments or movements. Many studies (Castellucci et al., 2016; Esht & Singh, 2021) stated that poorly designed educational institution furniture can have negative effects on students' health. For example, uncomfortable or improper furniture size leads to poor posture among students, which may result in neck, shoulder, and back pain. Prolonged sitting in furniture with ineffective support can cause musculoskeletal disorders (MSDs) such as stiffness, discomfort, or even long-term spinal problems. Irritation from sitting can distract students and reduce their ability to concentrate on their studies. Furniture that has limited movement can prevent students from adjusting position, which is important for maintaining comfort and focus. Also, poor posture or constant discomfort during childhood and adolescence leads to long-term health problems in life afterwards. Therefore, it is crucial for educational institutions to invest in ergonomic furniture designed with students' health and comfort in mind. Appropriate size, proper lumbar support, and furniture that promotes flexibility and movement can all contribute to a healthier and more comfortable learning environment.

Many researchers have shown interest in application of ergonomic principles to the design and assessment of furniture in educational environments. Notable contributions come from researchers such as Altaboli et al. (2023), Evans et al. (1988), Langová et al. (2021), Lu & Lu (2017), Lueder & Allie (1999), Mokdad & Al-Ansari (2009), Brewer et al. (2009), Obinna et al. (2021), Openshaw & Taylor (2006), Sahabo & Kabara (2023), Sejdiu et al. (2023), and Sousa et al. (2022).

Al-Hinai et al. (2018), Ansari et al. (2018), Igbokwe et al. (2019), Khoshabi et al. (2020), Shohel Parvez et al. (2022), Taifa and Desai (2017) and Thariq et al. (2010) specifically studied ergonomically mounted desktop chairs design. The most important data for ergonomic design is anthropometric data.

Anthropometric measurements are a foundational aspect of ergonomic school furniture design, ensuring that the furniture is personalized to the physiological needs of students. However, performing these measurements is challenging and time-consuming, especially for large populations, due to various constraints like time, cost, and expertise. Few publications tried to predict hard-to-measure data using easy-to-measure data. Jeong and Park (1990) examined students, aged between 6 to 17 and found that stature can

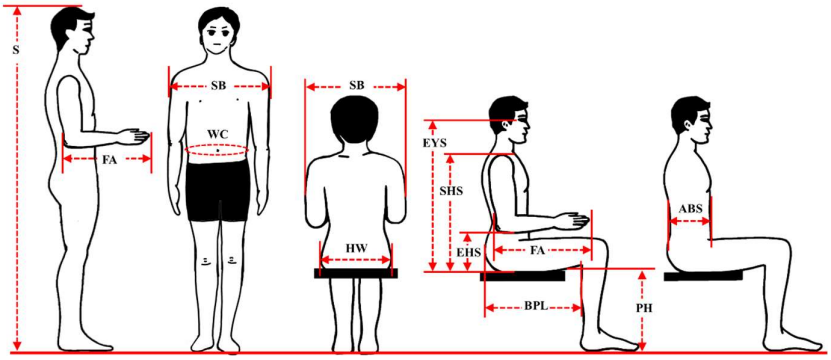

Figure 1 Anthropometric measurements

predict the body dimensions for school furniture design. However, sex differences significantly influenced interactions between body dimensions. Al-Haboubi (1992) considered different nationalities in East Asia in predicting body dimensions using stature and weight. Kaya et al. (2003) applied adaptive neuro-fuzzy inference system and stepwise regression analysis to predict anthropometric measurements. The six-dimensional outputs are still not enough to design chairs and desks for school children. The elbow-seat height is missing, which is used to define the seat to desk height and is one of the most crucial dimensions. Also, these input dimensions are not easy to measure. Chao and Wang (2010) proposed the process of using old anthropometric data to determine constant body ratio (CBR) and then applied a total of 483 CBR benchmarks to predict hard to measure body dimensions. To design classroom furniture for first graders, Oyewole et al. (2010) measured anthropometry of twenty first graders and built regression equations for predicting body dimensions. Agha & Alnahhal (2012) applied neural network and multiple linear regression to define five critical dimensions for primary school furniture design by four easy to measure anthropometry. They concluded that although neural networks have better performance, mathematical models from multiple linear regression can be applied by others. Ismaila et al. (2014) proposed models to obtain students' dimensions for the secondary school furniture design by using only stature. Castellucci et al. (2015) suggested using popliteal height over stature for school furniture selection. In Thailand, Pochana & Sungkhapong (2015) recommended to use age, stature, and weight as predictors for estimating primary school students' body dimensions. Wutthisrisatienkul & Puttapanom (2019) also used stature and weight to estimate anthropometric measurements for secondary school furniture. However, none of the literature proposed models for predicting all anthropometric dimensions necessary for the mounted desktop chairs design.

Therefore, the objective of this study is to propose linear regression models to predict Thai university students' anthropometric dimensions needed for the mounted desktop chairs design. There are two sets of inputs; the first set is stature and weight and the second set is easy to measure dimensions. Moreover, new criteria determinants for some chairs' dimensions and a recommended size are proposed.

2. Materials and Methods

2.1 Anthropometric Measurements

Prior to starting the experiment, a consent form containing information about the study, topic, objectives, benefits, procedures, procedures' time duration, and possible risks involved with the experiment was given and signed by each student.

Table 1 Definition of anthropometric measurements

Anthropometry	Definition
Stature (S)	Vertical distance from the floor to the top of the head
Forearm-fingertip length (FA)	Horizontal distance from the back of the elbow to the tip of the middle finger, with a 90° angle elbow flexion
Waist circumference (WC)	Horizontal circumference of the trunk at the level of the navel
Shoulder breadth (SB)	Horizontal distance across the maximum side parts of the right and left deltoid muscles
Body mass (weight)	Total body weight
Eye height, sitting (EYS)	Vertical distance from the seat to the outer corner of the eye
Shoulder height, sitting (SHS)	Vertical distance from the seat to the acromion
Elbow height, sitting (EHS)	Vertical distance from the seat to the lowest point of the elbow, with a 90° angle elbow flexion
Buttock-popliteal Length (BPL)	Horizontal distance from the buttock to the popliteal surface, with a 90° angle knee flexion
Popliteal height, sitting (PH)	Vertical distance from the floor to the popliteal surface behind the knee, with a 90° angle knee flexion
Abdominal depth, sitting (ABS)	Depth of the abdomen (at the level of the navel) while sitting
Hip Width, sitting (HW)	Maximum horizontal distance across the hip while sitting

Anthropometric measurements were conducted on students wearing their light school uniforms with empty pockets and without shoes. They sat in a relaxed and upright posture on adjustable chairs. Their knees were bent at a 90-degree angle, and their feet were flat on adjustable footrests. The measurement procedure was conducted based on ISO 7250-1:2017 (Basic human body measurements for technological design) (ISO, 2017). Figure 1 shows all anthropometric measurements which were selected and collected for this study while Table 1 describes the definition of each measurement according to ISO 7250 (ISO, 2017).

2.2 Mounted Desktop Chairs Design Dimensions

The dimensions of the mounted desktop chairs are presented in Figure 2. Table 2 explains the definition of each dimension.

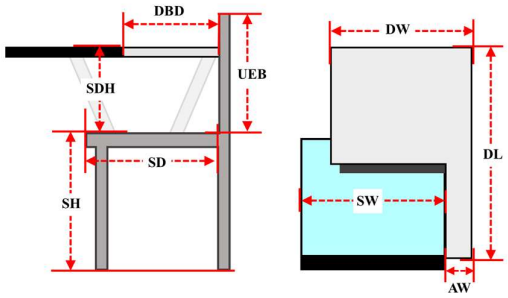

Figure 2 Mounted desktop chairs design dimensions

Table 2 Definition of mounted desktop chairs design dimensions

Chair dimension	Definition
Seat Height (SH)	Vertical distance from the floor to the highest point of the front edge of the seat
Seat to Desktop Height (SDH)	Vertical distance from the seat to the top of the desktop surface
Seat Depth (SD)	Horizontal distance for the front to the back of the seat
Seat Width (SW)	Horizontal distance from the left to the right edges of the seat
Upper Edge of Backrest (UEB)	Vertical distance from the seat to the top edge of the backrest
Desktop-Backrest Distance (DBD)	Horizontal distance between the desktop to the backrest
Desktop Length (DL)	Horizontal distance for the front to the back of the desktop
Desktop Width (DW)	Horizontal distance from the left to the right edges of the desktop
Armrest Width (AW)	Width of the armrest

2.3 Data Sample and Data Analysis

The volunteers were normal, healthy undergraduate students from two Thai public universities in the northern part of Thailand. The sample included 857 students (430 females and 427 males) aged between 18 and 25. After data collecting was done, the data of 800 subjects were used to create predictive models and the data of 57 subjects were used to validate the models.

According to mounted desktop chairs design dimensions, nine relevant anthropometric measurements needed for mounted desktop chairs designing (outputs): Eye height sitting (EYS), Shoulder height sitting (SHS), Elbow height sitting (EHS), Forearm-fingertip length (FA), Buttock-popliteal Length (BPL), Popliteal height sitting (PH), Abdominal depth sitting (ABS), Shoulder breadth (SB) and Hip Width sitting (HW) (Al-Hinai et al., 2018; Ansari et al., 2018; Igbokwe et al., 2019; Khoshabi et al., 2020; Shohel Parvez et al., 2022; Taifa & Desai, 2017; Thariq et al., 2010). In this study, there are twelve easy to measure anthropometric data (inputs); Stature (S), Eye height (EY), Shoulder height (SH), Elbow height (EH), Fist (grip axis) height (FIG), Waist circumference (WC), Forearm-fingertip length (FA), Upper arm length (UA), Grip reach (forward reach) (GRF), Popliteal height (PHST), Shoulder breadth (SB) and Body Mass Index (BMI). The BMI was calculated by dividing the subject's weight in kilograms by the square respective his/her stature in meters.

Linear regression was used to investigate the relationships between two or more anthropometric measurements. In this study, the first step is analyzing the relationship between each input and each output using Pearson's Correlation. Then, forward stepwise regression was applied to determine good and simple predictive models. The method of model fitting began with the highest correlation input first added to the models, tested each input as it was added to the model, then saved those inputs that helped to improve the model's coefficient of determination (R^2) and repeated the process until the R^2 and the adjusted R^2 were satisfactory.

3. Results and Discussion

After analyzing the relationship between each input and each output by using Pearson's correlation coefficient, the result shown in Table 3 yielded that Stature (S) and Forearm-fingertip length (FA) had high correlations with seven outputs; Eye height sitting (EYS), Shoulder height sitting (SHS), Elbow height sitting (EHS), Forearm-fingertip length (FA), Buttock-popliteal Length (BPL), Popliteal height sitting (PH), and Shoulder breadth (SB). Moreover, only Body Mass Index (BMI) and Waist circumference (WC) had high correlations with Abdominal depth sitting (ABS) and Hip Width sitting (HW). Therefore, S, FA, BMI and WC were selected to be inputs or predictors.

Table 3 shows Pearson's correlation Coefficients between these inputs and all outputs and the last two rows are correlations amongst inputs. Roebuck et al. (1975) showed that lengths of some body parts could be expressed as a fraction of stature. Oyewole et al. (2010), and Wutthisrisatienkul & Puttapanom (2019) presented that stature is a good input to predict PH, BPL, SHS, and EHS when BMI is a good input to predict HW. Since in Thailand, a student's record contains information of stature and weight, hence, the combination of stature and BMI were investigated.

Table 3 Pearson's correlation coefficient

Anthropometry	Pearson's Correlation Coefficient			
	S	BMI	FA	WC
EYS	0.893	0.117	0.795	0.256
SHS	0.905	0.082	0.785	0.227
EHS	0.842	0.095	0.799	0.232
BPL	0.890	0.087	0.896	0.255
PH	0.890	0.068	0.844	0.241
ABS	0.411	0.875	0.465	0.876
SB	0.783	0.380	0.750	0.511
HW	0.081	0.878	0.098	0.699
FA	0.887	0.110	-	0.272
WC	0.262	0.789	0.272	-

From Table 3, S has a high correlation with FA and BMI has a high correlation with WC. Consequently, two sets of inputs: {S, BMI} and {FA, WC}.

A linear regression model is widely measured by coefficient of determination (R^2). R^2 often rises when an input is added to the model, however it does not always mean the additional input helps to improve the model. Hence, an adjusted R^2 is used to verify the improvement. If the adjusted R^2 also increases, the model is improved and vice versa (Montgomery & Runger, 2010). Table 4 illustrates the R^2 and the adjusted R^2 of each simple or multiple linear regression equation. The red terms in the equations are added inputs that yield not better adjusted R^2 and the P-values are greater than 0.05 which means that these inputs have no significant effect on the models. For example, from the table, adjusted R^2 is 82, when using only stature (S) to predict shoulder height sitting (SHS) as Eq. (1). However, after BMI is added as Eq. (2), adjusted R^2 is decreasing to 81.9 and P-value for S and BMI are 0 and 0.924 respectively. Thus, it can be concluded that only S has a significant effect on predicting SHS, and Eq. (2) is not superior to Eq. (1).

$$SHS = 7.00 + 0.310*S \quad (1)$$
$$SHS = 7.01+0.310*S-0.00093*BMI \quad (2)$$

Table 4 Simple and multiple linear regression models

Output	Input	{S, BMI}					{FA, WC}				
		S		S, BMI			FA		FA, WC		
SHS	Eq	7.00+0.310*S		7.01+0.310*S-0.00093*BMI			18.5+0.890*FA		18.5+0.888*FA+0.00112*WC		
	P-Value	0.00	0.00	0.00	0.00	0.924	0.00	0.00	0.00	0.00	0.728
	R^2	82		82			86.9		86.9		
	R^2(adj)	82		81.9			86.9		86.8		
EYS	Eq	17.7+0.343*S		17.3+0.342*S+0.0258*BMI			33.8+0.899*FA		33.5+0.883*FA+0.0131*WC		
	P-Value	0.00	0.00	0.00	0.00	0.026	0.00	0.00	0.00	0.00	0.054
	R^2	79.7		79.8			72.8		73.1		
	R^2(adj)	79.7		79.8			72.7		73.1		
EHS	Eq	-14.4+0.230*S		-14.5+0.229*S+0.0119*BMI			-5.13+0.643*FA		-5.20+0.640*FA+0.00232*WC		
	P-Value	0.00	0.00	0.00	0.00	0.258	0.00	0.00	0.00	0.00	0.500
	R^2	73.8		73.9			70.4		70.4		
	R^2(adj)	73.8		73.8			70.4		70.3		
FA	Eq	-2.79+0.287*S		-3.05+0.286*S+0.0177*BMI			-		-		
	P-Value	0.001	0.00	0.00	0.00	0.076	-		-		
	R^2	78.7		78.8			-		-		
	R^2(adj)	78.7		78.8			-		-		
BPL	Eq	2.38+0.262*S		2.34+0.262*S+0.00264 BMI			9.21+0.816*FA		9.14+0.813*FA+0.00256*WC		
	P-Value	0.002	0.00	0.002	0.00	0.769	0.00	0.00	0.00	0.00	0.440
	R^2	79.1		79.1			80.2		80.2		
	R^2(adj)	79.1		79.1			80.2		80.2		
PH	Eq	1.91+0.243*S		1.93 + 0.243*S - 0.00137*BMI			10.9+0.697*FA		10.8 + 0.694*FA+0.00229*WC		
	P-Value	0.005	0.00	0.006	0.00	0.924	0.00	0.005	0.00	0.006	0.00
	R^2	80.4		80.5			71.2		71.3		
	R^2(adj)	80.4		80.4			71.2		71.2		
ABS	Eq	-4.29 + 0.152*S		0.85+0.0155*S+0.781*BMI			23.9-0.0862*FA		4.87-0.0604*FA+0.234*WC		
	P-Value	0.124	0.00	0.559	0.110	0.026	0.00	0.124	0.00	0.559	0.110
	R^2	17.1		77.8			0.3		72.9		
	R^2(adj)	16.9		77.7			0.0		72.7		
SB	Eq	-6.03+0.294*S		-9.41+0.283*S+0.230*BMI			3.11+0.882*FA		1.26+0.750 FA+0.0991*WC		
	P-Value	0.00	0.00	0.00	0.00	0.258	0.008	0.00	0.003	0.00	0.00
	R^2	63.1		73.2			58.4		71.1		
	R^2(adj)	63.0		73.1			58.3		71.1		
HW	Eq	29.4 + 0.0339*S		23.8 - 0.00248*S + 0.521*BMI			30.3+0.107*FA		25.4-0.0549*FA+0.155*WC		
	P-Value	0.00	0.00	0.00	0.589	0.076	0.00	0.00	0.00	0.00	0.00
	R^2	1.6		77.6			2.3		70.9		
	R^2(adj)	1.5		77.6			2.1		70.9		

Table 5 Linear regression predicting models

{S, BMI}			{FA, WC}		
Regression equations	**R^2 (%)**	**S**	**Regression equations**	**R^2 (%)**	**S**
SHS = 7.00 + 0.310*S	82	1.16112	SHS= 18.5 + 0.890*FA	86.9	0.792806
EYS = 17.7 + 0.343*S	79.7	1.3822	EYS = 33.8 + 0.899*FA	72.8	1.20000
EHS = - 14.4 + 0.230 S	73.8	0.9218	EHS= - 5.13 + 0.643*FA	70.4	1.05306
FA = - 2.32 + 0.284*S	78.7	1.3822	FA = FA	100	0
BPL = 2.38 + 0.262*S	79.1	1.07342	BPL = 9.21 + 0.816*FA	80.2	1.04489
PH = 1.91 + 0.243*S	80.5	0.95117	PH = 10.9 + 0.697*FA	71.2	1.14175
ABS = 3.04 + 0.797*BMI	77.8	1.34192	ABS = 2.30 + 0.234*WC	72.7	1.26319
SB = - 10.3 + 0.269*S + 0.369*BMI	73.2	1.4058	SB = 1.26 + 0.74*FA + 0.0991*WC	71.1	1.50831
HW = 23.5 + 0.521*BMI	77.6	0.90235	HW = 23.3 + 0.152*WC	70.4	0.979693

Therefore, using this analysis, Table 5 shows all final equations of the two input sets: {S, BMI} and {FA, WC}. All of R^2-values are greater than 70%, and the normal probability plot of the residuals, the residuals versus fitted values plot and the residuals versus orders plot were drawn for each equation and they all yielded that all the predictive equations are good and usable. To validate these equations, the data of 57 subjects which were not used in the model creation process was used for testing. Table 6 shows the means and standard deviations of the actual and predicted outputs; clearly, they are quite similar. To be sure, a paired sample *t*-test was conducted on testing data and the *P*-values are shown in Table 7. All the *P*-values for all outputs are greater than 0.05 which present that the mean difference is equal to zero, thus there is no significant difference between actual and predicted outputs. Moreover, comparison between two sets of outputs shows there is no significant difference either.

Table 6 Means and standard deviations of actual and predicted anthropometric measurements

Out-put	**Actual**		**Predicted**			
			{S, BMI}		**{FA, WC}**	
	Mean	StDev	Mean	StDev	Mean	StDev
SHS	58.89	11.39	58.81	10.50	59.03	10.58
EYS	74.93	13.39	75.03	12.86	74.74	10.80
EHS	23.97	5.08	24.04	5.78	23.81	3.91
FA	45.11	9.44	45.15	8.82	45.11	9.44
BPL	46.31	8.78	46.17	7.50	46.02	6.29
PH	42.61	7.02	42.52	6.45	42.34	4.59
ABS	21.62	10.08	21.61	10.41	21.42	9.04
SB	43.38	12.24	43.26	13.90	43.06	11.91
HW	35.58	4.08	35.59	4.42	35.66	3.76

Table 7 *P*-values of paired sample *t*-tests

Output	**Actual & {S, BMI}**	**Actual & {FA, WC}**	**{S, BMI} & {FA, WC}**
SHS	0.25	0.11	0.79
EYS	0.24	0.15	0.75
EHS	0.13	0.07	0.69
FA	0.74	1	0.65
BPL	0.07	0.06	0.82
PH	0.11	0.06	0.76
ABS	0.98	0.12	0.81
SB	0.58	0.1	0.83
HW	0.74	0.18	0.89

Table 8 presents criteria determinant for each mounted desktop chairs' dimension. Some criteria have been suggested and some criteria have just been introduced by this study. "Design for extreme" anthropometry principle was used for designing one size mounted desktop chairs for Thai university students.

In this study, a high seat is recommended that why 95th percentile of popliteal height is chosen over 5th percentile. Most literature (O Ismaila et al., 2013), (Esmaeel et al., 2020) suggested 5th percentile of popliteal height because a high chair leads the compression around the underside of the thigh causing blood circulation. However, Huang et al. (2016) discovered that low level seat pan height led to the maximum compressive loads on the lumbar joints compared with medium level and high level because when sitting on a lower level seat, only upper leg parts are supported. Hence most of the body weight goes down to the torso and feet since the knee angle is less than 90°. The reading distance of 40 cm (Bettencourt and Jacobs, 1995) is considered for Seat to Desktop Height. If the desktop pad is lower than the value of eye height sitting minus 40, a user will have a hard time seeing written letters. Salvendy (2012) showed that, 95th percentile shoulder breadth of male is wider than 95th percentile of hip width sitting of females. Thus, shoulder breadth should be considered in defining a seat width also. Al-Hinai et al. (2018) proposed using chest depth to define Desktop-Backrest Distance and this is only one study that mentioned Desktop-Backrest Distance. Therefore, Abdominal depth sitting is proposed and one quarter of the depth should be added to make a little bit

more room. Since no literature mentions about Desktop Length, the idea of the length should be able to support Forearm-fingertip portion with 25° angle shoulder flexion (Chafin et al., 1991). The desk width should be the width of the opened book which is around 2 times of A4 paper width.

4. CONCLUSIONS

Mounted desktop chairs' users often encounter discomfort and fatigue due to inconvenient adjustments or restricted movements. These challenges underscore the importance of prioritizing ergonomic design principles and nine difficult-to-measure anthropometric measurements are necessary. However, in this study, these nine hard-to-obtain anthropometrics can be simply predicted using either Stature and Body Mass Index or Forearm-fingertip length and Waist circumference. Moreover, there are new criteria determinants that have not been suggested by any study such as Desktop-Backrest Distance (DBD), Desktop Width (DW), Desktop Length (DL). These new proposed criteria determinants should help to improve the design of mounted desktop chairs. Also, because the sample age is between 18 and 25, which is working age, the results of this study can be applied to office furniture or workstations that restrict movements.

Table 8 Recommended dimensions for Thai university students.

Dims.	Anthropometry	Criteria Determinants	Design Dims.
SH*	PH	95th percentile of popliteal height + 2 cm for shoes allowance	43 cm
SDH*	EHS, EYS	Max {95th percentile of elbow height sitting, 95th percentile eye height sitting-40}	29 cm
SD	BPL	5th percentile of Buttock-popliteal Length	39.90 cm
SW*	HW, SB	Max {95th percentile of hip width sitting, 95th percentile shoulder breadth}	47 cm
UEB	SHS	5th percentile of shoulder height sitting	37.20 cm
DBD*	ABS	1.25 times 95th percentile of Abdominal depth sitting	37.50 cm
DL*	FA, SHS, EHS	95th percentile of Forearm-fingertip length, shoulder height sitting, and elbow height sitting	66.94 cm
DW*	-	2 times of A4 paper width	42 cm
AW	-	Literature review suggestion (Lueder & Allie, 1999)	10 cm

* New proposed criteria determinant

5. ACKNOWLEDGMENT

This study was supported financially by the Master Scholarship from the Faculty of Engineering, Naresuan University. Also, the authors gratefully acknowledge all participants and data collection team.

6. REFERENCES

Agha, S. R., & Alnahhal, M. J. (2012). Neural network and multiple linear regression to predict school children dimensions for ergonomic school furniture design. *Applied Ergonomics, 43*(6), 979-984.

Al-Haboubi, M. H. (1992). Anthropometry for a mix of different populations. *Applied Ergonomics, 23*(3), 191-196.

Al-Hinai, N., Al-Kindi, M., & Shamsuzzoha, A. (2018). An ergonomic student chair design and engineering for classroom environment. International *Journal of Mechanical Engineering and Robotics Research, 7*(5), 534-543.

Altaboli, A., Muttardi, R., Alahmar, H., Aliskandarani H., & Alshaikhi, A. (2023). *Anthropometric Evaluation of University Classroom Furniture*.

Ansari, S., Nikpay, A., & Varmazyar, S. (2018). Design and development of an ergonomic chair for students in educational settings. Health scope, 7(4).

Bettencourt, C. M., & Jacobs, K. (1995). *Ergonomics for Therapists*. Butterworth-Heinemann.

Brewer, J. M., Davis, K. G., Dunning, K. K., & Succop, P. A. (2009). Does ergonomic mismatch at school impact pain in school children? *Work-a Journal of Prevention Assessment & Rehabilitation*, 34(4), 455-464.

Castellucci, H. I., Arezes, P. M., & Molenbroek, J. F. M. (2015). Analysis of the most relevant anthropometric dimensions for school furniture selection based on a study with students from one Chilean region. *Applied Ergonomics, 46*, 201-211.

Chaffin, D. B., Andersson, G. B., & Martin, B. (1991). Occupational Biomechanics, John Wiley & Sons. *Inc, New York.*

Chao, W.-C., & Wang, E. M.-y. (2010). An approach to estimate body dimensions through constant body ratio benchmarks. *Applied Ergonomics, 42*(1), 122-130.

Esmaeel, A., Starovoytova, D., Maube, O., & Asad, R. (2020). Design of Classroom Furniture for Use at Tertiary Institutions.

Evans, W., Courtney, A., & Fok, K. (1988). The design of school furniture for Hong Kong schoolchildren: An anthropometric case study. *Applied Ergonomics*, 19(2), 122-134.

Huang, M., Hajizadeh, K., Gibson, I., & Lee, T. (2016). The influence of various seat design parameters: a computational analysis. *Human Factors and Ergonomics in Manufacturing & Service Industries, 26*(3), 356-366.

Igbokwe, J., Osueke, G., Opara, U., Ileagu, M., & Ezeakaibeya, K. (2019). Considerations of anthropometrics in the design of lecture hall furniture. Int. J. Res.-Granthaalayah, 7(8), 374-386.

Ismaila, S., Akanbi, O., & Ngassa, C. (2014). Models for estimating the anthropometric dimensions using standing height for furniture design. *Journal of Engineering, Design and Technology, 12*(3), 336-347.

Ismaila, S., Musa, A., Adejuyigbe, S., & Akinyemi, O. (2013). Anthropometric design of furniture for use in tertiary institutions in Abeokuta, South-Western Nigeria. *Engineering Review,* 33(3), 179-192.

ISO, I. (2017). 7250-1: Basic human body measurements for technological design-Part 1: Body measurement definitions and landmarks. *International Organization for Standardization, Geneva, Switzerland.*

Jeong, B. Y., & Park, K. S. (1990). Sex differences in anthropometry for school furniture design. *Ergonomics, 33*(12), 1511-1521.

Kaya, M. D., Hasiloglu, A. S., Bayramoglu, M., Yesilyurt, H., & Ozok, A. F. (2003). A new approach to estimate anthropometric measurements by adaptive neuro-fuzzy inference system. *International Journal of Industrial Ergonomics, 32*(2), 105-114.

Khoshabi, P., Nejati, E., Ahmadi, S. F., Chegini, A., Makui, A., & Ghousi, R. (2020). Developing a Multi-Criteria Decision-Making approach to compare types of classroom furniture considering mismatches for anthropometric measures of university students. PloS one, 15(9), e0239297.

Langová, N., Blašková, S., Gáborík, J., Lizoňová, D., & Jurek, A. (2021). Mismatch Between the Anthropometric Parameters and Classroom Furniture in The Slovak Primary Schools. Acta Facultatis Xylologiae Zvolen res Publica Slovaca, 63(1), 131-142.

Lueder, R., & Allie, P. (1999). Chairs with armrests: Ergonomic design issues. Proceedings of the Human Factors and Ergonomics Society Annual Meeting.

Lu, C.-W., & Lu, J.-M. (2017). Evaluation of the Indonesian National Standard for elementary school furniture based on children's anthropometry. *Applied Ergonomics*, 62, 168-181.

Montgomery, D. C., & Runger, G. C. (2010). Applied statistics and probability for engineers. John wiley & sons.

Mokdad, M., & Al-Ansari, M. (2009). Anthropometrics for the design of Bahraini school furniture. *International Journal of Industrial Ergonomics*, 39(5), 728-735.

Obinna, F. P., Sunday, A. A., & Babatunde, O. (2021). Ergonomic assessment and health implications of classroom furniture designs in secondary schools: a case study. *Theoretical Issues in Ergonomics Science*, 22(1), 1-14.

Openshaw, S., & Taylor, E. (2006). Ergonomics and design a reference guide. *Allsteel Inc., Muscatine, Iowa.*

Oyewole, S. A., Haight, J. M., & Freivalds, A. (2010). The ergonomic design of classroom furniture/computer work station for first graders in the elementary school. *International Journal of Industrial Ergonomics, 40*(4), 437-447.

Roebuck, J. A., Kroemer, K. H. E., & Thomson, W. G. (1975). *Engineering Anthropometry Methods*. Wiley.

Sahabo, M., & Kabara, A. (2023). Anthropometrics and Ergonomics of Secondary School Students in Four Yola Metropolis, Adamawa State, Nigeria. *Journal of Applied Sciences and Environmental Management,* 27(6), 1217-1222.

Salvendy, G. (2012). *Handbook of human factors and ergonomics.* John Wiley & Sons.

Sejdiu, R., Sylejmani, B., Idrizi, L., Bajraktari, A., & Sejdiu, M. (2023). Discrepancy between pupils' body and classroom furniture in elementary schools: A case study in the Republic of Kosovo. *Work*, 75(2), 447-459.

Shohel Parvez, M., Tasnim, N., Talapatra, S., Ruhani, A., & Hoque, A. M. (2022). Assessment of musculoskeletal problems among Bangladeshi University students in relation to classroom and library furniture. *Journal of The Institution of Engineers (India): Series C*, 1-14.

Taifa, I. W., & Desai, D. A. (2017). Anthropometric measurements for ergonomic design of students' furniture in India. *Engineering Science and Technology, an International Journal,* 20(1), 232-239.

Thariq, M. M., Munasinghe, H., & Abeysekara, J. (2010). Designing chairs with mounted desktop for university students: Ergonomics and comfort. *International Journal of Industrial Ergonomics*, 40(1), 8-18.

Wutthisrisatienkul, T., & Puttapanom, S. (2019). School furniture ergonomic assessment via simplified measurements and regression models. *Songklanakarin Journal of Science & Technology, 41*(1), 89-95

NUEJ
Naresuan University
Engineering Journal

How to Apply a Metaheuristic Algorithm to Physician Scheduling Problem

Atchara Thongsamai[1], Sirikarn Chansombat[2], and Saisumpan Sooncharoen[1*]

[1] Centre of Operations Research and Industrial Applications (CORIA), Department of Industrial Engineering, Faculty of Engineering, Naresuan University, Phitsanulok 65000, Thailand
[2] Faculty of Logistics and Digital Supply Chain, Naresuan University, Phitsanulok 65000, Thailand

[*]Corresponding author e-mail: saisumpans@nu.ac.th

(Received: 13 March 2024, Revised: 30 April 2024, Accepted: 18 May 2024)

Abstract

Hospitals spend a considerable percentage of their budget on medical personnel. However, proper physician scheduling helps to lower this cost. The emergency department is an area where physicians are available 24/7, so keeping the physicians satisfied is important. According to the scheduler specialist, creating a physician schedule takes a long time. It does not provide physicians with satisfaction and equality in terms of working hours, number of night shifts, and number of days off. This paper uses Random Search Optimization (RSO) to generate physician schedules and guidelines by applying metaheuristics to the physician scheduling problem. The goal is to reduce all overtime work to a minimum. We compared the performance of RSO with mathematical model and manual method. The results showed that RSO reduced total overtime by 50%, distributed the burden effectively, and had a procedure time of less than 12 seconds.

Keywords: Artificial Intelligence, Soft computing, NP-hard problem, Personnel scheduling, Optimization

1. INTRODUCTION

Scheduling problems are the assignment of work to limited resources over a period of time to achieve an objective. Scheduling problems are decisions of resource allocation or task sequencing (Salvendy, 2001). It is the allocation process for the increased effectiveness of activities that plays an important role in the industrial sector (Lenstra and Kan, 1981). It is a large problem with complexity and constraints (Rahimi et al., 2022). The physician scheduling problem is a Non-deterministic Polynomial-time hard (NP-hard) (Ozder et al., 2020). Although the physician scheduling problem is similar to the nurse scheduling problem, there are differences in terms of preferences, requirements, and specialty expertise (Hidri et al., 2020).

Erhard et al. (2018) classified physician scheduling problems into three types according to planning horizon: staffing, rostering, and re-planning problems. Staffing problems focus on strategically solving problems and involves long-term planning - one year. Rostering problems focus on solving tactical or operational level problems, with a planning period ranging from three to twelve months. Re-planning problems focus on the operational level and solving problems in the short-term. These problems are related to unexpected occurrences and can affect regular daily planning.

According to a search for articles on physician scheduling problems in the international database Scopus, the first article was published in 1958 and physician scheduling problems are still being researched today. Figure 1 represents the number of articles published each year on physician scheduling problems. Mathematical model, heuristics, and metaheuristics are used to solve physician scheduling problems, with mathematical model being the most commonly used.

Hidri et al. (2020) published an article on real-world physician scheduling problems in the Intensive Care Unit (ICU), solving this problem using Integer Linear Programming (ILP) with the purpose of minimizing total overtime. The manual method is a physician's allocation of work based on the scheduler's decision. The scheduler makes every effort to arrange it following hospital regulations, physician preferences, and patient demands. ILP decreases the overtime of physicians by 50% compared to manual methods. Furthermore, Hidri et al. compared the answer performance with the Genetic Algorithm (GA) and Simulated Annealing (SA), which reduced the total overtime by 39% and 37%, respectively. However, Hidri et al. did not clarify the physician scheduling procedure of GA and SA.

This paper proposes personnel scheduling and explains how to apply Random Search Optimization (RSO) to solve the physician scheduling problem with the objective of minimizing total overtime. RSO provides comparable results to the mathematical model while taking less time to solve the problem. In addition, establishing a preliminary agreement is also similar to the constraint in Hidri et al (2020). article, guiding other researchers interested in applying metaheuristics to the physician scheduling problem.

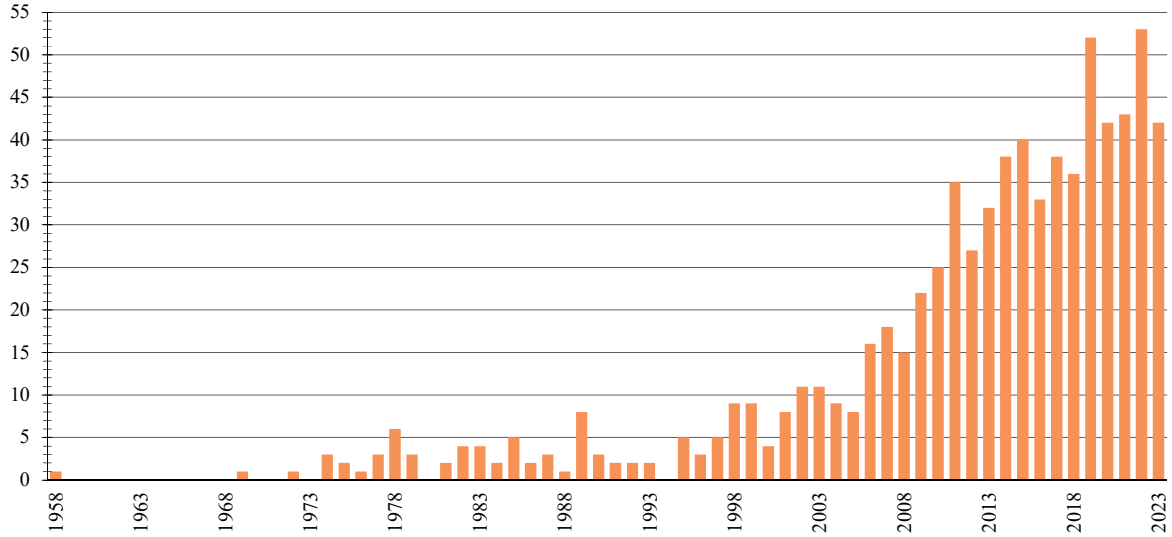

Figure 1 Number of articles published each year on physician scheduling problems

The following section is a literature review on physician scheduling using the Preferred Reporting Items for Systematic reviews and Meta-Analyses (PRISMA). Section 3 describes the elements of real-world problems from the dataset of Hidri et al. Section 4 depicts the flowchart and explains how to use the personnel scheduling Section 5 presents the results of an experimental study conducted on real data. The last section provides conclusions and suggestions for future research.

2. Literature Review

The researchers used PRISMA in the literature review presented by Liberati et al. (2009). The article collection period is from 2017 to August 2023. Figure 2 depicts the steps of a literature review with the following steps:

1. A search using the keywords "physician" and "schedule*" yielded 18,300 articles.
2. Selecting the desired period (2017 to 2023) yielded 4,779 articles.
3. Select only the subject area of interest and yield 299 articles (Computer science, Engineering, Decision sciences, Business, Mathematics, Economics, and Materials sciences).
4. The researcher made a preliminary selection of 29 articles based on the title and abstract.
5. Read the full-text article, which yielded 25 articles.
6. At last, 23 articles were of quality and related to the keywords.

Table 1 summarizes the 23 articles. We divide problem-solving approaches into three categories: 1) Mathematical model in this topic summarizes articles that use the mathematical model to apply the physician scheduling problem and the application area. 2) Heuristic in this topic is a summary of articles that solve problems using heuristics and demonstrate which methodologies are utilized to describe the physician scheduling procedure, and 3) Metaheuristic in this topic is a summary of the articles that used metaheuristics to solve problems. These sectional problems are large and frequently unsolvable using mathematical models.

2.1 Mathematical Model

The most popular mathematical model out of the proportions of solutions are depicted in Figure 3. When compared to other methods, the planning horizon is short (one week to three months). This method, which consists of an objective function and hard-soft constraints, achieves a single best solution value, and does not require parameterization. Mixed Integer Linear Programming (MILP) was used in an article by Gross, Fugener, et al. (2018) that is physician scheduling in university hospitals in Germany takes a time solution of twenty-one seconds, but according to Gross et al. when using a computer system the problem should be solved within ten seconds.

Guler and Gecici (2020) used MILP to create physician scheduling during the COVID-19 outbreak. They established three new departments (COVID-19 ICU, COVID-19 emergency, and COVID-19 service) to accommodate patients. It took one minute to find the answer, but the workload was very unevenly distributed due to different medical specialties.

Camiat et al. (2021) predicted patient demand using ten years of historical data from Sacre-Coeur Montreal Hospital. They use MILP to search for the answer. The solution for physician scheduling in the emergency department can meet demands well, but it cannot meet all the demands.

Schoenfelder and Pfefferlen (2018) used MILP an anesthesiology department physician scheduling in a hospital in Berlin, Germany. They define the penalty

coefficient when constraints are violated, and the model takes eighty-five seconds to solve problems. They can reduce almost all the severely punishable violations of the restriction.

Damcı-Kurt et al. (2019) used MILP to create schedule general physicians in United States hospitals and determine the penalty coefficients when violating constraints. Although the answer cannot be quantified in monetary terms, physician schedule improvements benefit both physicians and hospitals.

Fugener and Brunner (2019) used MILP to create physician scheduling in German university hospitals. This model can reduce overtime by 80% but takes up to 12 hours to solve.

Tan et al. (2019) used MILP to reduce physician scheduling time in the emergency room at West China Hospital of Sichuan University by dividing the physician scheduling into two phases: dividing the medical team and allocating work to the physician.

Integer Linear Programming (ILP) was used in an article by Hidri et al. (2020) that physician schedules in the ICU is divided into three buildings, each of which provides a different service, reducing the solution time to two hours.

Cappanera et al. (2022) divided physician scheduling of emergency departments in a European hospital into two phases: holiday determination and physician assignment by use ILP. Because more preferences from physicians complicate the problem, answers can be found within 6 hours.

Sample Average Approximation (SAA and tool) was used in an article by Marchesi et al. (2020) that is physician scheduling in the emergency department with the uncertain demand of patients, the model can reduce queue frequency and the average time door-to-doctor.

Tohidi et al. (2021) used SAA to create physician scheduling in an outpatient polyclinic in Canada, that provides general and specialized examinations to outpatients. It entails relocating some parts out of the hospital into the community to make them more accessible to patients. According to the results, as the problem size increases, the range between the best and worst solution will decrease because the increase in physician preferences making the problem more complex and resulting in fewer solutions and space possibilities. It also takes longer to solve these problems. Although this model reduced costs by 64%, the schedule generation must be updated every two years.

Integer Programming (IP) was used in an article by Liu et al. (2022) during the COVID-19 outbreak in China, physician scheduling generation to screen and treat patients promptly. Though the solution time was appropriate, it was unable to respond to all patient arrivals.

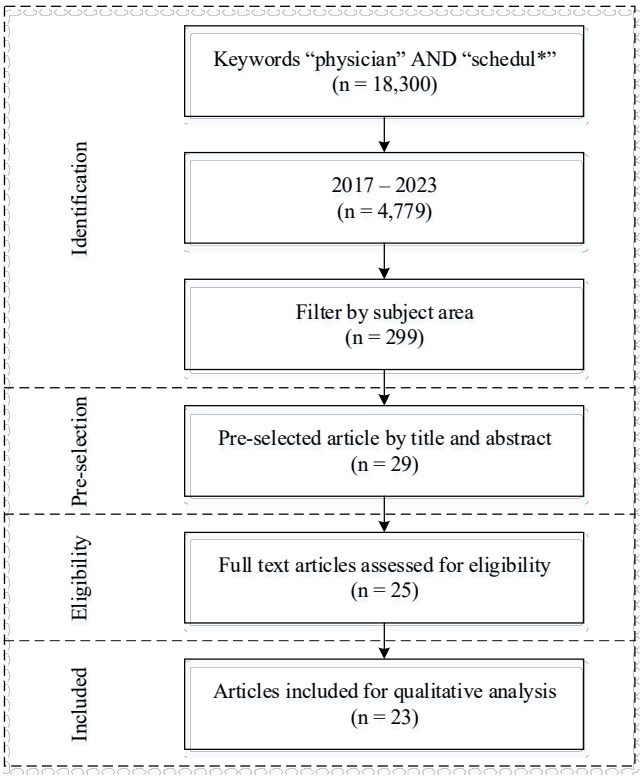

Figure 2 PRISMA flow for this study

Table 1 Literature review of physician scheduling

Article	Problem characteristics														Objective	Method		
	Classification	Planning horizon	Real data	Overlapping shifts	No. of shifts	Flexible shifts	No. of physicians	Stochastic demand	Fairness	Preferences	Requirement	Labor law	Breaks	Ergonomic		Mathematics	Heuristics	Metaheuristics
Gross, Fügener, et al. (2018)	Ro	4w	✓		n/a		133		✓	✓		✓			Maximize coverage demand and physicians satisfied	MILP		
Schoenfelder and Pfefferlen (2018)	Ro	1m	✓		7		34		✓	✓	✓	✓			Reduce physician scheduling time and regulation violations	MILP		
Damcı-Kurt et al. (2019)	Ro	3m	✓		n/a		36		✓		✓				Minimize the sum of penalties	MILP		
Fugener and Brunner (2019)	Ro	1w	✓		n/a	✓	17	✓							Minimize the number of assigned physicians	MILP	CG	
Lan et al. (2019)	Ro	1w	✓		4		150		✓	✓				✓	Minimize the dissatisfaction of physicians, cost, and deviation			SCA-VNS
Tan et al. (2019)	Ro	1m	✓	✓	2		25			✓	✓	✓			Minimize the deviation variables	MILP		
Tohidi et al. (2019)	Ro	1w			2		133		✓	✓	✓				Minimize the violation of the soft constraints		IVND	
Guler and Gecici (2020)	Ro	1m	✓		2-3		81		✓	✓		✓			Minimize the deviation variable	MILP		
Hidri et al. (2020)	Ro	1m	✓		2		18		✓	✓	✓	✓			Minimize the total overtime	ILP		
Kraul (2020)	S	1y	✓		n/a		52		✓						Minimize the violation between resource assignment and treatment requirements			GA
Mansini and Zanotti (2020)	Ro	2w			n/a		19		✓			✓			Minimize the total overtime		ALNS	
Marchesi et al. (2020)	Ro	4w	✓	✓	11		85			✓					Minimize the total number of waiting patients	SAA and tool		
Camiat et al. (2021)	Ro	13w	✓		3		35		✓	✓	✓			✓	Minimize the sum of difference between demand and supply	MILP		
Cildoz et al. (2021)	S	1y	✓		19	✓	42		✓	✓				✓	Maximize fairest feasibly		G-NO	
Erhard (2021)	Ro	6w	✓		12	✓	n/a		✓						Minimize the total cost		CG	
Liu and Xie (2021)	Ro	1w	✓		3		n/a	✓							Minimize total waiting time and working time			LS-TS
Tohidi et al. (2021)	Ro	1w	✓		2		147	✓	✓	✓		✓		✓	Maximize the number of visiting patients and minimize the cost of physicians	SAA and tool		

Table 1 (Continued)

Article	Problem characteristics														Objective	Method		
	Classification	Planning horizon	Real data	Overlapping shifts	No. of shifts	Flexible shifts	No. of physicians	Stochastic demand	Fairness	Preferences	Requirement	Labor law	Breaks	Ergonomic		Mathematics	Heuristics	Metaheuristics
Wang et al. (2021)	Re	1d	✓		17		n/a		✓						Minimize the risk tolerance level and rescheduling costs		Iterative	
Cappanera et al. (2022)	Ro	1m	✓		4		27		✓	✓					Minimize unfair distribution weekend and workday	ILP		
Li et al. (2022)	Ro	5d	✓		8		7			✓					Minimize average waiting time of patients and respects the physicians preferences			GA
Liu et al. (2022)	Ro	1w	✓		24		14					✓			Minimize the total working time	IP		
Lan et al. (2023)	Ro	1m	✓		6		30					✓			Maximize response to patient demand			PSO-VND
Wang et al. (2023)	Ro	1w	✓	✓	6		n/a	✓							Minimize the total patient waiting time			TS
This paper	Ro	4w	✓		2		18		✓	✓	✓	✓			Minimize the total overtime			RSO

Classification: *S* (Staffing), *Ro* (Rostering), and *Re* (Replanning), **Planning horizon**: *d* (Day), *w* (Week), *m* (Month), and *y* (Year), **Mathematics**: *MILP* (Mixed Integer Linear Programming), *ILP* (Integer Linear Programming), and *SAA* (Sample Average Approximation), *IP* (Integer Programming: branch and price), **Heuristics**: *CG* (Column Generation) and *IVND* (Iterated Variable Neighborhood Descent Algorithm), *ALNS* (Adaptive Large Neighborhood Search), *G-NO* (Hybrid Greedy Randomized Adaptive Search Procedure and Network Flow Optimization), *Iterative* (Exact Iterative Algorithm), **Metaheuristics**: *SCA-VNS* (Hybrid Sine Cosine Algorithm and Variable Neighborhood Search Algorithm), *GA* (Genetic Algorithm), *LS-TS* (Local Search based Tabu Search), *PSO-VND* (Hybrid Particle Swarm Optimization and Variable Neighborhood Descent), *TS* (Tabu Search), *RS* (Random Search).

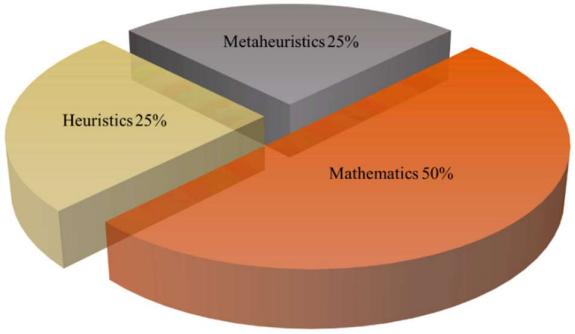

Figure 3 The proportion of methods in 23 articles used in this study

2.2 Heuristics

Heuristics are another technique for solving the physician scheduling problem, with the planning period ranging from one day to one year. Fugener and Brunner (2019) use Column Generation (CG) to create schedule physicians in a German university hospital. With only ten minutes of problem-solving, this method can reduce overtime by 80% as a flexible work shift arrangement.

Erhard (2021) uses CG to create a physician schedule using one to six weeks instances. Although it is not the best solution, it only takes ten minutes instead of a week. Also, use a flowchart to demonstrate how the algorithm works.

Tohidi et al. (2019) considered physician scheduling in ambulatory polyclinics, but the large problem size makes mathematical model unsuitable. As a result, Iterated Variable Neighborhood Descent Algorithm (IVNS) is used, resulting in high-quality solutions with little deviation. And uses pseudocode to explain the algorithm process.

Mansini and Zanotti (2020) used Adaptive Large Neighborhood Search (ALNS) from the destruction and repair processes to improve physician scheduling in general surgery. Although the best solution was not found in small instances, it was found in larger scale instances within an hour. And uses pseudocode to explain the algorithm process.

Cildoz et al. (2021) considered physician scheduling in a hospital compound of Navarre in Spain to determine the number of physicians and generate the initial solution using Hybrid Greedy Randomized Adaptive Search Procedure and Network Flow Optimization (G+NO), which is superior to the mathematical model. The use of flowcharts and pseudocode helps to explain the algorithm process.

Wang et al. (2021) presented a physician rescheduling model in a psychiatric hospital in China. They made an iteration to find the answer. They made an iteration to find the answer, which when entered into a local situation, generated a new solution. A minimized risk tolerance level has also been considered. Physician rescheduling improves resource allocation efficiency and decreases physician workload. This method uses pseudocode to explain the algorithm process.

2.3 Metaheuristics

Metaheuristics is another popular method for solving problems, because it encompasses a wide variety of techniques. Even though it may not be the best solution, it is a solution that can be accepted at the appropriate time. The size of the planning horizon found is five days to one year.

Kraul (2020) studied physician scheduling at a training hospital in Germany, he used GA and found that GA can improve their physician scheduling by more than 110% and have more equality. It uses a pseudocode to explain the algorithm process.

Li et al. (2022) used calibrated waiting time approximated to estimate patient waiting time in the outpatient department. And solving the problem with GA, which can provide good answers in minutes. Increasing physician preferences lengthens patient waiting time.

Lan et al. (2019) divided physician scheduling in the outpatient department into two steps: personnel allocation using an Iterated Hungarian Algorithm and physician scheduling using Hybrid Sine Cosine Algorithm and Variable Neighborhood Search Algorithm (SCA-VNS). The average objective function outperforms other algorithms, has a narrow distribution of answers, and finds answers quickly. It uses a flowchart and pseudocode to explain the algorithm process.

Liu and Xie (2021) physician scheduling in an emergency department using Local Search based Tabu Search (LS-TS). TS generates an initial solution and LS searches for a solution in nearby areas, the answers are highly effective.

Lan et al. (2023) considered physician scheduling in China during the COVID-19 outbreak. They used Hybrid Particle Swarm Optimization and Variable Neighborhood Descent (PSO-VND) to solve the problem. PSO generates the initial solution and then uses VND to improve it. This algorithm outperforms other algorithms, and pseudocode is used to explain the algorithm process.

Wang et al. (2023) physician scheduling in emergency departments in Chinese hospitals, and the forecast service demand is estimated which is close to reality. Although Tabu Search (TS) can reduce patient waiting times, it cannot meet all demands, and flowcharts are used to explain the algorithm process.

According to the literature review, some studies apply the metaheuristic to solve physician scheduling problems. Erhard et al. (2018) conducted a review of physician scheduling from 1985 to 2016 but did not find the application of RSO to the physician scheduling problem, as they did in their analysis of the 2017 to 2023 literature in this study. Some articles, based on heuristics and metaheuristics, use mathematical model equations to explain the physician scheduling process complicated. Flowcharts and pseudocode were used in some articles to explain the physician scheduling process. However, when we reviewed it, we found that these articles still did not explain the process in any detail.

3. Problem Description

In this paper, real-life physician scheduling problems as discussed by Hidri et al. (2020) are used. RSO is used to solve problems to minimize total overtime. This issue is physician scheduling in the emergency department, in which physicians must provide nonstop services 24/7. The ICU department is divided into three sections, each in a different building. These buildings provide dissimilar services as follows:

Building 1: The ICU department's main building.

Building 2: This building provides treatment for burn patients and women with fetal dystocia.

Building 3: Specializes in the treatment of serious car accidents. In this building, there is a specialized team of physicians that is ready to intervene outside the ICU department.

The three buildings have varying workloads, with Building 1 having the most patients and an intensive workload. Buildings 2 and 3 are with a lower workload, respectively.

The working hours in the case ICU department were divided into two shifts, with a day shift beginning at 07:00 a.m. and ending at 19:00 p.m. and a night shift beginning at 19:00 p.m. and ending at 07:00 a.m. Physician scheduling is monthly (four weeks or twenty-eight days). In September, 18 physicians were assigned to the ICU department, the minimum that is required. The existing physicians will be divided into six different teams each month.

We used the hard constraints and specific constraints of Hidri et al. (2020) and transformed them into agreement, which we divided into two categories as follows:

General agreement

1. A team of physicians is appointed to work in the ICU department at the start of each month. During the planning horizon, appointed physicians are not permitted to change teams.

2. A physician must work a minimum of 208 hours per month.

3. Each physician must be appointed to one unique team for one month (four weeks or twenty-eight days). This is to create coordination and understanding between the members of a team.

4. On each team, there should be at three physicians, but no more than six, to ensure that hospital services could be appropriately rendered, but not to exceed hospital capacity.

5. If the team is assigned to work during the night shift, it cannot be assigned to work the next day shift.

6. During a day shift, the team must be allocated to only one building.

7. All physicians on the team must perform the same tasks in the same building at the same time.

8. Each building is handled by a unique team at the same time, therefore, all three buildings would have their own teams.

9. Physicians are able to work overtime for extra money.

Specific agreement

10. A physician assigned to Building 2 and 3 must work only one shift each day, including Saturday and Sunday.

11. A physician assigned to Building 1 must work only one shift per day on weekdays, due to the intensive workload from Monday to Friday.

12. On the night shift, only one team was appointed to serve the three buildings, because the intensive patient demand is reduced at night.

13. If a team is appointed to Building 1, they must work there Monday through Friday to ensure the well-being of the patients.

14. A physician cannot be assigned to work at Building 1 for two consecutive weeks because of the intense workload.

15. On Saturday or Sunday, Building 1 must be ensured by the same team during the day shift and night shift (work 24 hours).

16. The teams working on Saturday or Sunday at Building 1 should have a day off before the weekend and also a day off after the weekend, therefore if a team works Saturday, then they should have Friday and Sunday off. If the team works on Sunday, they should have Saturday and Monday off. Such teams should work only one day on Saturday or Sunday.

17. The team working in Buildings 2 and 3 need to work both Saturday and Sunday and should be of the same team.

We tested the program using the following criteria: “Each physician must have two consecutive days off per week”. Then it was found that the program became unresponsive as it was unable to find a possible solution. As a result, these criteria will not be considered in this paper.

4. Random Search Optimization Personnel Scheduling

The optimization of algorithms applied to Non-deterministic Polynomial-time complete (NP-complete) or NP-hard. This method can solve large and complex problems, and it is classified into two types: Conventional Optimization Algorithms (COAs) and Approximation Optimization Algorithms (AOAs) (Pongcharoen, 2001; Pongcharoen et al., 2001), as shown in Figure 4.

COAs are mathematically based, with procedures, variables, and complex equations. Even if it is the best solution, it takes a long time to solve the problem. Later, various methods were used to solve a wide range of problems. This method is appropriate for small problems because they are too restrictive in terms of finding a fixed solution (Pongcharoen et al., 2004).

AOAs are applied to larger, more complex problems. With many problems today requiring immediate solutions, AOAs will provide answers that are close (Near optimum solution) to or optimum. AOAs require less time to find solutions than COAs (Pongcharoen et al., 2004).

Rastrigin (1963) proposed RSO, which works by iterative move to a better position in the search space. RSO is extremely efficient and necessitates very little modeling time (Schumer and Steiglitz, 1968).

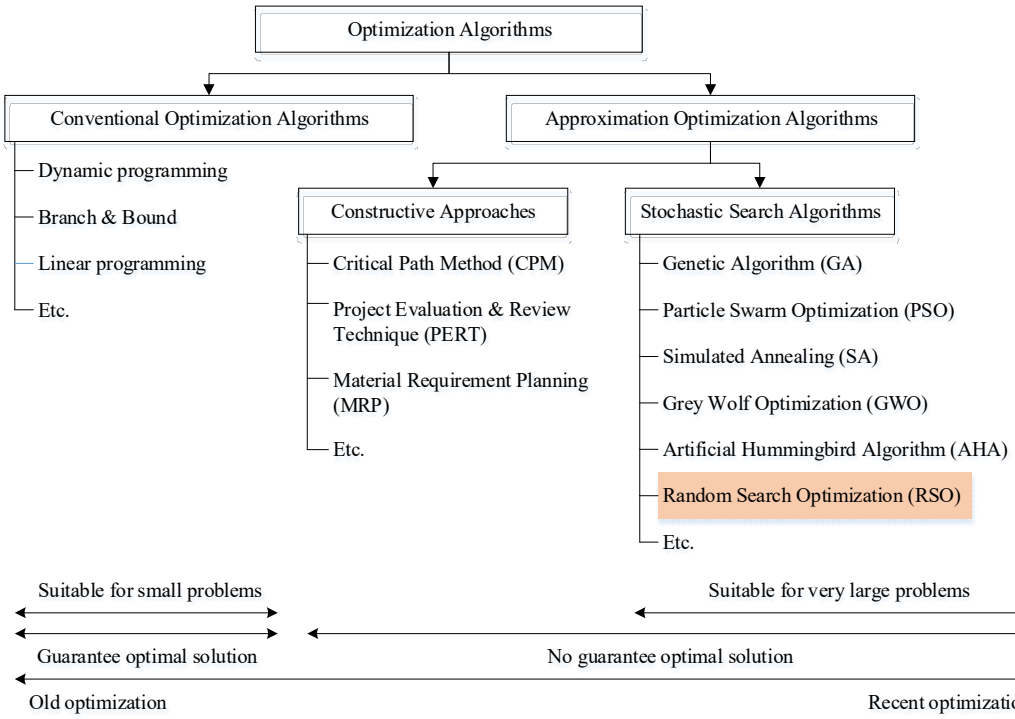

Figure 4 Optimization algorithms

4.1 Flowchart of Random Search Optimization for Physician Scheduling Problem

A personnel scheduling was developed that uses RSO that find the answer using an iterative. The objective was to minimize the overtime. The personnel scheduling was developed in a modular style using the Visual Basic for Applications (VBA) programming language. Figure 5 shows a flowchart that represents the proposed RSO used in the personnel scheduling, which includes the following steps:

1) Started by inputting data from the user-related information.
   a) number of physicians.
   b) number of buildings.
   c) work periods information - number of shifts, planning horizon.
   d) the severity rate is the percentage change in the initial solution (0 - 100).
   e) the step size (s) is round of swaps (Schrack and Choit, 1976).
2) RSO parameters set by the user include.
   a) number of populations (n).
   b) number of iterations (i).
   c) number of replications - an experiment was repeated using 30 different random seed numbers.
3) Problem encoding - a generated initial population ($x_1, x_2, x_3, \ldots, x_n$) and generating a representation for an example of a single solution as shown in Table 2.
4) Candidate solutions ($x_1, x_2, x_3, \ldots, x_n$) may be unfeasible. A repair process (Pongcharoen et al., 2004) satisfies constraints.

5) The evaluated value for all solutions in the initial population was computed and ranked, which can be calculated from Equation (1).

$$Total\ overtime = \sum_{m=1}^{6} [(NS_m * 12) - 208] * NP_m \quad (1)$$

where
NS_m is the number of shifts in team m (m = 1, ..., 6).
NP_m is the number of physicians in team m (m = 1, …, 6).

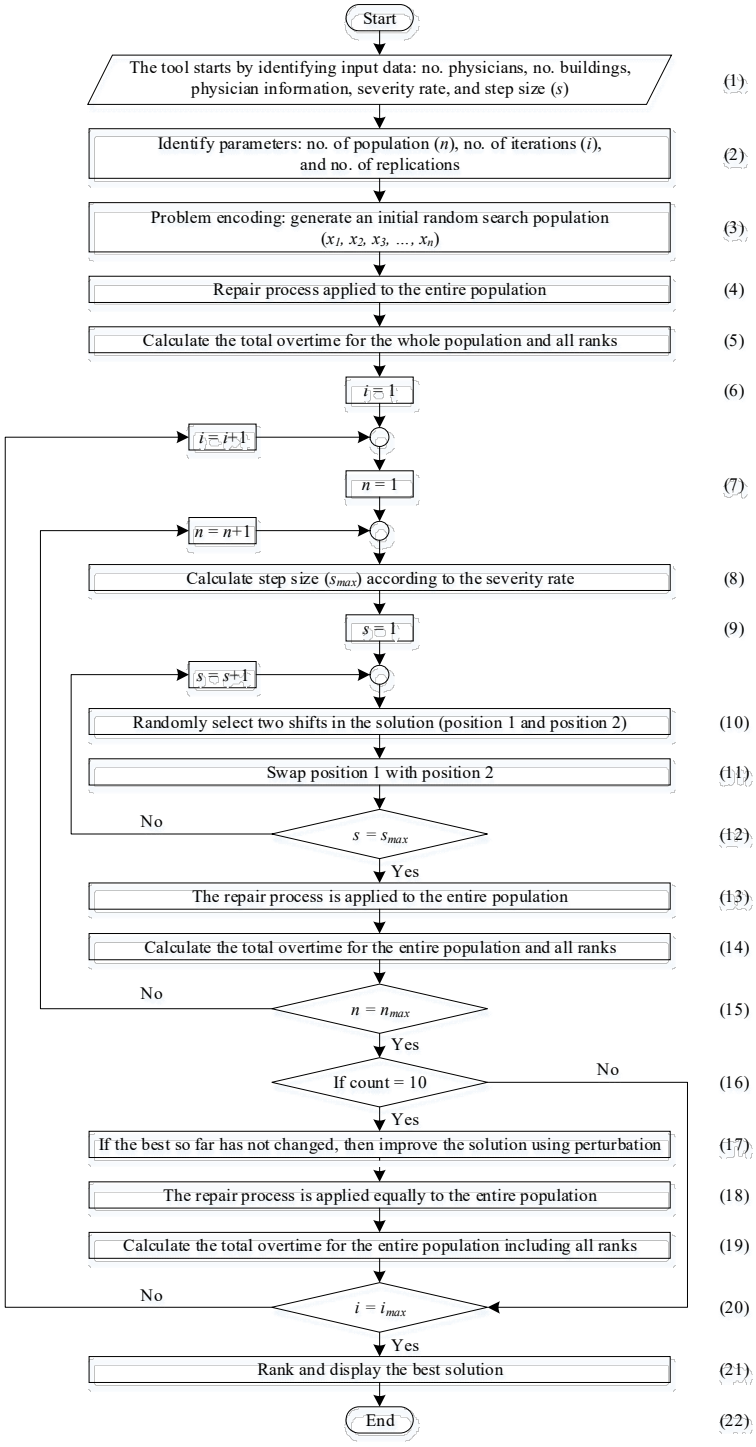

Figure 5 Random search optimization personnel scheduling flowchart

Equation (1) calculates the sum of overtime physicians for six teams, with working hours per shift of 12 hours and a minimum working hours of 208 hours per month.

6) Performs iterations from i: = 1 to i_{max}.
7) Started improving the solution for the first population.
8) Calculate s_{max} to find the round of swaps to improve the solution based on the severity rate, which can be calculated from Equation (2).

$$s_{max} = Rnd * 28 * 6 \quad (2)$$

$$s_{max} \leq \text{Severity rate} * 28 * 6 \quad (3)$$

where
Rnd is random numbers in the interval [0,1].
Equation (2) determines the maximum step size, which must be less than or equal to Equation (3). The number of working days is 28 days (four weeks or one month), and there are 6 teams.

9) Start switching positions for the first round.
10) Randomly select two shifts in the solution (position 1 and position 2).
11) Swap position 1 with position 2 shown in Figure 6.
12) If step size (s) is less than s_{max}, go back to step 9.
13) Apply the same repair procedure to all populations ($x_1, x_2, x_3, \ldots, x_n$).
14) The evaluated value for all solutions in the initial population was computed and ranked.
15) If there are remaining populations go to step 7.
16) If the best so far has not changed after being tested 10 times, then go to step 16, otherwise go to step 19.
17) Improve the solution by perturbation (generate a new initial solution).
18) Apply the same repair procedure to all populations ($x_1, x_2, x_3, \ldots, x_n$).
19) The evaluated value for all solutions in the initial population was computed and ranked.
20) If there are remaining iterations go to step 6.
21) Ranked the individuals and displayed the best solution.
22) End.

Table 2 Representation of a one population candidate solution

Day	Building 1		Building 2		Building 3	
	Day shift	Night shift	Day shift	Night shift	Day shift	Night shift
1	6	1	2	1	5	1
2	6	4	2	4	3	4
3	6	3	5	3	1	3
4	6	1	2	1	5	1
5	6	4	5	4	2	4
6	3	3	2	3	1	3
7	5	5	2	5	1	5
8	4	3	1	3	2	3
9	4	6	5	6	1	6
10	4	2	3	2	1	2
11	4	3	1	3	5	3
12	4	3	5	3	6	3
13	2	2	5	2	6	2
14	3	3	5	3	6	3
15	6	4	5	4	1	4
16	6	3	5	3	2	3
17	6	4	1	4	5	4
18	6	1	3	1	5	1
19	6	2	4	2	5	2
20	3	3	4	3	5	3
21	1	1	4	1	5	1
22	3	5	2	5	6	5
23	3	4	2	4	1	4
24	3	5	2	5	1	5
25	3	1	2	1	4	1
26	3	1	4	1	2	1
27	5	5	6	5	4	5
28	1	1	6	1	4	1

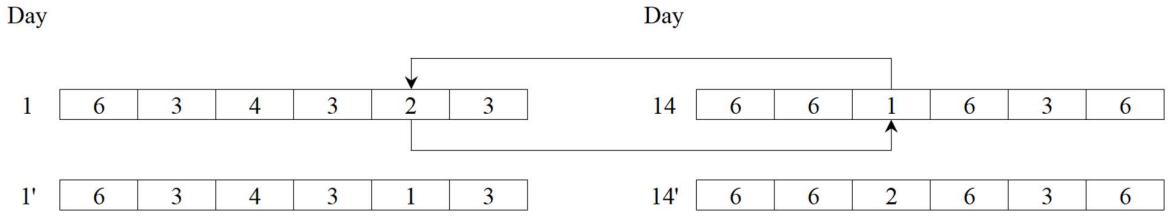

Figure 6 Swapping procedure

5. COMPUTATIONAL EXPERIMENTS AND DISCUSSION

In this paper used RSO to solve physician scheduling for the ICU department. To allocate work to physicians, we use the data set from an article of Hidri et al. (2020). We compared our method to manual method and ILP. In September, 18 physicians were assigned to the ICU department, which this month is significant because the number of physicians is limited. At the beginning of every month, physicians will be divided into 6 different teams. The computational experiments were performed on a personal computer with Ryzen 5, 2.10 GHz CPU, and 8 GB RAM

5.1 The Results and Analysis of Random Search Optimization

The article by Sooncharoen et al. (2020) discusses production scheduling for the capital goods industry in a variety of size problems (small, medium, large, and extra-large) by applying gray wolf optimization. It was discovered that the amount of search (N/I) 100/25 produced the best average of answers. As a result, the N/I = 100/25 is utilized in this paper, where N/I is the combination of the population and the iteration.

The RSO physician schedule is presented in Table 3. September is an interesting month because it has the fewest physicians assigned to the ICU department. Table 4 shows an analysis of physician schedules, workload, overtime, underload, and days off. The goal is to minimize total overtime, and the parameters listed below are used to compare to other methods.

NS_m is the number of day shifts in team m (m = 1, ..., 6).
NP_m is the number of physicians in team m (m = 1, …, 6).
OT_m is the overtime of team m (m = 1, …, 6). which can be calculated from Equation (4), if the result is positive it means overtime, but if it is negative, it means underload.

$$OT_m = [(NS_m * 12) - 208] * NP_m \quad (4)$$

UL_m is the under load of team m (m = 1, …, 6).
NNS_m is the number of night shifts in team m (m = 1, …, 6).
NDO_m is the number of days off in team m (m = 1, …, 6).

In this context and according to Table 3, teams 5, 4, 3, and 1 work on weekdays (Monday to Friday) in weeks 1, 2, 3, and 4, respectively, as an agreement (11). An agreement (12) requires that night shift physicians take care of all three buildings, team 6 works on night shift on days 1st, 5th, 7th, 9th, 11st, 13rd, 19th, 25th, and 26th. According to the agreement (15), team 2 working in Building 1 on the 6th, 14th, and 21st must work 24 hours.

Table 4 demonstrates that the total overtime is 288 hours, with no underload. The number of day shifts ranges from 18 to 19, which indicates that the physician scheduling is fair. The number of night shifts varies from 2 to 9 and the number of days off ranges from 9 to 12.

5.2 Comparative Study with Other Methods and Discussion

Hidri et al. (2020) uses mathematical model for presenting physician scheduling in the intensive care unit. The hospital uses half of the cost on medical personnel resource allocations. Their article aims to minimize total overtime, thereby resulting in reduced costs. Currently, physician scheduling is produced by a team of specialized schedulers, is known as a manual physician schedule, that takes more than two weeks to complete. This manual method does not account for the fairness, preferences, and requirements of physicians. So, they used ILP and defined hard constraints and non-classic constraints to produce physician scheduling. The outcome is the best answer and not infringing constraints. The ILP physician schedule can reduce total overtime by 50%, eliminate under-loading, and distribute duty properly. They also use metaheuristics to generate a physician scheduling of GA and SA physicians to compare its performance to that of ILP. However, because we do not know the procedure of the meta-heuristics method, GA and SA are not compared in this paper.

Table 5 shows physician scheduling using ILP and manual methods. The manual physician schedule on days 6th, 13rd, 20th, and 27th by teams 6, 3, 4, and 5 respectively, do not have a day off before work on Saturdays they must work twenty-four hours, which violates the agreement (16). In weeks 2, 3, and 4, teams 4, 5, and 2, respectively, were not allocated to work. It demonstrates that the workload distribution is unfair, even if it takes more than two weeks to complete. However, the ILP physician schedule only takes about two hours to produce, with no infringing constraints, and is still the best solution.

Table 6 shows an analysis of the ILP and manual methods. The manual method has 13 to 25-day shifts, 2 to 7-night shifts, and 5 to 16 days off, which is an unfair distribution of work and days off. Teams 2, 4, and 5 failed to reach their minimum workload, violating the agreement (2), resulting in increased total overtime. The ILP physician schedule has distributions of day shifts and days off that are good and that demonstrate equality, but the number of night shifts ranges from 2 to 8. Because the day shift is a good distribution, eliminates under-loading, and total overtime is less than the manual method.

Table 3 Random Search Optimization physician schedule

Day	Building 1		Building 2		Building 3	
	Day shift	Night shift	Day shift	Night shift	Day shift	Night shift
1	5	6	1	6	2	6
2	5	2	3	2	4	2
3	5	2	4	2	3	2
4	5	1	4	1	6	1
5	5	6	3	6	4	6
6	2	2	3	2	1	2
7	6	6	3	6	1	6
8	4	5	2	5	1	5
9	4	6	1	6	3	6
10	4	5	2	5	1	5
11	4	6	3	6	2	6
12	4	3	5	3	2	3
13	6	6	1	6	5	6
14	2	2	1	2	5	2
15	3	4	5	4	1	4
16	3	5	6	5	2	5
17	3	4	6	4	2	4
18	3	2	6	2	1	2
19	3	6	4	6	5	6
20	1	1	5	1	4	1
21	2	2	5	2	4	2
22	1	4	6	4	3	4
23	1	2	3	2	6	2
24	1	5	6	5	4	5
25	1	6	3	6	4	6
26	1	6	5	6	3	6
27	4	4	2	4	5	4
28	3	3	2	3	5	3

Table 4 Analysis of the Random Search Optimization physician schedule

Team	NS_m (Shifts)	NP_m (Person)	OT_m (Hours)	UL_m (Hours)	NNS_m (Shifts)	NDO_m (Days)
1	18	3	24	0	2	11
2	19	3	60	0	7	12
3	19	3	60	0	2	10
4	19	3	60	0	4	10
5	19	3	60	0	4	9
6	18	3	24	0	9	12
Total	112	18	288	0	28	64

Table 5 Integer Linear Programming and manual physician schedule

Day	Integer Linear Programming (ILP)						Manual Method					
	Building 1		Building 2		Building 3		Building 1		Building 2		Building 3	
	Day shift	Night shift	Day shift	Night shift	Day shift	Night shift	Day shift	Night shift	Day shift	Night shift	Day shift	Night shift
1	1	4	3	4	6	4	6	1	3	1	4	1
2	1	4	6	4	3	4	6	4	2	4	1	4
3	1	5	3	5	6	5	6	5	2	5	1	5
4	1	3	2	3	4	3	6	5	2	5	1	5
5	1	3	5	3	2	3	6	4	2	4	1	4
6	6	6	2	6	5	6	6	6	5	6	1	6
7	4	4	2	4	5	4	2	2	5	2	1	2
8	3	6	2	6	5	6	3	5	1	5	6	5
9	3	4	2	4	5	4	3	5	1	5	6	5
10	3	2	5	2	1	2	3	2	1	2	6	2
11	3	6	5	6	1	6	3	2	1	2	6	2
12	3	5	4	5	1	5	3	5	1	5	6	5
13	2	2	6	2	4	2	3	3	2	3	6	3
14	1	1	6	1	4	1	1	1	2	1	6	1
15	6	5	4	5	2	5	4	2	6	2	3	2
16	6	5	2	5	3	5	4	2	6	2	3	2
17	6	2	4	2	1	2	4	1	6	1	3	1
18	6	5	4	5	1	5	4	1	6	1	3	1
19	6	5	3	5	1	5	4	2	6	2	3	2
20	2	2	1	2	3	2	4	4	1	4	3	4
21	4	4	1	4	3	4	6	6	1	6	3	6
22	2	5	1	5	6	5	5	1	3	1	4	1
23	2	1	6	1	3	1	5	1	3	1	4	1
24	2	6	5	6	4	6	5	6	3	6	4	6
25	2	6	5	6	4	6	5	6	3	6	4	6
26	2	6	3	6	4	6	5	1	3	1	4	1
27	1	1	3	1	4	1	5	5	6	5	4	5
28	5	5	3	5	4	5	3	3	6	3	4	3

Table 6 Analysis of the Integer Linear Programming and manual physician schedule

Team	Integer Linear Programming (ILP)						Manual Method					
	NS_m (Shifts)	NP_m (Person)	OT_m (Hours)	UL_m (Hours)	NNS_m (Shifts)	NDO_m (Days)	NS_m (Shifts)	NP_m (Person)	OT_m (Hours)	UL_m (Hours)	NNS_m (Shifts)	NDO_m (Days)
1	19	3	60	0	3	11	21	3	132	0	7	8
2	19	3	60	0	4	11	13	3	0	156	6	16
3	18	3	24	0	2	10	22	3	168	0	2	8
4	19	3	60	0	5	11	17	3	0	12	3	12
5	18	3	24	0	8	11	14	3	0	120	6	15
6	19	3	60	0	6	10	25	3	276	0	4	5
Total	112	18	288	0	28	64	112	18	576	288	28	64

Table 7 compares the performance of RSO and ILP utilizing *PRO* (Percent Reduction of Overtime compared to the manual method), *PRU* (Percent Reduction of Underload is compared to the manual method), *ADO* (Average Days Off), and *ANS* (Average Number of Night shifts). As can be shown, both methods can reduce total overtime by 50% while eliminating under-load (100%). The *ADO* is computed by dividing 64 days off every month by the number of teams. On weekdays, two teams cease working (5 days * 2 teams * 4 weeks = 40 times), while three teams stop working on weekends (2 days * 3 teams * 4 weeks = 24 times). The *ANS* is computed using a month with 28-night shifts divided by the number of physician teams.

Table 7 Comparison of RSO and ILP

Method	*PRO* (%)	*PRU* (%)	*ADO* (Days)	*ANS* (Shifts)
RSO	50	100	10.67	4.67
ILP	50	100	10.67	4.67

The ILP and RSO can decrease total overtime in half when compared to the manual method, allowing all physicians to satisfy a minimum workload. Both techniques produce an optimal distribution of day shifts and decrease processing time by more than 99% as shown in Table 8 (*PRP*: Percent Reduce of Processing time compared to the manual method), but RSO is still unable to distribute the number of days off as effectively as ILP. However, both have disadvantages in terms of night shift workload distribution because they have a wider distribution range and a significantly different number of shifts than *ANS*.

Table 8 Processing time for producing a physician schedule using the manual method, ILP, and RSO

Method	*Processing time*	*PRP*
Manual	2 weeks	-
ILP	2 hours	99.16667
RSO	12 seconds	99.99862

6. CONCLUSION

The scheduling problem is an NP-hard problem, with varying properties depending on the area of application. Physician scheduling is the assignment of a work to a medical practitioner. This subject is currently receiving more attention and is frequently solved using a mathematical model approach. This paper uses data from the article of Hidri et al. (2020), which is a real-life situation involving the assignment workload to physicians in the ICU department. The ICU department of this hospital has a unique structure as well as characteristics. This work modified their constraints by adopting the general and specific agreement to provide guidelines for future research. RSO is constantly seeking a better position than its previous position in the search space. We are comparing the performance of ILP with RSO, and it appears that both techniques are very effective, as indicated in Table 7. According to Table 8, the ILP and RSO can reduce processing time by more than 99%. However, as seen in Table 4 and Table 6, both techniques fail to allocate the night shift fairly.

Future work aims to deal with the optimal solution, such as minimizing the total unbalanced workload, minimizing the total cost, or maximizing the total fairness. Thongsamai et al. (2024). discussed the physician scheduling problem but have not yet applied other metaheuristics like the Artificial Hummingbird Algorithm (AHA) to improve the optimal solutions. Statistical parameter tuning, modifying, and hybridizing metaheuristics can also improve the optimal solutions.

7. ACKNOWLEDGMENT

The first author is grateful to the Faculty of Engineering, Naresuan University (NU) for supporting this research financially and also providing research facilities. This work was also part of a research project financially supported by the Faculty of Engineering, Naresuan University under grant no. R2565C010. We are very thankful to Mr. Kevin Mark Roebl of English Editing Services, Division of International Affairs and Language Development (DIALD), NU, for proofreading this manuscript.

8. REFERENCES

Camiat, F., Restrepo, M. I., Chauny, J. M., Lahrichi, N., and Rousseau, L. M. (2021). Productivity-driven physician scheduling in emergency departments. *Health Systems*, *10*(2), 104-117. https://doi.org/10.1080/20476965.2019.1666036

Cappanera, P., Visintin, F., and Rossi, R. (2022). The emergency department physician rostering problem: obtaining equitable solutions via network optimization. *Flexible Services and Manufacturing Journal*, *34*(4), 916-959. https://doi.org/10.1007/s10696-021-09426-7

Cildoz, M., Mallor, F., and Mateo, P. M. (2021). A GRASP-based algorithm for solving the emergency room physician scheduling problem. *Applied Soft Computing*, *103*, 107151. https://doi.org/10.1016/j.asoc.2021.107151

Damcı-Kurt, P., Zhang, M., Marentay, B., and Govind, N. (2019). Improving physician schedules by leveraging equalization: Cases from hospitals in U.S. *Omega (United Kingdom)*, *85*, 182-193. https://doi.org/10.1016/j.omega.2018.06.011

Erhard, M. (2021). Flexible staffing of physicians with column generation. *Flexible Services and Manufacturing Journal*, *33*(1), 212-252. https://doi.org/10.1007/s10696-019-09353-8

Erhard, M., Schoenfelder, J., Fugener, A., and Brunner, J. O. (2018). State of the art in physician scheduling. *European Journal of Operational Research*, *265*(1),

1-18.
https://doi.org/10.1016/j.ejor.2017.06.037

Fugener, A. and Brunner, J. O. (2019). Planning for overtime: The value of shift extensions in physician scheduling. *INFORMS Journal on Computing*, *31*(4), 732-744.
https://doi.org/10.1287/IJOC.2018.0865

Gross, C. N., Fugener, A., and Brunner, J. O. (2018). Online rescheduling of physicians in hospitals. *Flexible Services and Manufacturing Journal*, *30*(1-2), 296-328.
https://doi.org/10.1007/s10696-016-9274-2

Guler, M. G. and Gecici, E. (2020). A decision support system for scheduling the shifts of physicians during COVID-19 pandemic. *Computers and Industrial Engineering*, *150*, 106874.
https://doi.org/10.1016/j.cie.2020.106874

Hidri, L., Gazdar, A., and Mabkhot, M. M. (2020). Optimized procedure to schedule physicians in an intensive care unit: A case study. *Mathematics*, *8*(11), 1-24.
https://doi.org/10.3390/math8111976

Kraul, S. (2020). Annual scheduling for anesthesiology medicine residents in task-related programs with a focus on continuity of care. *Flexible Services and Manufacturing Journal*, *32*(1), 181-212.
https://doi.org/10.1007/s10696-019-09365-4

Lan, S., Fan, W., Liu, T., and Yang, S. (2019). A hybrid SCA–VNS meta-heuristic based on Iterated Hungarian algorithm for physicians and medical staff scheduling problem in outpatient department of large hospitals with multiple branches. *Applied Soft Computing Journal*, *85*, 105813.
https://doi.org/10.1016/j.asoc.2019.105813

Lan, S., Fan, W., Yang, S., and Pardalos, P. M. (2023). Physician scheduling problem in Mobile Cabin Hospitals of China during Covid-19 outbreak. *Annals of Mathematics and Artificial Intelligence*, *91*(2-3), 349-372.
https://doi.org/10.1007/s10472-023-09834-5

Lenstra, J. K. and Kan, A. H. G. R. (1981). Complexity of vehicle routing and scheduling problems. *Networks*, *11*(2), 221-227.
https://doi.org/10.1002/net.3230110211

Li, N., Li, X., and Forero, P. (2022). Physician scheduling for outpatient department with nonhomogeneous patient arrival and priority queue. *Flexible Services and Manufacturing Journal*, *34*(4), 879-915.
https://doi.org/10.1007/s10696-021-09414-x

Liberati, A., Altman, D. G., Tetzlaff, J., Mulrow, C., Gøtzsche, P. C., Ioannidis, J. P. A., Clarke, M., Devereaux, P. J., Kleijnen, J., and Moher, D. (2009). The PRISMA statement for reporting systematic reviews and meta-analyses of studies that evaluate health care interventions: Explanation and elaboration. *Italian Journal of Public Health*, *6*(4), 354-391.
https://www.scopus.com/inward/record.uri?eid=2-s2.0-76549089252&partnerID=40&md5=dc8847f1671dc34e0b515045479a8b14

Liu, R., Fan, X., Wu, Z., Pang, B., and Xie, X. (2022). The Physician Scheduling of Fever Clinic in the COVID-19 Pandemic. *IEEE Transactions on Automation Science and Engineering*, *19*(2), 709-723.
https://doi.org/10.1109/TASE.2021.3114339

Liu, R. and Xie, X. (2021). Weekly scheduling of emergency department physicians to cope with time-varying demand. *IISE Transactions*, *53*(10), 1109-1123.
https://doi.org/10.1080/24725854.2021.1894656

Mansini, R. and Zanotti, R. (2020). Optimizing the physician scheduling problem in a large hospital ward. *Journal of Scheduling*, *23*(3), 337-361.
https://doi.org/10.1007/s10951-019-00614-w

Marchesi, J. F., Hamacher, S., and Fleck, J. L. (2020). A stochastic programming approach to the physician staffing and scheduling problem. *Computers and Industrial Engineering*, *142*, 106281.
https://doi.org/10.1016/j.cie.2020.106281

Ozder, E. H., Ozcan, E., and Eren, T. (2020). A Systematic Literature Review for Personnel Scheduling Problems. *International Journal of Information Technology & Decision Making*, *19*(6), 1695-1735.
https://doi.org/10.1142/S0219622020300050

Pongcharoen, P. (2001). *Genetic algorithms for production scheduling in capital goods industries* [dissertation, University of Newcastle upon Tyne]. Newcastle upon Tyne.

Pongcharoen, P., Hicks, C., and Braiden, P. M. (2004). The development of genetic algorithms for the finite capacity scheduling of complex products, with multiple levels of product structure. *European Journal of Operational Research*, *152*(1), 215-225.
https://doi.org/10.1016/S0377- 2217(02)00645-8

Pongcharoen, P., Stewardson, D. J., Hicks, C., and Braiden, P. M. (2001). Applying designed experiments to optimize the performance of genetic algorithms used for scheduling complex products in the capital goods industry. *Journal of Applied Statistics*, *28*(3-4), 441-455.
https://doi.org/10.1080/02664760120034162

Rahimi, I., Gandomi, A. H., Deb, K., Chen, F., and Nikoo, M. R. (2022). Scheduling by NSGA-II: Review and Bibliometric Analysis. *Processes*, *10*(1), 98.
https://doi.org/10.3390/pr10010098

Rastrigin, L. A. (1963). The convergence of the random search method in the extremal control of a many parameter system. *Automation and Remote Control*, *24*(11), 1337–1342.

Salvendy, G. (2001). *Handbook of Industrial Engineering: Technology and Operations Management*. John Wiley & Sons, Inc.

Schoenfelder, J. and Pfefferlen, C. (2018). Decision support for the physician scheduling process at a German Hospital. *Service Science*, *10*(3), 215-229. https://doi.org/10.1287/serv.2017.0192

Schrack, G. and Choit, M. (1976). Optimized relative step size random searches. *Mathematical Programming*, *10*(1), 230-244. https://doi.org/10.1007/BF01580669

Schumer, M. A. and Steiglitz, K. (1968). Adaptive Step Size Random Search. *IEEE Transactions on Automatic Control*, *13*(3), 270-276. https://doi.org/10.1109/TAC.1968.1098903

Sooncharoen, S., Pongcharoen, P., and Hicks, C. (2020). Grey Wolf production scheduling for the capital goods industry. *Applied Soft Computing Journal*, *94*, 106480. https://doi.org/10.1016/j.asoc.2020.106480

Tan, M., Gan, J., and Ren, Q. (2019). Scheduling emergency physicians based on a multiobjective programming approach: A case study of west China Hospital of Sichuan University. *Journal of Healthcare Engineering*, *2019*, 5647078. https://doi.org/10.1155/2019/5647078

Thongsamai, A., Chansombat, S., and Sooncharoen, S. (2024). The applications of Artificial Hummingbird Algorithm (AHA) in the optimization problems: A review of the state-of-the-art. *Engineering and Applied Science Research*, *51*(2), 164-179. https://ph01.tci-thaijo.org/index.php/easr/article/view/254296

Tohidi, M., Kazemi Zanjani, M., and Contreras, I. (2019). Integrated physician and clinic scheduling in ambulatory polyclinics. *Journal of the Operational Research Society*, *70*(2), 177-191. https://doi.org/10.1080/01605682.2017.1421853

Tohidi, M., Kazemi Zanjani, M., and Contreras, I. (2021). A physician planning framework for polyclinics under uncertainty. *Omega (United Kingdom)*, *101*, 102275. https://doi.org/10.1016/j.omega.2020.102275

Wang, F., Zhang, C., Zhang, H., and Xu, L. (2021). Short-term physician rescheduling model with feature-driven demand for mental disorders outpatients. *Omega (United Kingdom)*, *105*, 102519. https://doi.org/10.1016/j.omega.2021.102519

Wang, Z., Liu, R., and Sun, Z. (2023). Physician Scheduling for Emergency Departments Under Time-Varying Demand and Patient Return. *IEEE Transactions on Automation Science and Engineering*, *20*(1), 553-570. https://doi.org/10.1109/TASE.2022.3163259

9. BIOGRAPHIES

Miss. Atchara Thongsamai

Graduated with a Bachelor of Engineering Program in Industrial Engineering, Industrial Engineering Department, Faculty of Engineering, Naresuan University.

Currently studying in a Master of Engineering Program in Management Engineering, Industrial Engineering Department, Faculty of Engineering, Naresuan University.

Dr. Sirikarn Chansombat

Is a lecturer in the Faculty of Logistics and Digital Supply Chain, Naresuan University.

She graduated a bachelor degree in Industrial Engineering and received a Ph.D. in Management Engineering from Naresuan University.

Dr. Saisumpan Sooncharoen

Is a lecturer at the Industrial Engineering Department, Faculty of Engineering, Naresuan University, Phitsanulok.

Completed a Ph.D. Management Engineering from Naresuan University.

NUEJ
Naresuan University
Engineering Journal

Mobile-Centric Supervised Machine Learning Approach for Elderly Fall Detection Using YOLOv8

Poramin Saengtipkanya , Kritchai Junoakson, Krisda Khankasikam and Khaninnat Chotphornseema*

Department of Applied Science, Faculty of Science and Technology, Nakhon Sawan Rajabhat University, Nakhon Sawan, Thailand

* Corresponding author e-mail: Khaninnat.C@nsru.ac.th

(Received: 22 May 2024, Revised: 18 June 2024, Accepted: 29 June 2024)

Abstract

The global surge in the elderly population has underscored the need for advanced safety systems tailored to seniors, particularly those living independently. Central to these systems is the pivotal role of fall detection in ensuring their welfare. This paper presents a cutting-edge fall detection system designed specifically for the elderly, leveraging supervised machine learning techniques with a mobile-centric approach. Departing from traditional hospital-centric setups, our system offers cost-effectiveness and improved mobility, facilitating deployment across diverse environments. The methodology comprises three core stages: data collection and annotation, model training, and inference. We curated a dataset of 1500 images categorized into three classes: standing, falling, and fallen, meticulously annotated using RoboFlow. Subsequent model training utilized YOLOv8, culminating in the inference stage, which underwent quantitative evaluation employing 10-fold cross-validation, yielding an average accuracy of 97.88%. Qualitative assessment across four distinct scenarios further validated our system, achieving an average accuracy of 95.92%. These results underscore the efficacy of our approach and lay the foundation for practical implementation and widespread adoption. Subsequent to the successful development of the core algorithm, we operationalized it for real-world applications by seamlessly integrating it with smartphones via TensorFlowLite. This integration underscores the synergy between algorithm design and software development, further facilitating the practical deployment and widespread acceptance of our system in diverse settings.

Keywords: Fall detection, Elderly care, Supervised machine learning, YOLOv8, TensorFlowLite

1. INTRODUCTION

Over the past decade, there has been a notable surge in the demographic comprising individuals aged 60 and above. This demographic shift holds significant implications for various sectors, particularly the healthcare industry. With projections extending to the year 2100, the sustained growth in the elderly population is expected to play a pivotal role in shaping the trajectory of healthcare services globally. Concurrently, the issue of falls among the elderly has remained a longstanding concern. According to statistical insights provided by the World Health Organization (WHO), the prevalence of falls among individuals aged 65 and above is anticipated up to 35%. Moreover, this risk escalates significantly to 42%, for individuals aged 70 and older (Kumar et al., 2021). These statistics underscore the urgent need for comprehensive strategies and interventions to mitigate the risks associated with falls in the elderly population.

Research in human fall detection can be categorized into several main types: wearable sensors, vision-based systems, acoustic detection, radar-based systems, and hybrid approaches. Recent advancements in wearable sensor technology have significantly enhanced the field of fall detection systems, particularly in the context of elderly care and safety monitoring. Wearable sensors offer continuous monitoring capabilities, making them ideal for detecting sudden movements and changes in posture associated with falls. Alvarez, Li, and Philips (2021) proposed a system that integrates wearable sensors with machine learning algorithms to improve fall detection accuracy. Their approach leverages real-time data processing to distinguish fall events from normal activities, demonstrating robust performance in various settings. Chen, Yu, and Wang (2020) developed a wearable sensor-based fall detection system using machine learning techniques. Their study emphasizes the importance of sensor fusion and algorithm optimization in achieving high detection accuracy and reliability. By analyzing accelerometer and gyroscope data, their system effectively distinguishes fall incidents from other daily movements. Lopes, Rodrigues, and Plawiak (2020) conducted a comprehensive review of wearable solutions for elderly fall detection. They highlighted the integration of multiple sensor modalities and the optimization of algorithms to enhance detection accuracy while minimizing false positives. Their findings underscored the importance of sensor placement and data fusion techniques in achieving reliable fall detection outcomes. Kim and Kim (2021) focused on real-time fall detection using wearable sensors and machine learning algorithms. Their research

highlighted advancements in sensor technology and algorithmic efficiency, contributing to improved responsiveness and reliability in detecting falls.

Vision-based systems analyze images or video to identify posture changes and potential falls. Recent advancements in vision-based fall detection systems have leveraged RGB-D cameras and deep learning techniques to enhance accuracy and reliability in detecting falls, particularly focusing on elderly care and safety monitoring. Ma, Zhang, and Li (2020) proposed an RGB-D camera-based fall detection system utilizing deep learning algorithms. Their approach integrates RGB-D camera data to capture both color and depth information, enabling precise detection of falls based on human body movements and orientations. Palacios-Navarro, Carrasco-Jiménez, and Perez-Cisneros (2021) developed a fall detection system that fuses thermal and depth information from sensors. By combining thermal imaging with depth data, their system achieves robust fall detection capabilities, particularly in low-light conditions or privacy-sensitive environments. Bouloudi, Charfi, and Soudani (2019) utilized Kinect depth images and support vector machine (SVM) algorithms for real-time fall detection. Their study demonstrated high accuracy in identifying falls by analyzing depth images captured by Kinect sensors and applying machine learning classifiers. Yu, Wang, and Hao (2020) proposed a fall detection system based on RGB-D cameras and convolutional neural networks (CNNs). Their approach leverages CNNs to process RGB-D camera data, achieving efficient and accurate fall detection through automated feature extraction and classification.

Acoustic-based fall detection systems have emerged as a promising approach for detecting falls using sound signals and machine learning techniques. These systems capitalize on the unique acoustic signatures generated during falls to distinguish them from other activities and background noise. Khan and Porikli (2019) proposed an acoustic fall detection system utilizing deep learning-based sound analysis. Their study demonstrated the effectiveness of deep learning algorithms in analyzing acoustic patterns associated with falls, achieving high accuracy in real-time fall detection scenarios. Grzeszick and Jager (2020) developed a fall detection system based on convolutional neural networks (CNNs) applied to acoustic signals. Their approach focuses on extracting features from audio recordings to classify falls, showcasing the robustness of CNNs in acoustic-based fall detection applications. Wang and Liu (2020) explored the use of acoustic signals and machine learning techniques for fall detection. Their study investigated various machine learning algorithms to analyze acoustic features, aiming to improve detection accuracy by leveraging different classification models. Pannurat, Nantajeewarawat, and Haddawy (2020) proposed a fall detection system using environmental sound signals and machine learning. Their approach integrates environmental sounds with machine learning models to detect falls in diverse acoustic environments, highlighting the versatility of acoustic-based methods in different settings.

Radar-based fall detection systems have garnered attention for their ability to monitor human motion and detect falls using radar signals. These systems utilize radar technology to detect changes in movement patterns associated with falls, providing reliable monitoring in various environments. Miao, Zhang, and Wang (2019) explored radar-based fall detection using machine learning algorithms. Their study focused on enhancing detection accuracy by integrating radar signals with machine learning techniques, demonstrating effective fall detection capabilities. Zhou, He, and Wu (2020) investigated ultra-wideband radar for fall detection, emphasizing signal processing and system design aspects. Their research highlighted the advantages of ultra-wideband radar in detecting falls with high accuracy and reliability in complex environments. Wang and Guo (2020) proposed a fall detection system utilizing ultra-wideband radar combined with deep learning methods. Their study leveraged deep learning algorithms to analyze radar signals, achieving robust performance in detecting falls under different conditions. Mahmood and Hassan (2020) investigated a frequency-modulated continuous-wave radar-based fall detection system employing deep learning techniques. Their study showcased the effectiveness of radar signals and deep learning algorithms in accurately detecting falls, highlighting advancements in radar-based fall detection technologies.

Moreover, hybrid approaches combine multiple methods to enhance accuracy. Alsheikh and Selim (2020) proposed a hybrid fall detection system integrating wearable sensors and RGB-D cameras. Their study demonstrated the effectiveness of combining sensor modalities to improve detection accuracy and reduce false alarms in real-world scenarios. Mahmud and Wang (2019) conducted a comprehensive review on sensor fusion techniques for fall detection. Their review highlighted the integration of different sensor types, such as accelerometers, gyroscopes, and environmental sensors, with advanced fusion algorithms to enhance system robustness and reliability. Eskofier, Lee, and Kupnik (2020) investigated sensor fusion and machine learning approaches for robust fall detection in real-world environments. Their research emphasized the synergy between sensor fusion techniques and machine learning algorithms to achieve high accuracy and adaptability across various conditions. Hossain, Muhammad, and Alhamid (2020) proposed a hybrid fall detection system utilizing both wearable sensors and ambient sensors. Their study focused on integrating data from multiple sensor sources to improve detection sensitivity and reliability, particularly in home-based

healthcare settings. He and Wang (2020) explored multi-sensor fusion techniques combined with deep learning for fall detection. Their research highlighted the advantages of integrating data from different sensors with deep learning models to achieve robust and accurate fall detection performance.

In addition to the previously mentioned methodologies, an increasingly prevalent approach in the development of human fall detection systems is the YOLO-based technique. The related research is as follows: Luo (2023) addresses the critical challenge of fall detection in smart home applications, aiming to mitigate injuries among the elderly. Although both vision and non-vision-based techniques are available, vision-based approaches are preferred for their practicality, despite challenges related to accuracy and computational cost. The research introduces a novel dataset for posture and fall detection, employing YOLO networks to enhance detection efficacy. Various YOLO versions, including YOLOv5n and YOLOv6s, are evaluated on the dataset based on accuracy metrics such as the F1 score, recall, and mean Average Precision (mAP). Experimental results indicate that YOLOv5s outperforms other versions, demonstrating superior performance in real-world fall detection scenarios. Gao (2023) focuses on developing a YOLO-based model for effective fall detection in IoT smart home applications, essential for minimizing injuries among the elderly. Vision-based approaches have gained popularity due to their practicality, but they often encounter issues such as low accuracy and high computational costs. The research aims to address these challenges by creating an accurate and lightweight fall detection system suitable for IoT platforms. A YOLO-based network is trained and tested to accurately identify human falls. Experimental findings highlight the system's potential for integration into IoT-enabled smart homes. Kan et al. (2023) tackle the significant health concern of falls among the elderly by proposing a lightweight approach named CGNS-YOLO for human fall detection. Despite the advancements of YOLOv5 in fall detection, challenges such as computational demands and hardware integration persist. The CGNS-YOLO method integrates GSConv and GDCN modules to optimize YOLOv5s, reducing model size and enhancing feature extraction efficiency. A normalization-based attention module (NAM) improves precision by focusing on relevant fall-related data. Incorporating the SCYLLA Intersection over Union (SIoU) loss function further boosts detection accuracy and convergence speed. Evaluation on the Multicam and Le2i Fall Detection datasets reveals a 1.2% increase in detection accuracy, with a significant reduction in model parameters and floating-point operations. Overall, CGNS-YOLO demonstrates superior efficacy and suitability for real-world deployment in fall detection applications. Wang et al. (2023) introduce an improved YOLOv5s algorithm for lightweight fall detection, crucial for addressing health risks associated with elderly falls at home. Enhancements include the application of a k-means clustering algorithm for accurate anchor boxes, replacing the backbone with a ShuffleNetV2 network for simplified computing, integrating an SE attention mechanism for enhanced feature extraction, and adopting an SIOU loss function for improved detection accuracy and training speed. Experimental results demonstrate a 3.5% increase in mean Average Precision (mAP), a 75% reduction in model size, and a 79.4% decrease in computation time compared to conventional YOLOv5s. The algorithm offers superior detection accuracy and speed, making it suitable for deployment in cost-effective embedded devices with limited performance. Gomes et al. (2022) leverage deep learning for fall detection, a crucial aspect of elderly safety. They integrate the YOLO object detection algorithm with temporal classification models and the Kalman filter to identify and track falls in video streams. The proposed methods, YOLOK + 3DCNN and YOLOK + 2DCNN + LSTM, outperform existing models on key metrics. Raza, Yousaf, and Velastin (2022) explore human fall detection using YOLO from a real-time and AI-on-the-edge perspective. Addressing the challenges of using wearable sensors in public settings, they propose a vision-based solution using YOLO and its variants (YOLOv1-v4 and tiny YOLOv4). The method leverages the UR Fall dataset for feature extraction and demonstrates the ability to detect falls and other activities in real-time using simple video camera images, without the need for ambient sensors. The approach supports deployment on edge devices like Raspberry Pi and OAK-D, highlighting its practical applicability. Zhao et al. (2021) introduce YOLO-Fall, an advanced convolutional neural network model tailored for detecting falls in open spaces, particularly in industrial settings where safety hazards are prevalent. Traditional fall detection models often struggle with accuracy and computational demands, limiting their practical deployment. YOLO-Fall addresses these challenges by incorporating novel enhancements: an SDI attention module for improved feature extraction, GSConv and VoV-GSCSP modules to reduce model parameters and complexity, and a DBB module in the final ELAN for enhanced feature diversity. Experimental results show that YOLO-Fall achieves a 2.7% improvement in mean Average Precision (mAP) compared to YOLOv7-tiny, while reducing model parameters by 3.5% and computational requirements by 5.4%. These advancements position YOLO-Fall as a precise and lightweight solution for real-world fall detection applications. Yin et al. (2021) address the critical issue of elderly fall detection using YOLO algorithms, considering the challenges posed by aging populations. Traditional machine learning methods often lack real-time performance and robustness in complex scenarios.

The study utilizes modified versions of YOLOv4 and YOLOv5s to achieve end-to-end prediction of fall events in real-time. Training on a custom fall dataset and testing in real scenarios demonstrate that YOLOv5s offers lightweight deployment, good robustness, and real-time accuracy compared to YOLOv4. Wang and Jia (2020) address the increasing issue of falls among the elderly, highlighting the need for efficient fall detection methods. Current video-based methods are often complex and lack real-time accuracy. The authors propose a solution using the YOLOv3 network model, which includes creating a fall detection dataset and optimizing the model on a GPU server. Their model demonstrates superior recognition performance compared to other algorithms.

After reviewing the literature on human fall detection, this section will discuss the details of YOLO (You Only Look Once). YOLO is a pioneering object detection algorithm that revolutionized computer vision by enabling real-time detection with high accuracy. Developed by Joseph Redmon et al., YOLO employs a single convolutional neural network (CNN) to predict bounding boxes and class probabilities directly from images in a single pass. This approach eliminates the need for multiple stages and significantly speeds up the detection process, achieving up to 45 frames per second on a GPU. YOLO's unified framework, use of anchor boxes for precise bounding box prediction, and its balance between speed and accuracy have made it a cornerstone in various applications requiring fast and reliable object detection.

In this research, we choose to use YOLOv8, referred to hereafter as YOLO version 8, which represents a significant advancement in the YOLO series of object detection models. This version introduces several key improvements over its predecessors, enhancing both accuracy and efficiency in object detection tasks. YOLOv8 integrates advanced architectural changes, such as the use of CSPNet (Cross Stage Partial Network) and PANet (Path Aggregation Network). These enhancements optimize feature extraction and aggregation, leading to improved detection performance across various object sizes and orientations. In terms of speed, YOLOv8 maintains real-time inference capabilities despite its increased complexity. This is achieved through optimizations in model architecture, implementation of efficient layers, and streamlined computational processes. Training efficiency has also been enhanced in YOLOv8. The model benefits from novel data augmentation techniques, refined loss functions like focal loss, and efficient training strategies such as transfer learning with pre-trained models. These improvements contribute to faster convergence during training and better overall model performance. Backbone network improvements are crucial in YOLOv8, leveraging a more powerful base network that enhances feature representation and extraction. This upgrade ensures that the model can accurately detect objects under diverse environmental conditions and challenging scenarios. Overall, YOLOv8 sets a new benchmark in object detection with state-of-the-art performance metrics. Its combination of superior accuracy, real-time processing speed, efficient training methodologies, and robust backbone architecture makes it a preferred choice for a wide range of applications in computer vision, including autonomous driving, surveillance systems, and medical diagnostics.

Upon reviewing the literature on elderly fall detection, it is evident that current systems primarily focus on developing highly efficient detection hardware. Moreover, the software and algorithms used in these systems are often complex and resource-intensive, leading to significant costs for access. In practical real-world applications, these high-performance falls detection systems offer limited accessibility options for the middle class. The available alternatives are either to place elderly individuals in a healthcare center, incurring substantial expenses, or to invest in installing a home-based fall detection system, which requires considerable expenditure on both hardware and costly software. Furthermore, once installed, these systems lack portability and cannot be relocated for use in different settings. Therefore, users of these systems are constrained to remain within the premises where the system is originally set up. Additionally, a stable Wi-Fi connection is crucial for optimal system operation.

Hence, the author aims to propose a fall detection system characterized by affordability and accessibility for all users. This system should be highly portable. Consider a scenario where one must care for an elderly individual who stays alone at home while the caregiver is at work during the day. If the caregiver's job involves frequent relocations, a portable fall detection system becomes essential. Consequently, the author envisions developing a fall detection application for elderly individuals using a smartphone as the detection device. Upon detecting a fall, the system can send alerts through Wi-Fi or mobile network SIM. Another notable feature of this system is its portability, allowing it to be carried anywhere. Additionally, in the event of a power outage, the smartphone can continue to operate on battery power until it is depleted.

The subsequent sections of the paper follow this structure: the section titled "The Proposed Methods" presents the methodologies proposed in this paper, offering detailed elucidations. Following that, the section "Experimental Results" delves into the specifics of data processing and experimentation, accompanied by an exhaustive analysis of the outcomes. Lastly, the "Conclusion" section provides a summary of the findings and outlines avenues for future research.

2. THE PROPOSED METHODOLOGY

This section presents a comprehensive fall detection system specifically designed for elderly individuals, utilizing supervised machine learning methods, and emphasizing mobile-based deployment. The proposed methodology is delineated into three core stages: data collection and labeling, training, and inference. The schematic representation of our system is illustrated in Figure 1.

Our method amalgamates state-of-the-art machine learning techniques with a mobile-centric approach, providing an economically viable and scalable solution for fall detection within elderly care contexts. The subsequent section will delve into the intricate details of each of these three stages, elucidating their significance and implementation nuances.

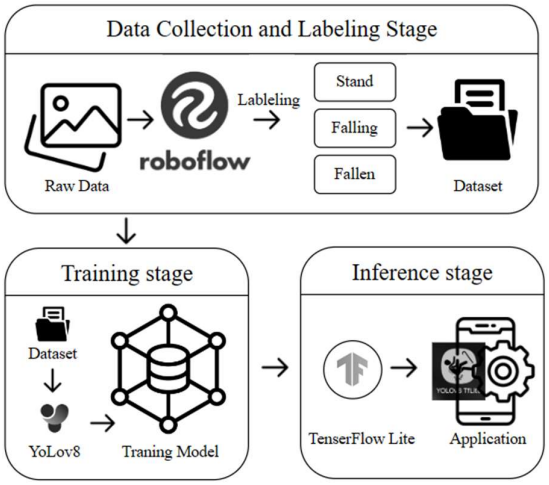

Figure 1 The schematic of the proposed system

2.1 The data collection and labeling stage

The data collection and labeling stage involved acquiring a diverse dataset comprising 1,500 images across three distinct classes: standing, falling, and fallen. All 1500 images were selected from free access image datasets specifically curated for elderly fall detection, namely the UP-Fall Detection Dataset, Multicam Dataset, and UR Fall Detection Dataset. The UP-Fall Detection Dataset, Multicam Dataset, and UR Fall Detection Dataset are invaluable resources for research in elderly fall detection. Each dataset offers curated images specifically annotated to depict various scenarios of falls among elderly individuals. The UP-Fall Detection Dataset provides a comprehensive collection capturing diverse environments and fall types, enhancing realism in training and evaluation. The Multicam Dataset contributes multiple camera angles, simulating varied surveillance perspectives crucial for robust model training. Meanwhile, the UR Fall Detection Dataset focuses on annotated images tailored for studying algorithmic intricacies in fall detection, aiding in algorithm development and evaluation. Together, these datasets facilitate comprehensive research on fall detection algorithms, covering a wide range of environmental conditions and fall scenarios. These images underwent meticulous labeling using the RoboFlow platform, ensuring accurate classification within the designated classes while maintaining consistency and reliability across the dataset. The schematic depiction of this stage is illustrated in Figure 2.

Following the augmentation of noise types to diversify the dataset, the original 1,500 images have been significantly enriched, resulting in a total of 7,500 images. This augmentation strategy aims not only to expand the dataset size but also to imbue the model with robustness and adaptability to varying real-world conditions. The inclusion of four types of noise: grayscale, saturation, mosaic, and brightness serves as a strategic augmentation approach to simulate a spectrum of environmental challenges commonly encountered in real-life scenarios. Each type of noise introduces specific variations to the original images, thereby enhancing the model's ability to generalize and accurately detect falls amidst diverse conditions. Grayscale noise, for instance, alters the color space of the images to simulate scenarios with varying lighting conditions, such as low-light environments or overexposed settings. This augmentation challenges the model to detect falls irrespective of lighting variations, thereby improving its resilience in real-world deployment.

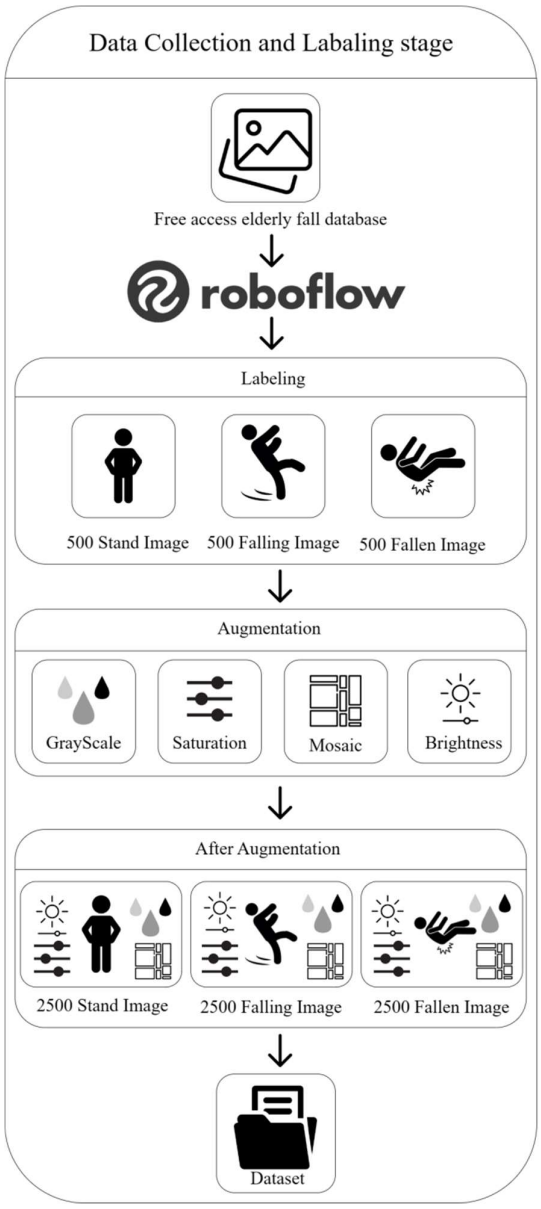

Figure 2 Overview of the data collection and labeling stage

Saturation noise adjusts the saturation levels of the images, resulting in desaturated or muted colors. This augmentation mimics scenes with subdued or washed-out colors, such as foggy or hazy conditions, challenging the model to discern falls amidst diminished visual cues. Mosaic noise pixelates sections of the images, distorting their details to replicate scenarios where the image quality is degraded or obscured. This augmentation prompts the model to identify falls despite partial or obscured visual information, thereby enhancing its adaptability to diverse imaging conditions. Brightness noise modifies the brightness levels of the images, resulting in darker or brighter overall appearances. This augmentation emulates environments with varying degrees of illumination, ranging from dimly lit spaces to glaringly bright conditions, challenging the model to accurately detect falls under diverse lighting circumstances.

Through this comprehensive augmentation strategy, we aim to equip our model with the resilience and adaptability necessary to reliably detect falls in a wide range of real-world conditions, thus enhancing its practical utility within elderly care settings.

The characteristics of each type of noise are visually depicted in Figure 3, showcasing the diversity of challenges introduced to the dataset.

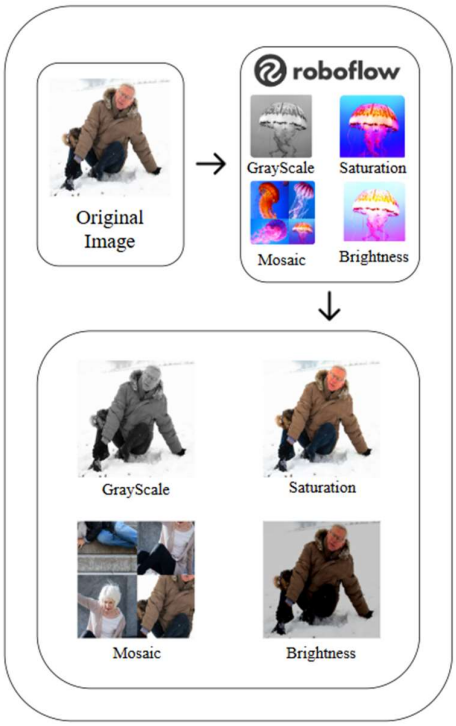

Figure 3 Examples of all four types of noise

This step ensures the availability of high-quality data crucial for training our fall detection model.

2.2 The training stage

Subsequently, the training stage incorporates state-of-the-art deep learning architecture, YOLOv8, to facilitate the development of our fall detection model. Leveraging the capabilities of TensorFlow, a powerful machine learning framework, we seamlessly integrate YOLOv8 into our training pipeline. This strategic decision is rooted in YOLOv8's renowned robustness in object detection tasks and its real-time processing capabilities, making it an ideal candidate for our mobile-centric approach to fall detection. The schematic

depiction of this stage, as outlined above, is visually represented in Figure 4.

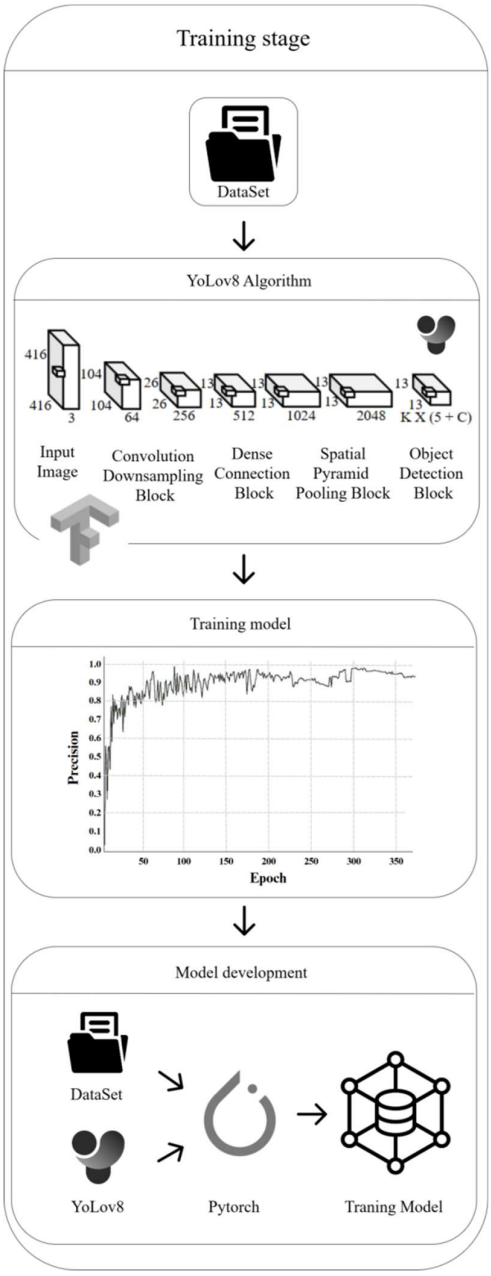

Figure 4 Overview of the training stage

By harnessing TensorFlow's extensive functionalities, we optimize the implementation of YOLOv8, ensuring efficient utilization of computational resources during training. TensorFlow's flexibility allows us to fine-tune model parameters and hyperparameters, enhancing the accuracy and reliability of our fall detection system. Moreover, TensorFlow provides a rich ecosystem of tools and libraries for data preprocessing, augmentation, and visualization, streamlining the entire training process.

Throughout numerous training iterations, our model undergoes a rigorous learning process, adapting to diverse scenarios and environmental conditions to accurately detect and classify instances of falls within input images.

Additionally, we carefully monitor the training progress by analyzing the learning rate over epochs. The learning rate graph, depicted in Figure 5, illustrates the dynamic adjustment of the learning rate during training. This adaptive learning rate scheme optimizes the convergence speed and stability of the training process, allowing our model to effectively learn from the training data while mitigating the risk of overfitting or divergence.

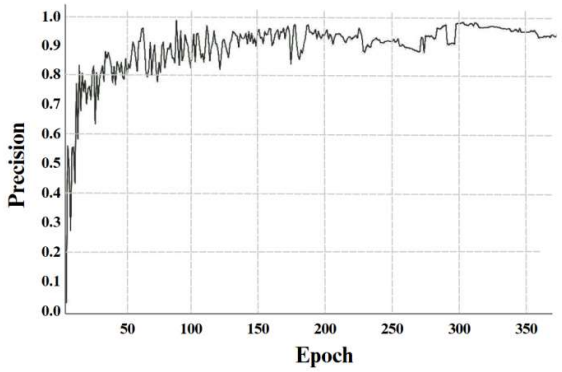

Figure 5 Graph of learning rate

In Figure 5, it is observed that the precision surpasses the threshold of 80% after approximately 50 epochs of training. Furthermore, the precision stabilizes at a level exceeding 80% after around 300 epochs of training. This phenomenon underscores the efficacy of the training regimen in enhancing precision metrics. Such observations reflect a convergence towards a stable and desirable precision performance, indicative of the model's adeptness in discerning and classifying data patterns. These findings bear significance in the context of model optimization and deployment, elucidating the trajectory of precision improvement over training epochs. The integration with TensorFlow not only accelerates model convergence but also facilitates seamless deployment across various platforms, including mobile devices, ensuring real-time fall detection capabilities in practical scenarios.

In summary, by harnessing the synergy between YOLOv8 and TensorFlow, we empower our fall detection model with cutting-edge object detection capabilities, paving the way for robust and efficient fall detection solutions in real-world applications.

2.3 The inference stage

The inference stage marks the deployment and evaluation of our trained fall detection system. Our next critical step involves deploying the trained system for real-world applications. Integration of YOLOv8 with TensorFlow provides a robust framework for developing and deploying advanced object detection systems. YOLO is renowned for its real-time processing speed and high accuracy in object detection across images and videos. TensorFlow, widely adopted in deep learning and machine learning applications, offers comprehensive support for training and inference processes, enhancing YOLO models effectively.

The TensorFlow Object Detection API enables seamless integration with YOLO models, empowering researchers and developers to leverage TensorFlow's capabilities throughout training and deployment phases. During training, TensorFlow efficiently trains models using annotated datasets, allowing the YOLO model to adapt and optimize its detection capabilities by adjusting model parameters and architecture for optimal performance metrics.

In deployment, TensorFlow facilitates the integration of pre-trained YOLO models into real-time applications or video streams, ensuring precise object detection in dynamic environments. The API's flexibility supports fine-tuning of pre-trained models tailored to specific use cases or to enhance detection performance further.

Furthermore, TensorFlow supports ongoing model refinement through continuous evaluation and optimization, enabling iterative improvements based on real-world performance feedback. Leveraging TensorFlow Lite, a lightweight version optimized for mobile and embedded devices, further enhances deployment efficiency.

The workflow of this stage is illustrated in Figure 6, depicting the overall process from model training to deployment and iterative refinement.

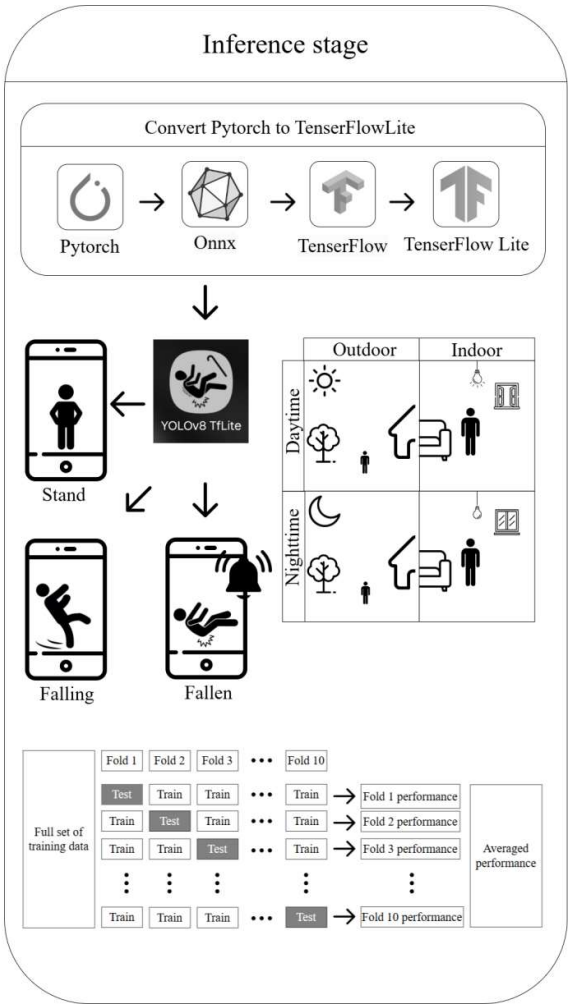

Figure 6 Overview of the Inference stage

The process begins with the conversion of our trained TensorFlow model into a TensorFlowLite format, tailored for seamless integration with mobile platforms. TensorFlowLite employs various optimization techniques to ensure minimal computational and memory footprint, thereby enabling efficient execution on resource-constrained devices such as smartphones. Once the model conversion is completed, we proceed to integrate the TensorFlowLite model into our mobile application, empowering smartphones with the capability to perform real-time fall detection. Leveraging the processing power of modern smartphones, our application can analyze video streams or accelerometer data in real-time, swiftly detecting and alerting caregivers or emergency services in the event of a fall. Furthermore, the deployment of our fall detection system on smartphones offers several advantages, including portability, ubiquity, and accessibility.

Users can carry their fall detection solution with them wherever they go, ensuring continuous monitoring

and assistance, particularly for elderly individuals living independently. Additionally, the integration of our fall detection system into smartphones opens up opportunities for further enhancements, such as incorporating additional sensors (e.g., gyroscopes, GPS) for context-aware fall detection or leveraging cloud services for centralized monitoring and data analytics. In summary, the exportation of our trained fall detection model to TensorFlowLite facilitates seamless integration into smartphones, enabling the deployment of our solution for real-time fall detection on a wide scale. By harnessing the ubiquity and processing power of smartphones, we empower individuals to lead safer and more independent lives while providing caregivers and emergency responders with timely alerts and assistance when needed.

Following the successful deployment of our fall detection system onto smartphones, the next pivotal aspect we delve into is the analysis of experimental results. This phase serves as the ultimate validation of our system's performance and effectiveness in real-world scenarios.

3. The Experimental Results

The experimental results provide crucial insights into the performance and effectiveness of our fall detection system, validating its capability to accurately identify falls and differentiate them from normal activities. In this section, we present a comprehensive analysis of both quantitative and qualitative evaluations conducted to assess the system's performance. Additionally, a utilization evaluation was also conducted.

3.1 Quantitative evaluation

Cross-validation is a statistical method used to assess the performance of machine learning models by partitioning the dataset into subsets known as "folds." Typically, in a 10-fold cross-validation setup, the data is divided into 10 equally sized folds. During each iteration, one fold is designated as the validation set, while the remaining nine folds are utilized for training the model. This process is repeated ten times, ensuring that each fold serves once as the validation set. The results from each iteration are averaged to derive a final performance metric, providing robust evaluation and minimizing overfitting risks by leveraging all available data for training and validation purposes.

For the quantitative evaluation of our fall detection system, we utilized a 10-fold cross-validation technique. Details of the fold division and the sequence of folds used for testing and training are depicted in Figure 7. The dataset comprises a total of 7,500 images, consisting of 3 classes with 2,500 images per class. These images were divided into 10 folds, each containing 750 images. Each fold consists of 750 images, with 250 images from each of the 3 classes. The average accuracy of our approach was calculated to be 97.88%. Comprehensive confusion matrices for each fold, accompanied by their respective accuracy scores, are presented in Table 1, providing a detailed illustration of the evaluation results.

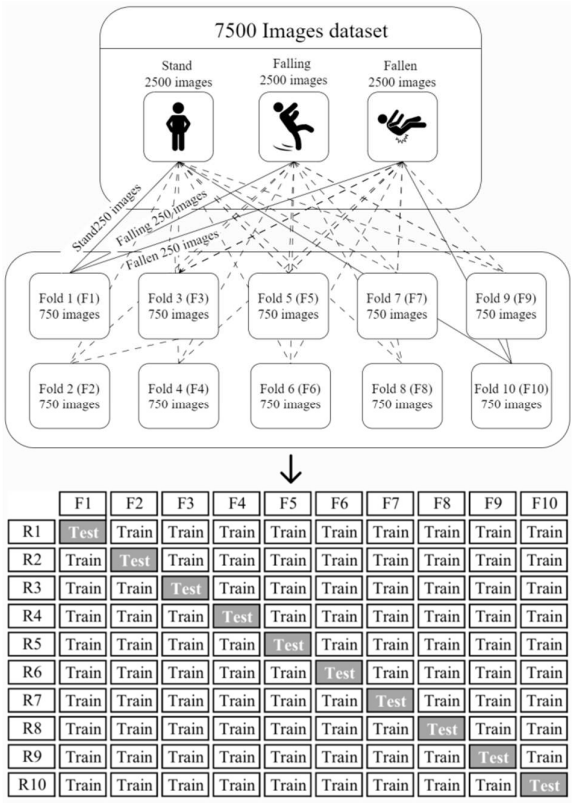

	F1	F2	F3	F4	F5	F6	F7	F8	F9	F10
R1	Test	Train	Train	Train	Train	Train	Train	Train	Train	Train
R2	Train	Test	Train	Train	Train	Train	Train	Train	Train	Train
R3	Train	Train	Test	Train	Train	Train	Train	Train	Train	Train
R4	Train	Train	Train	Test	Train	Train	Train	Train	Train	Train
R5	Train	Train	Train	Train	Test	Train	Train	Train	Train	Train
R6	Train	Train	Train	Train	Train	Test	Train	Train	Train	Train
R7	Train	Train	Train	Train	Train	Train	Test	Train	Train	Train
R8	Train	Train	Train	Train	Train	Train	Train	Test	Train	Train
R9	Train	Train	Train	Train	Train	Train	Train	Train	Test	Train
R10	Train	Train	Train	Train	Train	Train	Train	Train	Train	Test

Figure 7 10-fold cross-validations

In Table 1, the abbreviations ST, FG, and FN in the columns under "Actual class" and "Predicted class" denote stand, falling, and fallen, respectively. The accuracy of the fall detection model was evaluated using the following formula:

$$Accuracy = \frac{TP+TN}{TP+TN+FP+FN} \quad (1)$$

where *TP* represents True Positives, *TN* represents True Negatives, *FP* represents False Positives, and *FN* represents False Negatives. This metric measures the model's ability to correctly classify instances of falls and non-falls.

These results demonstrate the high accuracy and reliability of our fall detection system across diverse datasets, showcasing its robustness in real-world scenarios.

Table 1 Accuracy scores from 10-fold cross-validation

Fold	Actual Class	Predicted Class			Accuracy (%)
		ST	FG	FN	
1	ST	245	4	1	98.27%
	FG	2	245	3	
	FN	1	2	247	
2	ST	245	4	1	98.00%
	FG	2	245	3	
	FN	1	2	247	
3	ST	245	3	2	98.40%
	FG	1	246	3	
	FN	2	4	244	
4	ST	249	1	0	97.87%
	FG	3	243	4	
	FN	0	4	246	
5	ST	245	3	2	97.73%
	FG	1	246	3	
	FN	3	4	243	
6	ST	246	3	1	97.07%
	FG	2	244	4	
	FN	2	5	243	
7	ST	245	3	2	98.27%
	FG	5	237	8	
	FN	1	3	246	
8	ST	248	2	0	97.20%
	FG	1	245	4	
	FN	2	4	244	
9	ST	242	5	3	98.67%
	FG	2	244	4	
	FN	1	6	243	
10	ST	247	2	1	97.33%
	FG	1	246	3	
	FN	0	3	247	
Average					97.88%

3.2 Qualitative evaluation

In addition to quantitative assessment, we conducted a qualitative evaluation to analyze the system's performance under different conditions. The evaluation criteria included four scenarios: daytime outdoor residential (DOR), daytime indoor residential (DIS), nighttime outdoor residential (NOR), and nighttime indoor residential (NIR). From this assessment, we collected 300 images for each scenario, totaling 1200 images used for qualitative evaluation. These images were meticulously chosen to encompass various environmental factors and challenges typical of real-world fall detection scenarios. Examples of images from each scenario are illustrated in Figure 8. These scenarios represent subclasses within the main class of elderly fall images as discussed in section 2.1 of the image database.

Figure 8 Examples of images from four scenario

The evaluation was based on confusion matrices obtained from the classification results for each scenario. The confusion matrices provide insights into the system's ability to accurately detect falls and differentiate them from non-fall activities. The results of the qualitative evaluation are summarized in Table 2, where the average accuracy of the qualitative approach is calculated to be 95.92%.

Table 2 Accuracy scores from four scenarios

Scenario	Actual Class	Predicted Class			Accuracy (%)
		ST	FG	FN	
DOR	ST	97	2	1	97.33%
	FG	0	97	3	
	FN	1	1	98	
DIR	ST	95	3	2	96.67%
	FG	1	97	2	
	FN	1	1	98	
NOR	ST	96	3	1	95.33%
	FG	0	98	2	
	FN	3	5	92	
NIR	ST	93	4	3	94.33%
	FG	1	97	2	
	FN	2	5	93	
Average					95.92%

These results demonstrate the system's effectiveness in accurately detecting falls across different environmental conditions. The low false positive and false negative rates indicate the system's reliability in distinguishing fall events from normal activities, thus showcasing its suitability for real-world deployment.

3.3 Utilization evaluation

In addition to the quantitative and qualitative evaluations discussed in preceding sections, serving as benchmarks for academic performance, this study

presents a pragmatic assessment focusing on four critical dimensions: real-time detection capabilities, simultaneous detection of falls among multiple individuals with varying statuses, system repositioning flexibility, and fall-triggered alert notifications.

The study conducted tests on real-time and simultaneous fall detection by capturing fifteen 1-hour videos, totaling 15 hours of footage. Results indicate the smartphone-based fall detection system operated flawlessly. Figure 9 provides sample images highlighting the system's real-time individual status detection, while Figure 10 demonstrates its simultaneous detection across diverse individual statuses.

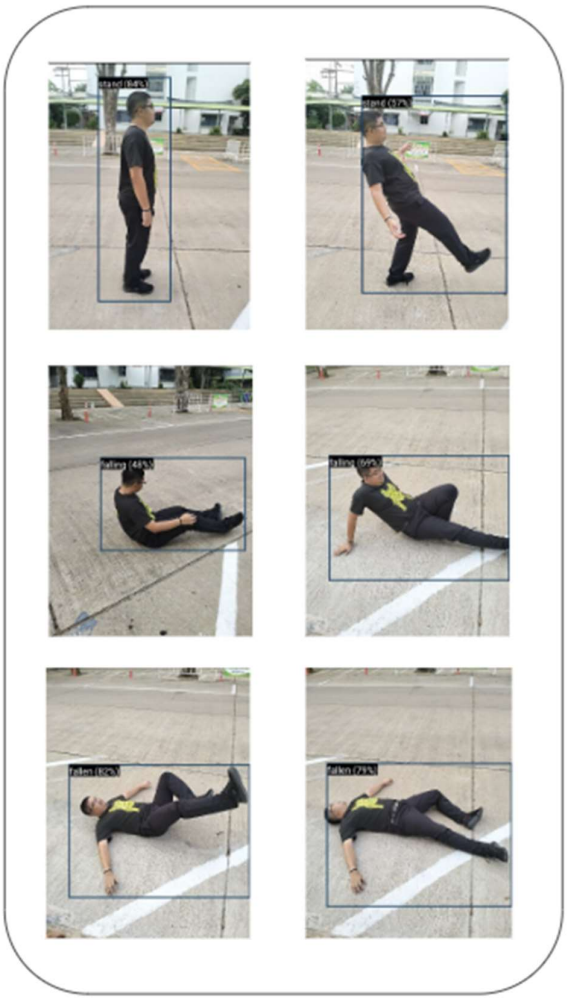

Figure 9 Real-time demonstration of the fall detection system accurately identifying individual statuses.

Figure 10 Simultaneous detection of falls across multiple individuals with varying statuses.

To evaluate system mobility and usability across different environments, varied indoor and outdoor locations were systematically tested during video recordings. Results revealed seamless transitions between locations without complications, as shown in Figure 11.

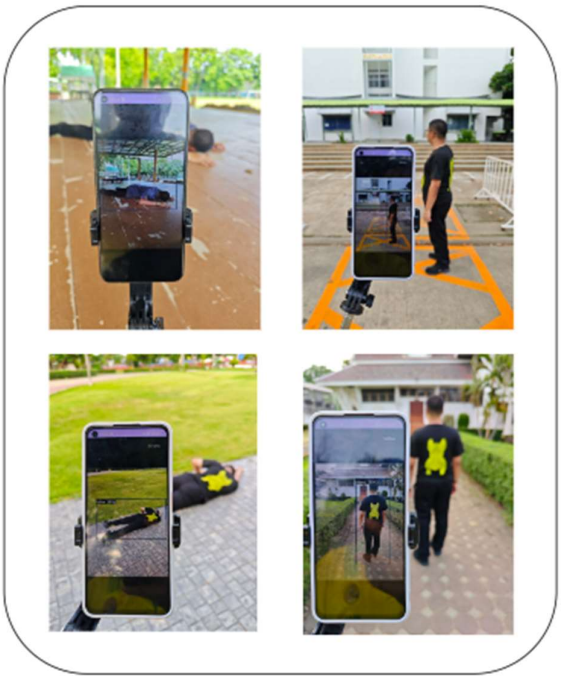

Figure 11 Example of location transition during testing.

Lastly, alert notifications were tested by integrating them with the LINE messaging app, triggering notifications for 45 instances of randomly simulated falls, occurring three times per hour during video recordings. The system successfully detected and alerted each instance without errors, depicted in Figure 12.

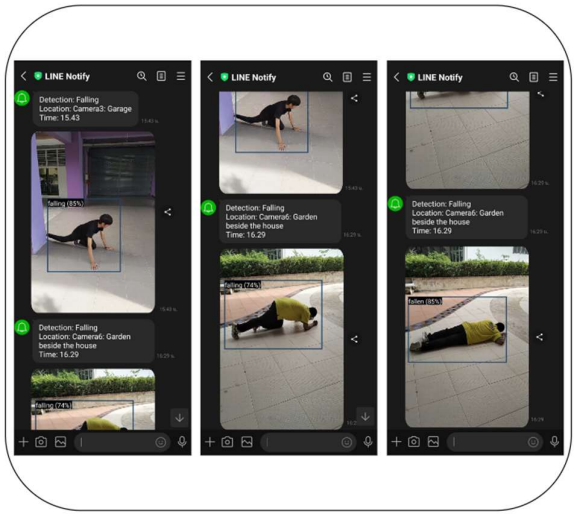

Figure 12 Notification display integrated with the LINE messaging app during fall detection testing.

This revision emphasizes that figures 9, 10, 11, and 12 were intentionally chosen not to depict elderly individuals. The testing methodology of the fall detection system included simulated falls specifically designed to assess its sensitivity and accuracy, particularly in scenarios involving elderly users. The deliberate decision to exclude images of elderly individuals from these figures was made to prevent any misinterpretation and to ensure clarity in demonstrating the system's capabilities across various scenarios.

Conducting tests with elderly individuals in fall detection research raises significant ethical considerations and potential risks. Safeguarding the safety and well-being of participants is paramount when conducting research involving vulnerable populations. Adherence to stringent research ethics guidelines is essential to mitigate any potential harm or discomfort that participants may experience. Testing the fall detection system involved rigorous evaluation under controlled conditions where simulated falls were carefully orchestrated to mimic real-world scenarios. This approach not only validated the system's ability to detect falls but also ensured that the testing process did not expose elderly individuals to actual risks associated with falling.

The validated fall detection system explored in this study holds significant promise for diverse applications across various sectors. Implementing this system in elderly care facilities, such as nursing homes or assisted living facilities stands to revolutionize elderly care by providing immediate alerts in the event of falls. This capability not only reduces response times but also enhances overall safety by ensuring prompt assistance during critical moments. In the realm of home healthcare, particularly for elderly individuals living independently, the system's continuous monitoring capabilities offer reassurance without compromising privacy. By detecting falls and triggering alerts, it enables timely intervention and support, crucial for managing emergencies effectively and maintaining independence. Hospitals can also benefit from integrating this fall detection system into their environments. In wards where patient mobility is a concern, the system serves as a valuable supplement to existing monitoring systems. It enhances patient safety by providing additional layers of detection and response mechanisms, thereby reducing the risks associated with falls within healthcare settings. Public spaces, such as airports, train stations, or recreational areas, can leverage the system to improve safety protocols. Rapid detection of falls allows for immediate medical assistance, minimizing potential consequences and ensuring a swift response to emergencies. Moreover, the system's adaptability extends to personal use through wearable devices or smartphone integration. This application empowers individuals by alerting caregivers or emergency services in real-time, regardless of their location. Such proactive measures not only enhance personal safety but also contribute to peace of mind for users and their families. By harnessing the accuracy and real-time capabilities validated in this study, stakeholders across these sectors can optimize safety protocols, improve response times, and ultimately enhance outcomes for individuals prone to falls, including the elderly and those with specific medical conditions.

4. CONCLUSION

In conclusion, this paper introduces a mobile-centric approach to fall detection tailored specifically for the elderly, addressing a critical need in the context of an aging global population. Our research underscores the urgency of developing cost-effective, scalable solutions to ensure the safety and well-being of seniors, particularly those living independently. By diverging from conventional hospital-based setups, our methodology offers a pragmatic response to the challenges posed by the demographic shift towards an increasingly elderly populace. Throughout our study, we have meticulously outlined the methodology employed in the design, development, and evaluation of our fall detection system. From the rigorous data collection and labeling process to the utilization of state-of-the-art supervised machine learning techniques, such as YOLOv8, our approach reflects a commitment to methodological rigor and innovation. Furthermore, the

seamless integration of our model with mobile platforms through TensorFlowLite underscores our emphasis on practicality and real-world applicability. The experimental results presented in this paper provide compelling evidence of the efficacy and reliability of our fall detection system. Through a combination of quantitative evaluation techniques, including 10-fold cross-validation, and qualitative analysis based on confusion matrices, we have demonstrated the robustness of our approach across diverse datasets and environmental conditions. These findings not only validate the effectiveness of our system but also underscore its potential for widespread adoption and deployment. Moreover, the practical implications of our research extend beyond academic discourse. The deployment of our fall detection system on smartphones holds transformative potential for elderly care and emergency response. By leveraging the ubiquity and processing power of mobile devices, we empower caregivers and elderly individuals with real-time monitoring and assistance capabilities, thereby enhancing safety, autonomy, and quality of life. Looking ahead, the field of fall detection systems for the elderly presents exciting opportunities for further research and innovation.

Future endeavors may explore enhancements such as context-aware fall detection, integration with additional sensors, or cloud-based analytics for comprehensive monitoring and analysis. By continuing to push the boundaries of technology and healthcare, we can strive towards a future where aging populations can age with dignity and security, supported by cutting-edge solutions tailored to their unique needs.

5. REFERENCES

Kumar, V., Badal, N., & Mishra, R., (2021). Elderly fall detection using IoT and image processing. Journal of Discrete Mathematical Sciences and Cryptography, 24(3), 681-695 https://doi.org/10.1080/09720529.2019.1692451

Alvarez, J., Li, C., & Philips, A. (2021). Enhancing fall detection accuracy using wearable sensors and machine learning algorithms. *Journal of Assistive Technologies*, *12*(3), 217-230. https://doi.org/10.1108/JAT-12-2020-0078

Chen, Y., Yu, H., & Wang, Y. (2020). A wearable sensor-based fall detection system using machine learning algorithms. *IEEE Sensors Journal*, *20*(15), 8765-8773. https://doi.org/10.1109/JSEN.2020.2993583

Lopes, I. M., Rodrigues, J. J., & Pławiak, P. (2020). A review of wearable solutions for elderly fall detection. *Sensors*, *20*(3), Article 829. https://doi.org/10.3390/s20030829

Kim, T., & Kim, M. S. (2021). Real-time fall detection using machine learning algorithms and wearable sensors. *Sensors*, *21*(6), Article 2086. https://doi.org/10.3390/s21062086

Ma, X., Zhang, T., & Li, M. (2020). RGB-D camera-based fall detection system using deep learning. *Journal of Visual Communication and Image Representation*, 69, 103010. https://doi.org/10.1016/j.jvcir.2020.103010

Palacios-Navarro, G., Carrasco-Jiménez, J. C., & Pérez-Cisneros, M. (2021). Fall detection system using thermal and depth information fusion. *Sensors*, *21*(2), Article 429. https://doi.org/10.3390/s21020429

Bouloudi, F., Charfi, I., & Soudani, A. (2019). Real-time fall detection using Kinect depth images and a support vector machine. *Sensors*, *19*(11), Article 2457. https://doi.org/10.3390/s19112457

Yu, Z., Wang, Q., & Hao, K. (2020). Human fall detection system based on RGB-D cameras and convolutional neural networks. *Journal of Ambient Intelligence and Humanized Computing*, *11*(5), 1897-1906. https://doi.org/10.1007/s12652-019-01322-3

Khan, M. A., & Porikli, F. (2019). Acoustic fall detection using deep learning-based sound analysis. *Pattern Recognition*, *93*, 195-205. https://doi.org/10.1016/j.patcog.2019.05.017

Grzeszick, R., & Jager, F. (2020). Acoustic-based fall detection using convolutional neural networks. *Applied Acoustics*, *164*, 107315. https://doi.org/10.1016/j.apacoust.2020.107315

Wang, Z., & Liu, Y. (2020). Fall detection using acoustic signals and machine learning techniques. *IEEE Sensors Journal*, *20*(7), 3661-3670. https://doi.org/10.1109/JSEN.2019.2951383

Pannurat, N., Nantajeewarawat, E., & Haddawy, P. (2020). Fall detection using environmental sound signals and machine learning. *Sensors*, *20(6)*, Article 1746. https://doi.org/10.3390/s20061746

Miao, F., Zhang, X., & Wang, W. (2019). Radar-based fall detection using machine learning algorithms. *IEEE Transactions on Biomedical Engineering*, *66*(2), 419-428. https://doi.org/10.1109/TBME.2018.2839078

Zhou, K., He, Y., & Wu, F. (2020). Ultra-wideband radar for fall detection: Signal processing and system design. *Digital Signal Processing*, *98*, 102647. https://doi.org/10.1016/j.dsp.2019.102647

Wang, Z., & Guo, L. (2020). Fall detection using ultra-wideband radar and deep learning. *IEEE Access*, *8*, 53657-53666. https://doi.org/10.1109/ACCESS.2020.2986087

Mahmood, A., & Hassan, M. (2020). Frequency-modulated continuous-wave radar-based fall detection using deep learning. *IEEE Transactions on Industrial Informatics*, *16*(7), 4361-4370. https://doi.org/10.1109/TII.2019.2953813

Alsheikh, M. A., & Selim, M. M. (2020). Hybrid fall detection system using wearable sensors and RGB-D cameras. *Journal of Ambient Intelligence and Humanized Computing*, *11*(10), 4427-4439. https://doi.org/10.1007/s12652-019-01344-x

Mahmud, M. S., & Wang, X. (2019). A review of sensor fusion techniques for fall detection. *IEEE Access*, *7*, 48819-48833. https://doi.org/10.1109/ACCESS.2019.2907910

Eskofier, B. M., Lee, S. I., & Kupnik, M. (2020). Sensor fusion and machine learning for robust fall detection in real-world environments. *Sensors*, *20*(7), Article 1901. https://doi.org/10.3390/s20071901

Hossain, M. S., Muhammad, G., & Alhamid, M. F. (2020). Hybrid fall detection system using wearable sensors and ambient sensors. *IEEE Access*, *8*, 132836-132847. https://doi.org/10.1109/ACCESS.2020.3015645

He, T., & Wang, H. (2020). Multi-sensor fusion for fall detection using deep learning techniques. *IEEE Transactions on Neural Systems and Rehabilitation Engineering*, *28*(4), 922-931. https://doi.org/10.1109/TNSRE.2020.2978803

Luo, B. (2023). Human fall detection for smart home caring using YOLO networks. *International Journal of Advanced Computer Science and Applications, 14*(4), 59-68. https://doi.org/10.14569/IJACSA.2023.0140409

Gao, P. (2023). Development of YOLO-based model for fall detection in IoT smart home applications. *International Journal of Advanced Computer Science and Applications, 14*(10), 1118-1125. https://dx.doi.org/10.14569/IJACSA.2023.01410117

Kan, X., Zhu, S., Zhang, Y., & Qian, C. (2023). A lightweight human fall detection network. *Sensors, 23*(22), 9069, 1-20. https://doi.org/10.3390/s23229069

Wang, Y., Chi, Z., Liu, M., Li, G., & Ding, S. (2023). High-performance lightweight fall detection with an improved YOLOv5s algorithm. *Machines, 11*(8), 818, 1-17. https://doi.org/10.3390/machines11080818

Gomes, M. E. N., Macêdo, D., Zanchettin, C., de-Mattos-Neto, P. S. G., & Oliveira, A. (2022). Multi-human fall detection and localization in videos. *Computer Vision and Image Understanding, 220*, 103442, 1-13 https://doi.org/10.1016/j.cviu.2022.103442

Raza, A., Yousaf, M. H., & Velastin, S. A. (2 0 2 2) . Human fall detection using YOLO: A real-time and AI-on-the-edge perspective. In *2022 12th International Conference on Pattern Recognition Systems (ICPRS)* (pp. 1-6). https://doi.org/10.1109/ICPRS54038.2022.9854070

Zhao, D., Song, T., Gao, J., Li, D., & Niu, Y. (2021). YOLO-Fall: A novel convolutional neural network model for fall detection in open spaces. In *2021 IEEE International Conference on Emergency Science and Information Technology (ICESIT)* (Vol. 12, pp.26137-26149). https://doi.org/10.1109/ACCESS.2024.3362958

Yin, Y., Lei, L., Liang, M., Li, X., He, Y., & Qin, L. (2021). Research on fall detection algorithm for the elderly living alone based on YOLO. In *2021 IEEE International Conference on Emergency Science and Information Technology (ICESIT)* (pp. 403-408). https://doi.org/10.1109/ICESIT53460.2021.9696459

Wang, X., & Jia, K. (2020). Human fall detection algorithm based on YOLOv3. In *2020 IEEE 5th International Conference on Image, Vision and Computing (ICIVC)* (pp. 50-54). IEEE. https://doi.org/10.1109/ICIVC50857.2020.9177447

NUEJ
Naresuan University
Engineering Journal

A Comparative Study of the Applicability of Regression Models in Predicting Student Academic Performance

Wenting Cui, Adisak Sangsongfar, and Noppadol Amdee*

Department of Industrial Technology Management, Faculty of Industrial Technology,
Muban Chom Bueng Rajabhat University, Ratchaburi, Thailand 70150

*Corresponding author e-mail: noppadolamd@mcru.ac.th

(Received: 22 February 2024, Revised: 9 June 2024, Accepted: 27 June 2024)

Abstract

Educational Data Mining (EDM) has witnessed a surge in educational systems, as it enables the analysis and prediction of student performance, facilitating proactive measures. This paper aims to present a comparative study of regression prediction using eight mainstream models: Linear Regression, Ridge Regression, Lasso Regression, Huber Regression, Support Vector Regression (SVR), K-Nearest Neighbors Regression (KNN), Decision Tree Regression (DT), and Neural Network Regression. The applicability of these eight models is analyzed across different courses and semester GPAs, considering three distinct scenarios. Our thorough analysis underscores the substantial influence of data granularity and integrity on bolstering the precision of final CGPA predictions. In the third scenario where Semester GPAs were utilized, Lasso Regression achieved an R-value of 0.9901 with remarkably low RMSE and MAE, establishing its dominance across all scenarios. Neural Network Regression, with an R-value of 0.9832 and minimal error metrics in the same scenario, also demonstrated robust predictive capabilities. These insights highlight the imperative of tailoring regression model selection to align with specific scenario nuances and the targeted predictive precision.

Keywords: Educational Data Mining, Regression models, Student Academic Performance

1. INTRODUCTION

The emergence of big data has garnered increasing attention in education. A pivotal challenge within educational data mining is the development of student models capable of accurately predicting academic performance (Bydžovská, H., 2016). In the early 2000s, Xiushan NIE et al. (2022) pioneered association rule mining techniques to identify students requiring course remediation, paving the way for a substantial body of research focused on student performance prediction through machine learning and data mining methodologies. The query rule "student performance prediction (topic) and predicting student performance (topic) and machine learning" was entered into the "Web of Science". The results show that over half of the literature has been published in the last five years, further demonstrating the increasing interest in student academic performance prediction.

As machine learning theories and methodologies continue evolving and related technologies advance rapidly, scholars have extensively researched student performance prediction. This research can be broadly categorized into five main areas: (1) investigations into the factors influencing students' performance, (2) studies focusing on predicting students' performance in online exams, (3) research on predicting students' performance in individual courses, (4) efforts aimed at predicting students' overall GPA performance, and (5) application in real teaching scenarios, such as college alert, personalized learning, adaptive learning system, learning resource recommendation, etc. From a large amount of research literature, the current student performance prediction is still mainly based on classification problems. The prediction models are mostly single, and the corresponding classification prediction results cannot be effectively analyzed for the prediction results (Ma, Y. et al., 2000). In the process of course grade prediction, the corresponding models fit differently depending on the predicted course. Moreover, the more technical literature is not the most suitable learning resource for education and teaching administrators who lack theoretical and technical knowledge of algorithms, perhaps due to factors such as poor readability and difficulty in understanding, which becomes one of the constraints for student achievement prediction research to be truly useful in real teaching scenarios.

To address the above issues, this paper intends to conduct regression type of grade prediction and use eight mainstream regression prediction algorithms: Linear Regression, Ridge Regression, Lasso Regression, Huber Regression, Support Vector Regression (SVR), K-Nearest Neighbors Regression (KNN), Decision Tree Regression (DT), and Neural Network Regression (NN), to analyze their characteristics under different course attributes. The eight algorithms are compared in terms of prediction accuracy, error analysis, and prediction distribution, and different training samples are selected to

provide a reference basis for suitable prediction algorithms for predicting college students' course grades.

2. LITERATURE REVIEW

Over the past few years, a notable surge in research has been focused on predicting student academic performance. The analyzed literature reveals that researchers often employ multiple algorithms to develop predictive models (Kumar et al., 2018). The most commonly utilized algorithms in predictive modeling encompass a variety of approaches, including Decision Trees, Bayesian Classifiers, Neural Networks, Support Vector Machines, K-Nearest Neighbors, and Logistic and Linear Regression. The selection of algorithms is contingent upon factors such as the problem type, the characteristics of the outcome to be predicted, and the variables employed in the prediction process. It is customary for researchers to experiment with multiple algorithms and assess their performance to identify the most accurate prediction methodology. Studies consistently demonstrate that the performance of algorithms varies across different datasets, with Neural Networks often outperforming other algorithms in terms of accuracy (Cavazos et al., 2017; Vijayalakshmi et al., 2019; Bravo et al., 2020; Makombe et al., 2020; Mengash, 2020; Waheed et al., 2020).

Numerous studies have undertaken comparisons of Decision Tree, Artificial Neural Networks (ANN), and Regression algorithms in their effectiveness at predicting student academic performance. These comparisons consistently demonstrate that ANN yields the best results (Mutanu & Machoka, 2019). In addition, a study by Iyanda (2018) found that Regression Neural Network outperformed MLP (Multi-Layer Perceptron). Furthermore, Hussain and Khan (2021) and Mai et al. (2022) utilized Gradient Boosting and Decision Tree algorithms to forecast students' overall performance. El Aouif et al. (2021) employed the K-Nearest Neighbor (KNN) algorithm for predicting learners' performance, while Cutad and Gerardo (2019) applied it for curriculum analysis.

In the specific articles examined, Tomasevic et al. (2020) employed Artificial Neural Networks (ANN), Support Vector Machines (SVM), K-Nearest Neighbors (KNN), and Decision Trees to predict student performance, drawing from a combination of grades, behavioral, and demographic data. Meanwhile, Sa'ad and Mustafa (2020) utilized ELM (Extreme Learning Machines), SVM, and ANN methodologies to forecast the dropout rate of PhD students, relying primarily on behavioral data. Bujang et al. (2021) explored Naive Bayes, KNN, and Logistic Regression models to predict semester-end grades using demographic and grade data. However, these studies primarily focused on specific prediction tasks and had limitations regarding the comparison methods used and the data types considered.

In the realm of regression problems, both Single and Multiple Linear Regression have been employed for prediction tasks. Hsu Wang (2019) utilized the multiple linear regression model to forecast students' online behavior and academic achievement. Similarly, Albalooshi et al. (2019) and Yang et al. (2018) employed this approach to assess learners' academic performance. Meanwhile, Single Linear Regression was utilized by Omer et al. (2020) for performance evaluation and by Tuononen and Parpala (2021) to predict students' thesis grades.

In our proposed approach, we focus on regression problems to determine the applicability of regression algorithms and emphasize the importance of selecting appropriate regression methods based on the specific scenario and desired predictive accuracy. Based on the analysis of the aforementioned related work, we have chosen eight of the most popular regression algorithms researchers use. The methodologies employed encompass a range of regression techniques, including Linear Regression, Ridge Regression, Lasso Regression, Huber Regression, SVR, KNN, DT, and Neural Network Regression, all aimed at predicting student academic performance.

3. METHODOLOGY

3.1 Proposed Approach

The proposed steps in this paper, based on eight main regression prediction methods for student performance, are as follows: First, retrieve student information from the university's academic affairs database. Second, data cleaning is performed, and the extracted data is converted into a suitable format. Third, data pre-processing on the cleaned data must be carried out to ensure its quality and relevance. Fourth, conduct course feature selection and choose different types of courses for prediction. Fifth, evaluate the application of the models, select appropriate algorithms for comparison and analysis, and recommend suitable algorithms for different courses. The specific algorithm flow is illustrated in Figure 1.

3.2 Regression algorithms used

In this paper, eight regression models were utilized following the steps of regression analysis. The models encompass Linear Regression, Ridge Regression, Lasso Regression, Huber Regression, SVR, KNN, DT, and Neural Network Regression. Each model possesses distinct characteristics and applicability. Linear regression establishes a linear relationship using the least squares method, while Ridge and Lasso regressions introduce regularization to control complexity and promote sparsity, respectively. Huber regression reduces

sensitivity to outliers through the Huber loss function. SVR handles nonlinear problems and complex structures, KNN captures local patterns, DT handles nonlinear relationships and interactions, and Neural Network Regression constructs complex models for large-scale and high-dimensional data. These models were chosen to analyze regression performance and accuracy comprehensively.

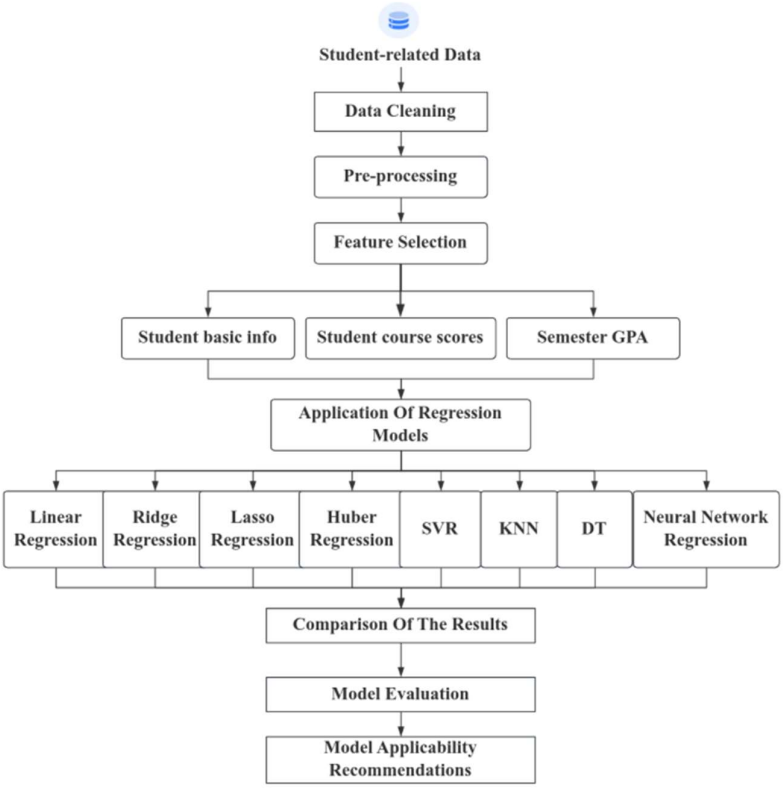

Figure 1. Predictive Comparison Flow Chart

3.3 Data description

The eight prediction algorithms were implemented for comparative analysis, and 21 courses in four grades of Computer Science and Technology under the School of Information Engineering of a university, namely 2017, 2018, 2019, and 2020, were used as experimental data. In this paper, for each student, thirty-four (34) data points were collected, including the final CGPA at graduation (Y), the values of thirty-three predictor variables (from X1 to X33), and a total of 628 students, 628 × 34 = 21,352 data points were collected. The collected data (Y, X1, X2, X3, ……, X33) were initially in different scales of measurements: X1 – X4 were encoded in different numbers, X5 – X25 varied from 0.00 to 100.00, X26 – X33 varied from 0.00 to 5.00, and Y varied from 0.00 to 5.00. The student-related attributes are given in Table 1. Before using them to establish a prediction model, the collected raw data must be pre-processed, as described in the following paragraphs.

Table 1 Student-related attributes

Attributes	Description	Value
Student ID	The ID for a student	TEXT
Sex	The Sex of the student	1 F, 2 M
Entry year	The year the student enrolled	2017-2021
Birth place	The place where the student birth	Encoded from 1-21
Dormitory type	The university dormitory types	1,2,3,4,6
Course scores	The grade obtained by the student	0-100
Semester GPA	The student's GPA at the end of each semester	0-5
Final CGPA	The student's CGPA at semester eight(graduation) or for all the semesters passed	0-5

3.4 Data cleaning and pre-processing

Since the extracted data from the academic affairs database could not be directly applied to the prediction model, it was necessary to clean and transform the data to meet the requirements of the prediction model. The following operations were performed on the original data:

(1) Data cleaning:

a) Most student performance data with zero course grades were deleted, as these data points had limited validity and could introduce noise.

b) Selecting only courses taken consistently across all years and having consistent assessment evaluations.

c) Normalizing the performance data. The grades for each course in each data set were normalized to the range [0,1], as shown in Table 2. This normalization helped alleviate the effects of inconsistent grade distributions across courses.

(2) Missing value processing: The data set was analyzed descriptively to identify missing values. Missing data in the student's course grades could be attributed to factors such as students taking breaks from school or changing majors. However, the proportion of missing grades was very small, so the samples with missing grades were removed.

(3) Establishing a training sample: 80% of the data was allocated for training, while the remaining 20% was reserved as a test sample.

Table 2 Normalization table

Attributes	Description	Value
X1 - X4	The basic information for a student	0.00 - 1.00
X5 - X25	Course scores for a student	0.00 - 1.00
X26 - X33, Y	X26 - X33 is the Semester GPA, Y is the final CGPA	0.00 - 1.00

3.5 Model evaluation

To validate the prediction models, 10-fold cross-validation was employed. The student-related data set was randomly divided into 10 subsets, with eight subsets used for training and the remaining two for testing. This process was repeated 10 times, and the accuracy of the models was computed based on the results.

The study focused on predicting the target variable, the overall final CGPA, which is a numeric variable ranging from 0.00 to 5.00.

Consistent with most literature, this paper utilized root mean square error (RMSE) and mean absolute error (MAE) as evaluation metrics. RMSE quantifies the deviation between predicted and true values, offering insights into the overall prediction accuracy. On the other hand, MAE reflects the actual magnitude of prediction errors. The formulas for both metrics are as follows:

$$RMSE = \sqrt{\frac{1}{m}\sum_{i=1}^{m}(y_i - \hat{y}_i)^2} \quad (1)$$

$$MAE = \frac{1}{m}\sum_{i=1}^{m}|y_i - \hat{y}_i| \quad (2)$$

where m is the sample size, Y_i is the true value, and $\hat{Y}_i$ is the predicted value.

3.6 Feature Selection

To conduct the experiments, a feature subset selection process was performed. Feature selection involves identifying and removing irrelevant features from the data set, specifically those that do not contribute significantly to the task at hand. This process is essential as it helps reduce the dimensionality of the data, thereby improving the efficiency of the learning algorithm, reducing execution time, and enhancing predictive accuracy.

To better understand the variables, we analyzed the correlation of all variables as the basis for feature selection in corresponding scenarios. As shown in Figure 2, X1-X4 shows a low correlation with the results, while X7, X8, X11-X13, X15-X17, X19-X22 show a high correlation with the CGPA(Y), all of which are core professional courses.

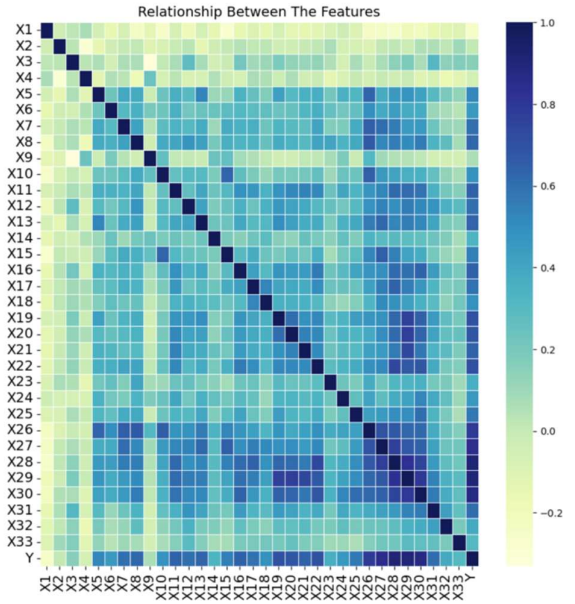

Figure 2. Relationship Between the Features

For our experiment, we considered three different combinations of predictors, all aiming to predict the final CGPA of students:

First Scenario: We utilized the students' university course scores from the first 2 years, encompassing the scores of 14 courses, as input features for predicting the final CGPA.

Second Scenario: We expanded the feature set to include the students' university course scores from the first 3 years, incorporating the scores of 21 courses to predict the final CGPA.

Third Scenario: Instead of relying on course scores, we utilized the students' Semester GPA at the end of each semester from the first 3 years of courses as input features for predicting the final CGPA.

By exploring these different scenarios, our objective was to analyze how different input features influence the accuracy of predicting the final CGPA. Through feature selection, we sought to identify the most relevant and informative predictors that would yield the best predictive performance.

4. RESULTS

4.1 Experiment of the First Scenario

In this experiment, we evaluated the performance of various regression methods, namely Linear Regression, Ridge Regression, Lasso Regression, Huber Regression, SVR, KNN, DT, and Neural Network Regression. These methods were tested specifically for the first scenario described in section 3.6.

Table 3 Prediction result for the First Scenario

Methods	R (Correlation coefficient)	RMSE	MAE
Linear Regression	0.8769	0.4162	0.1353
Ridge Regression	0.8774	0.4158	0.1352
Lasso Regression	**0.8777**	**0.1726**	**0.1351**
Huber Regression	0.6762	0.2809	0.2089
SVR	0.8034	0.2188	0.1579
KNN	0.8230	0.2076	0.1503
DT	0.5753	0.3217	0.2390
Neural Network	**0.8752**	**0.1743**	**0.1374**

As the results indicate in Table 3, The first three linear regression algorithms showed high correlation coefficients (R), indicating a strong linear relationship between input features and the target variable. These models demonstrated strong predictive capability, with R values ranging from 0.8769 to 0.8777. They also achieve MAE values ranging from 0.1351 to 0.1353, indicating their ability to provide predictions closer, on average, to the true CGPA values. Lasso Regression and Neural Network Regression achieved the lowest mean squared error (RMSE), indicating better overall predictive accuracy and reduced squared differences between predicted and actual CGPA values. Huber Regression and Decision Tree Regression demonstrated relatively lower performance in terms of correlation coefficient and predictive accuracy metrics, suggesting they may not effectively capture the underlying relationships between input features and the final CGPA.

In addition to quantitative metrics, the prediction results were qualitatively evaluated by plotting both the predicted and target values, as shown in Figure 3.

Figure 3 shows that the SVR and KNN models have considerable deviation between the predicted and target values at lower and higher CGPA ranges. The overlap between the predicted and target values is most pronounced for Lasso Regression and Neural Network Regression, indicating their superior performance.

Overall, Lasso Regression and Neural Network Regression are promising models for predicting final CGPA using the students' university course scores from the first 2 years.

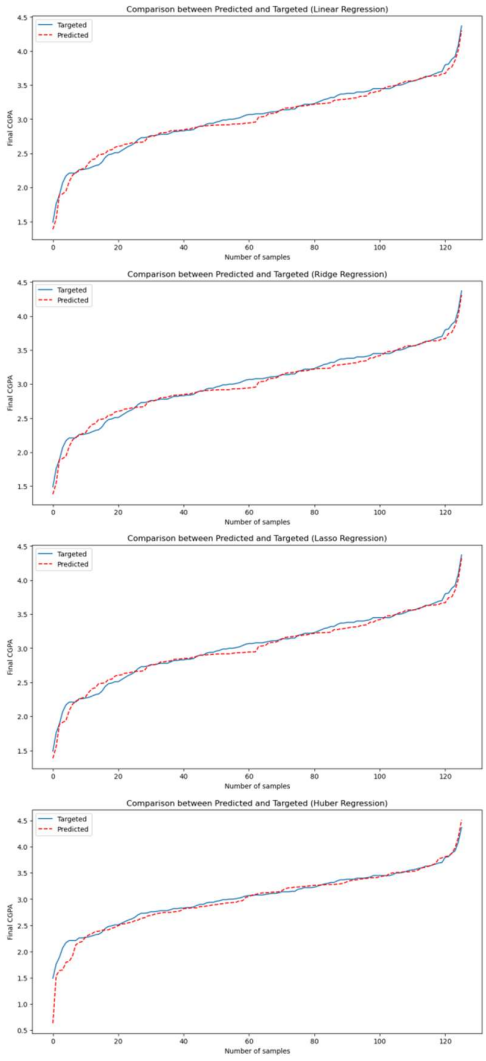

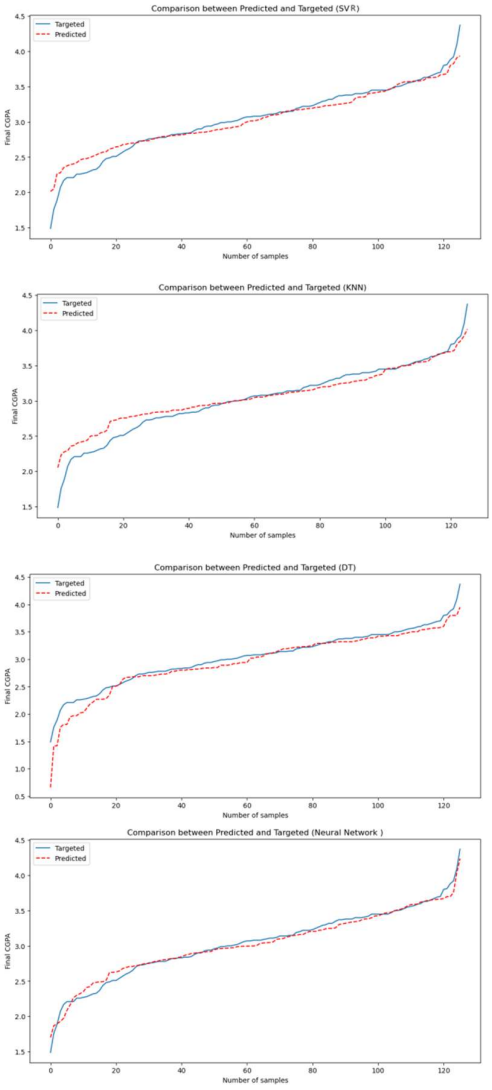

Figure 3: Prediction result of the eight methods for the First Scenario

4.2 Experiment of the Second Scenario

The experiments were repeated for the second scenario. Table 4 presents the results of the three prediction methods for this scenario.

Table 4 Prediction result for the Second Scenario

Methods	R (Correlation coefficient)	RMSE	MAE
Linear Regression	0.9436	0.3279	0.0855
Ridge Regression	0.9436	0.3279	0.0854
Lasso Regression	**0.9442**	**0.1070**	**0.0849**
Huber Regression	**0.9396**	**0.1114**	**0.0882**
SVR	0.8002	0.2025	0.1263
KNN	0.8373	0.1827	0.1374
DT	0.5247	0.3123	0.2497
Neural Network	**0.9248**	**0.1243**	**0.0986**

The prediction results for the second scenario are summarized in Table 4. Among the evaluated regression methods, Lasso Regression attained the highest correlation coefficient (R) of 0.9442, denoting a robust linear relationship between the input features and the target variable. Furthermore, it showcased the lowest RMSE value of 0.1070 and the lowest MAE value of 0.0849, suggesting superior predictive accuracy with minimal squared differences and closer predictions to the true values. Ridge Regression performed similarly to Lasso Regression, with a correlation coefficient (R) of 0.9436 and slightly higher RMSE and MAE values. Huber Regression also showed good performance with a correlation coefficient (R) of 0.9396 and relatively low RMSE and MAE values. On the other hand, SVR, KNN, and DT exhibited lower correlation coefficients and higher RMSE and MAE values, indicating less accurate predictions. Neural Network Regression achieved a correlation coefficient (R) of 0.9248, demonstrating a strong linear relationship, and showcased competitive performance with low RMSE and MAE values. Overall, Lasso Regression, Ridge Regression, and Neural Network Regression emerged as the top-performing methods for the second scenario, providing accurate predictions and capturing the underlying relationships between the input features and the target variable.

The prediction results evaluated by plotting both the predicted and target values also show that the three models have the best performance, as depicted in Figure 4.

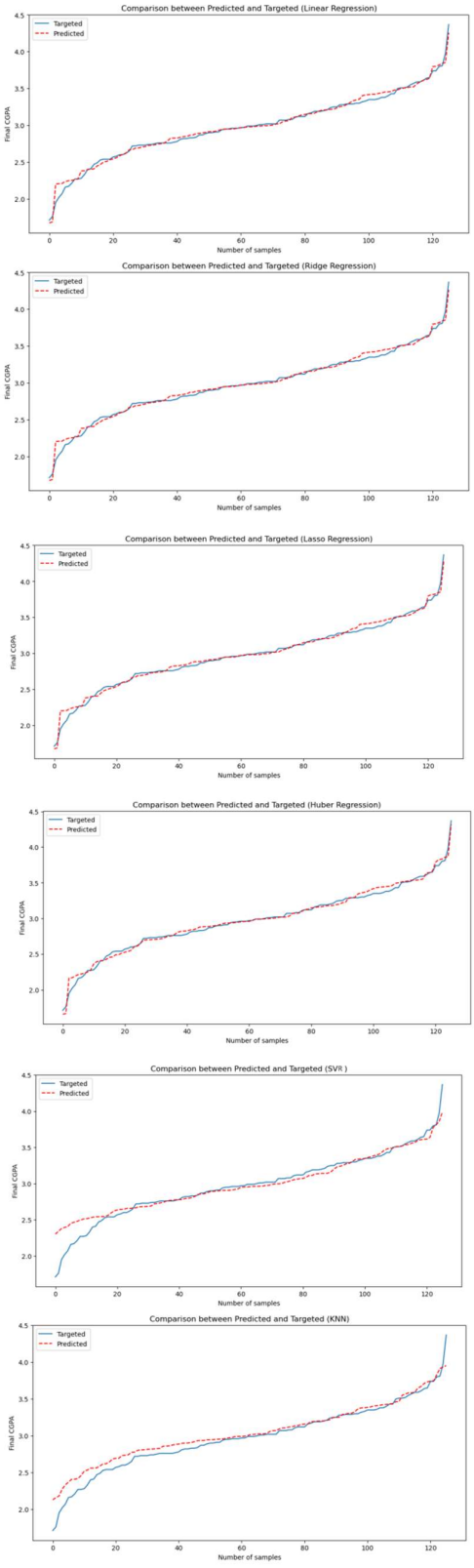

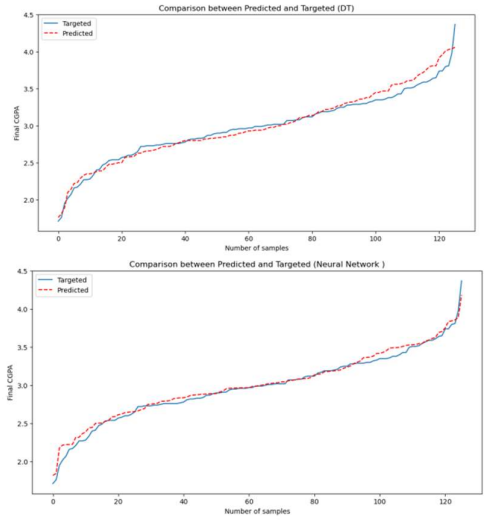

Figure 4: Prediction result of the eight methods for the Second Scenario

4.3 Experiment of the Third Scenario

The prediction results for the third scenario are summarized in Table 5.

Table 5 Prediction results for the Third Scenario

Methods	R (Correlation coefficient)	RMSE	MAE
Linear Regression	0.9905	0.2311	0.0413
Ridge Regression	0.9900	0.2341	0.0423
Lasso Regression	**0.9901**	**0.0546**	**0.0428**
Huber Regression	**0.9899**	**0.0550**	**0.0438**
SVR	**0.9882**	**0.0595**	**0.0459**
KNN	0.8549	0.2085	0.1462
DT	0.9076	0.1665	0.1262
Neural Network	**0.9832**	**0.0710**	**0.0555**

In the third scenario, the shift to Semester GPA as the predictive feature marked a significant advancement in modeling accuracy, as evidenced by the strikingly higher R values across all models. This transition from individual course scores to a cumulative measure of academic performance over three semesters encapsulates a more integrated view of student learning. The Lasso Regression and Huber Regression models, in particular, excelled with R values of 0.9901 and 0.9899, respectively, indicating an exceptionally strong linear relationship between the Semester GPA and the final CGPA. Moreover, these models' RMSE and MAE values were notably lower, suggesting a more precise prediction of student outcomes. The superior performance in the third scenario, as depicted in Figure 5, underscores the predictive power of aggregated academic metrics and the

effectiveness of regularization techniques in regression analysis.

When synthesized, the comparative analysis of the three scenarios reveals a clear trend: the predictive models' accuracy escalates with the use of more comprehensive and aggregated academic data. The third scenario, focusing on Semester GPA, provides a more stable and generalized prediction and aligns with the educational systems' objective to assess students' overall performance rather than isolated course achievements. The consistent dominance of Lasso Regression, as observed in Figure 5, reinforces its utility in educational data mining, where the ability to handle complex datasets and multicollinearity is paramount. Additionally, Neural Network Regression has consistently performed consistently throughout all scenarios, suggesting its capacity to model complex, nonlinear relationships effectively. These insights are invaluable for institutions seeking to optimize their predictive models, suggesting that the strategic employment of aggregated GPA data can substantially enhance the forecasting of student success.

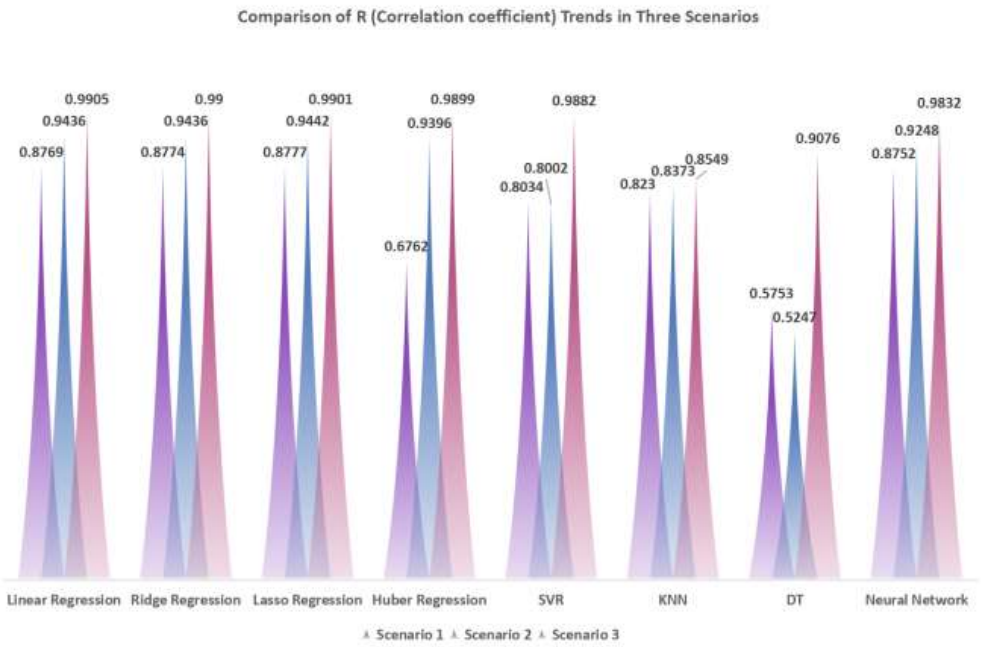

Figure 5: Comparison of Results Trends in Three Scenarios

4.4 Experimental Analysis

The experimental outcomes across three scenarios underscore the pivotal role of data quantity and type in enhancing predictive model accuracy. Initially, employing 14-course scores from the first two academic years, Lasso Regression distinguished itself with a high correlation coefficient and minimized error metrics, showcasing its adeptness at discerning patterns within a moderate feature set. This trend intensified in the subsequent scenario, expanding to 21-course scores across three years. Lasso Regression's performance peaked with an even higher correlation coefficient and significantly reduced RMSE and MAE, underscoring the value of comprehensive data in refining predictive accuracy.

The transition to utilizing Semester GPA as an aggregated performance metric in the culminating scenario engendered a significant leap in the predictive efficacy of the models, particularly Lasso Regression and Huber Regression, which showcased exceptional correlation values and minimized error metrics. This advancement illustrates a heightened sensitivity and precision when models are based on comprehensive academic data. The incremental refinement from discrete course scores to consolidated GPA metrics has enhanced the models' predictive capabilities. The consistent outperformance of Lasso Regression is attributed to its advanced feature selection and regularization techniques, which together advocate for the strategic use of aggregated and representative data in academic forecasting. These findings underscore educational institutions' need to adopt data-driven methodologies, providing a robust framework for evidence-based decision-making and strategic planning to augment student success.

4.5 Model Applicability Suggestions

Based on the findings from the experiments, certain regression models demonstrate better applicability for specific scenarios. Lasso Regression consistently performs well across all three scenarios, indicating its robustness and effectiveness in capturing the underlying relationships between input features and the target variable. Neural Network Regression is a competitive model, showing strong linear relationships and relatively accurate predictions. These two models, Lasso Regression and Neural Network Regression, can be recommended for various applications where accurate prediction and capturing complex interactions are crucial. However, it's crucial to consider each scenario's unique requirements and choose the regression method accordingly. This is because different models may exhibit varying performance levels based on the characteristics of the data and the relationships between the variables.

5. CONCLUSION AND DISCUSSION

5.1 Conclusion

The experimental analysis underscores the efficacy of Lasso Regression and Neural Network Regression in predicting student grades across varying scenarios, emphasizing their ability to capture complex relationships with high accuracy. Lasso Regression, in particular, has proven to be a robust model, consistently outperforming others with its high correlation coefficients and minimized RMSE values. The progression from the First to the Third Scenario illustrates the substantial impact of data quality and aggregation on predictive accuracy, with the use of Semester GPA in the Third Scenario yielding the most significant improvements. These findings underscore the importance of model selection tailored to specific scenarios and highlight Lasso Regression as a top performer, particularly suitable for applications requiring precise predictions and handling complex interactions. As we advance, further exploration into additional regression techniques and hybrid models could potentially enhance predictive accuracy and broaden the scope of regression analysis in diverse fields.

In conclusion, our comprehensive evaluation has demonstrated that the depth and quality of academic data significantly enhance the predictive accuracy of students' final CGPA. Lasso Regression has emerged as a consistently superior model, with its predictive power notably increasing as the data set expanded from 14-course scores to a more holistic measure of Semester GPA. The results highlight the profound impact of representative and aggregated data features on model efficacy, advocating for the strategic use of such data in educational modeling and decision-making processes.

5.2 Discussion

Our study contributes to the body of research on applying regression models in predicting student academic performance. Through a comparative analysis of eight regression models, we have identified Lasso Regression and Neural Network Regression as particularly effective in predicting final CGPA, especially when using Semester GPAs as input data. Our findings resonate with those of Lyu (2023), who found Random Forest to be the best model for predicting student grades based on past scores, highlighting the potential of machine-learning techniques in educational data mining.

Moreover, our results align with the study by Kumar et al. (2020), which applied regression analysis to accurately predict student performance, underscoring the importance of past academic records as a strong predictor of future performance. The high R values and low error metrics observed in our study are consistent with the effectiveness of regression models in capturing the nuances of student performance, as demonstrated in the work of Lyu (2023) and Kumar et al. (2020).

Our study extends the existing literature by examining the impact of data granularity and integrity on the precision of CGPA predictions. The dominance of Lasso Regression in our third scenario, with an R-value of 0.9901 and minimal error metrics, is particularly noteworthy. This aligns with the findings of Rusli and Ibrahim (2007), who reported high accuracy in predicting academic performance using artificial neural networks, suggesting that advanced regression techniques can outperform traditional methods.

Furthermore, our comparative study adds depth to the work of Arsad et al. (2014), who compared neural networks and linear regression for predicting academic achievement by providing a more comprehensive analysis of various regression models. Our results indicate that while Neural Network Regression showed robust predictive capabilities, Lasso Regression was superior in prediction accuracy.

In conclusion, our study emphasizes the importance of selecting the appropriate regression model tailored to the specific characteristics of the data and the predictive precision required. The high predictive accuracy of Lasso Regression and Neural Network Regression in our study, along with the support from the literature, validates the effectiveness of these models in predicting student academic performance. Future research should continue to explore the integration of various regression models and their potential for enhancing student performance prediction in educational settings.

6. ACKNOWLEDGMENT

Data from the School of Information and Engineering, Wenzhou Business College, supported this work. The authors thank Wenzhou Business College and Muban Chom Bueng Rajabhat University for their support.

7. REFERENCES

Albalooshi, F., Alobaidy, H., & Ghanim, A. (2019). Mining students outcomes: An empirical study. International Journal of Computing and Digital Systems, 8(3), 229–241. https://doi.org/10.12785/ ijcds/080303

Arsad, P. M., & Buniyamin, N. (2014, April). Neural Network and Linear Regression methods for prediction of students' academic achievement. In 2014 IEEE Global Engineering Education Conference (EDUCON) (pp. 916-921). IEEE. https://doi.org/10.1109/EDUCON.2014.6826206

Bravo, L. E. C., Molano, J. I. R., & Trujillo, E. R. (2020). Exploration of a system to determine the academic performance of engineering students through machine learning. International Journal of Advanced Science and Technology, 29(7), 11894–11905. http://sersc.org/journals/index.php/IJAST/article/view/27865

Bujang, S. D. A., Selamat, A., Ibrahim, R., Krejcar, O., Herrera-Viedma, E., Fujita, H., & Ghani, N. A. M. (2021). Multiclass prediction model for student grade prediction using machine learning. Ieee Access: Practical Innovations, Open Solutions, 9, 95608–95621. https://doi.org/10.1109/ACCESS.2021.3093563

Bydžovská, H. (2016). A Comparative Analysis of Techniques for Predicting Student Performance. International Educational Data Mining Society. https://doi.org/10.1109/FIE.2007.4417993

Cavazos, R., & Garza, S. E. (2017). Learning models for student performance prediction. Paper presented at the Mexican International Conference on Artifcial Intelligence. https://doi.org/10.1007/978-3-030-02840-4_14

Cutad, R. E. E., & Gerardo, B. D. (2019). A prediction-based curriculum analysis using the modifed artifcial Bee Colony Algorithm. International Journal of Advanced Computer Science and Applications, 10(10), 117–123. https://doi.org/10.14569/ijacsa.2019.0101017

El Aouifi, H., El Hajji, M., Es-Saady, Y., & Douzi, H. (2021). Predicting learner's performance through video sequences viewing behavior analysis using educational data-mining. Education and Information Technologies, 26(5), 5799-5814. https://doi.org/10.1007/s10639-021-10512-4

Hsu Wang, F. (2019). On prediction of online behaviors and achievement using self-regulated learning awareness in fipped classrooms. International Journal of Information and Education Technology, 9(12), 874–879. https://doi.org/10.18178/ijiet.2019.9.12.1320

Hussain, S., & Khan, M. Q. (2021). Student-performulator: Predicting students' academic performance at secondary and intermediate level using machine learning. Annals of Data Science. https://doi.org/10.1007/s40745-021-00341-0

Ibrahim, Z., & Rusli, D. (2007, September). Predicting students' academic performance: comparing artificial neural network, decision tree and linear regression. In 21st Annual SAS Malaysia Forum, 5th September. https://www.researchgate.net/publication/228894873

Iyanda, A. R., Ninan, O. D., Ajayi, A. O., & Anyabolu, O. G. (2018). Predicting student academic performance in computer science courses: A comparison of neural network models. International Journal of Modern Education & Computer Science, 10(6). https://dx.doi.org/10.5815/ijmecs.2018.06.01

Lyu, S. (2023, November). Student's Academic Performance Prediction Based on Machine Learning Regression Models. In 2023 International Conference on Image, Algorithms and Artificial Intelligence (ICIAAI 2023) (pp. 293-299). Atlantis Press. https://doi.org/10.2991/978-94-6463-300-9_29

Kumar, A., Eldhose, K. K., Sridharan, R., & Panicker, V. V. (2020, July). Students' Academic Performance Prediction using Regression: A Case Study. In 2020 International Conference on System, Computation, Automation and Networking (ICSCAN) (pp. 1-6). IEEE. https://doi.org/10.1109/ICSCAN49426.2020.9262346

Kumar, A., Selvam, R., & Kumar, K. (2018). Review on prediction algorithms in educational data mining. International Journal of Pure and Applied Mathematics, 118, 531–536. https://www.acadpubl.eu/jsi/2018-118-7-9/articles/8/77.pdf

Ma, Y., Liu, B., Wong, C. K., Yu, P. S., & Lee, S. M. (2000, August). Targeting the right students using data mining. In Proceedings of the sixth ACM SIGKDD international conference on Knowledge discovery and data mining (pp. 457-464). http://scholarbank.nus.edu.sg/handle/10635/39963

Mai, T. T., Bezbradica, M., & Crane, M. (2022). Learning behaviours data in programming education: Community analysis and outcome prediction with cleaned data. Future Generation Computer Systems, 127, 42–55. https://doi.org/10.1016/j.future.2021.08.026

Makombe, F., & Lall, M. (2020). A predictive model for the determination of academic performance in private

higher education institutions. International Journal of Advanced Computer Science and Applications (IJACSA), 11(9). http://dx.doi.org/10.14569/IJACSA.2020.0110949

Mengash, H. A. (2020). Using data mining techniques to predict student performance to support decision making in university admission systems. IEEE Access, 8, 55462–55470. https://doi.org/10.1109/ACCESS.2020.2981905

Mutanu, L., & Machoka, P. (2019). Enhancing computer students' academic performance through predictive modelling-a proactive approach. In Paper presented at the 2019 14th international conference on Computer Science & Education (ICCSE). https://doi.org/10.1109/ICCSE.2019.8845452

Omer, U., Farooq, M. S., & Abid, A. (2020). Cognitive learning analytics using assessment data and concept map: A framework-based approach for sustainability of programming courses. Sustainability (Switzerland), 12(17). https://doi.org/10.3390/su12176990

Sa'ad, M. I., & Mustafa, M. S. (2020, October). Student Prediction of Drop Out Using Extreme Learning Machine (ELM) Algorithm. In 2020 2nd International Conference on Cybernetics and Intelligent System (ICORIS) (pp. 1–6). IEEE. https://doi.org/10.1109/ICORIS50180.2020.9320831

Tomasevic, N., Gvozdenovic, N., & Vranes, S. (2020). An overview and comparison of supervised data mining techniques for student exam performance prediction. Computers & Education, 143, 103676. https://doi.org/10.1016/j.compedu.2019.103676

Tuononen, T., & Parpala, A. (2021). The role of academic competences and learning processes in predicting Bachelor's and Master's thesis grades. Studies in Educational Evaluation, 70. https://doi.org/10.1016/j.stueduc.2021.101001

Vijayalakshmi, V., & Venkatachalapathy, K. (2019). Comparison of predicting student's performance using machine learning algorithms. International Journal of Intelligent Systems and Applications, 11(12), 34. https://doi.org/10.5815/ijisa.2019.12.04

Waheed, H., Hassan, S.-U., Aljohani, N. R., Hardman, J., Alelyani, S., & Nawaz, R. (2020). Predicting academic performance of students from VLE big data using deep learning models. Computers in Human Behavior, 104, 106189. https://doi.org/10.1016/j.chb.2019.106189

Xiushan NIE, Yuling MA, Huiyan QIAO, Jie GUO, Chaoran CUI, Zhiyun YU, Xingbo LIU, & Yilong YIN. (2022). Surver on student academic performance prediction from the perspective of task granularity. Journal of Shandong University (Engineering Science), 52(2): 1-14. https://doi.org/10.6040/j.issn.1672-3961.0.2021.489

Yang, S. J. H., Lu, O. H. T., Huang, A. Y. Q., Huang, J. C. H., Ogata, H., & Lin, A. J. Q. (2018). Predicting students' academic performance using multiple linear regression and principal component analysis. Journal of Information Processing, 26, 170–176. https://doi.org/10.2197/ipsjjip.26.170

7. BIOGRAPHIES (OPTIONAL)

Miss Wenting Sui (Ph.D. Student)

Department of Industrial Technology Management, Faculty of Industrial Technology, Muban Chom Bueng Rajabhat University, Ratchaburi, Thailand

Dr.Adisak Sangsongfar

Department of Industrial Technology Management, Faculty of Industrial Technology, Muban Chom Bueng Rajabhat University, Ratchaburi, Thailand

Assistance Professor Dr.Noppadol Amdee

Department of Industrial Technology Management, Faculty of Industrial Technology, Muban Chom Bueng Rajabhat University, Ratchaburi, Thailand

NUEJ
Naresuan University
Engineering Journal

Effect of Weave Pattern on Experimental and Simulated Ballistic Behavior of Carbon Fiber Reinforced Polybenzoxazine Composites.

Kangsadan Inthakun*

Department of Chemical Science and Technology, Chulachomklao Royal Military Academy, Nakhon Nayok, Thailand

*Corresponding author e-mail: Kangsadan.in@crma.ac.th

(Received: 18 April 2024, Revised: 19 June 2024, Accepted: 4 July 2024)

Abstract

This research investigates the effect of weave patterns on the experimental and simulated ballistic performance of carbon fabric reinforced polybenzoxazine (CFR-poly(BA-a)) composites. The present study focuses on developing the materials using a strike panel impacted by a rigid 7.62×51 mm projectile at an impact velocity of 847±9.1. This study compares the ballistic performance of three different weave patterns of CFR-poly(BA-a) composite against the penetration of a 7.62×51 mm projectile by using an energy absorption equation that includes fiber/matrix cohesive failures to predict the appropriate thickness of the composite to protect against penetration. The damage area of the specimen composites is also studied using numerical simulation by using parameters of material properties composite under impact event using 7.62×51 mm projectiles and was performed on 4, 8, and 12 plies of CFR-poly(BA-a) composite. Laminates of three different carbon fabric weave patterns were fabricated using plain, 2x2 twill and unidirectional weaves. The ballistic performance of the composites was investigated by using CFR-poly(BA-a) composite as a strike panel dimensions 150 x 150 mm. The damage area of the specimen composites observed from the experiment results are in good agreement with the numerical simulation model, the error in the prediction of the damage pattern of the specimen composite was less than 3%. The numerical simulation model effectively anticipates the qualitative extent of damage for the composite specimen. The ballistic performance of the composite panel reinforced with a twill weave pattern of carbon fiber observed from the experiment result was superior to that of other weave patterns of carbon fiber due to the 2D woven structure being able to transmit load simultaneously in longitudinal and transverse weave directions. Therefore, it resisted stiffness, stress, and stress distribution. In addition, the twill weave pattern had low contact friction, crimp, and binding effect because of its minimum intersection point compared with plain weave and unidirectional fabrics, therefore relatively high mechanical properties, high energy absorption, and better protection against penetration of the impact velocity of the projectile on the ballistic performance, while also being thinner and lighter when compared with other weaves. These properties make it a more effective material for use in ballistic applications. The numerical simulation and experimental results of the ballistic performance reveal that the hardness of the three weave patterns of CFR-poly(BA-a) composites were able to effectively protect against a single projectile shot without penetration on the rear side of the strike panel, the penetration depth, and damage extent of the perforation were in good agreement with the numerical simulation model. These results suggest the composite could be developed and applied as a strike panel in hard ballistic armor. The findings demonstrate a correlation between numerical simulation outcomes from ballistic impact tests and experimental results, effectively predicting the behavior of CFR-poly(BA-a) composites with relatively low error and good correlation with the experimental data. This predictive capability allows for safe, rapid, and cost-effective design validation and testing by leveraging virtual ballistic impact test models of real-world assets for a person interested in studying them in the future.

Keywords: Composites, Carbon fibers, Woven fabric reinforced polymer (WFRP), Finite element analysis (FEA), Energy absorption.

1. INTRODUCTION

Military confrontations and wars have been a constant throughout world history. As attacking weapons have become more advanced, so too has the level of personal and property protection needed on the battlefield and in riot situations. Different materials have been used as body shields throughout history, from wooden shields to metal shields. Today, ballistic protective materials are primarily used for personnel protection (Al-Haik et al., 2016). These materials are typically lightweight and flexible, making them easy to wear and move in. Ballistic shields are designed as multilayer composite materials that typically consist of hard layers, such as ceramics or steel plates, and soft input materials. When a projectile strikes a hard plate, it can become deformed and cause the fragmentation of the fragile armor, posing a risk to the

user. The function of the soft input layer is to capture and absorb the remaining energy of blunt projectiles and projectile fragments that have damaged the first shielding layer (Pach et al., 2017). In terms of materials used in ballistic armor, steel plates have traditionally been widely used in armor applications in the past. The weight limitation and lack of flexibility of ceramic and steel plates make them less than ideal for use in certain applications, such as body armor (Yashas Gowda et al., 2018; Sherif et al., 2019; Chukov et al., 2019; Linul et al., 2019). Composite materials offer several advantages over traditional materials, such as ceramic and steel, for body armor applications. Composite materials can be designed to be lightweight, have excellent mechanical properties, high thermal properties, outstanding specific modulus, and specific strength (Buehler and Seferi, 2000; Ishida and Chaisuwan, 2003; Li et al., 2013; Delmonte, 1981; Shalin, 1995; Shen and Ishida, 1996). This makes composite materials a good choice for body armor that is both protective and comfortable to wear.

Composite materials are an amalgamation of at least two constituents. Fiber-reinforced polymers (FRPs) are composed of two phases, matrix phase and particle or fiber phase. Fiber textiles are found to be among the most efficient reinforcements for FRPs. Currently, developed fiber-reinforced polymers (FRPs) focus on the relationship between the weave structure property of fibers, different polymer matrices used to develop composites, their mechanical performances, and different composite fabrication techniques (Rajak, 2019). FRP composites are widely used in ballistic protections such as helmets and ballistic armor (Al-Haik et al., 2016; Rebouillat, 2016; Okhawilai and Rimdusit, 2017) due to their excellent mechanical properties including high strength high modulus, and especially extra energy absorption.

Carbon fiber-reinforced polymers (CFRPs) are a class of extremely strong and lightweight fiber reinforced polymers based on carbon/graphite fibers (Che et al., 2014). CFRPs offer a very high strength-to-weight ratio, high modulus-to-weight ratio (specific modulus), high damping capacity, good dimensional stability, excellent damage tolerance, and good corrosion and fatigue resistances, which makes them widely used in aerospace, robotics (Wang et al., 2003), construction, transportation, sporting goods, medical, and military applications (Dandekar et al., 2012).

The knitting pattern can affect the mechanical properties of a textile, which in turn affects the composite mechanical properties (Ratna et al., 2004; Hallal et al.,2012; Colorado et al., 2006). By carefully selecting the knitting pattern, it is possible to design FRPs with the desired mechanical properties. Woven fabric-reinforced polymer (WFRP) composites have excellent mechanical strengths, i.e., rigidity, strength, and dimensional stability compared to unidirectional fiber composites. WFRPs are particularly attractive for lightweight structures because of their high strength-to-weight ratios, directional tolerability, and strength dependencies on strain rates. These highly engineered materials are increasingly sought after for use in structures and protective devices required to operate and survive against severe dynamic loading events such as blast, ballistic and fragment impacts, and mechanical shock. Textile engineering concepts can be used to improve the mechanical properties of hybrid woven composites. This can be achieved by selecting the appropriate yarn size, as the correct choice of yarn size can provide the optimal force value and strength to resist the deformation of the woven fabric and ensure the good mechanical properties of the composites (Wahab, 2014).

The following are some research areas related to the use of textile engineering concepts to enhance the mechanical properties of hybrid woven composites Cavallaro (2016) investigated the effects of weave styles and crimp gradients (CGs) on the damage tolerance levels and energy absorption capacities of woven fabric reinforced polymer (WFRP) composites. A comparative study was conducted to determine the specific failure mechanisms including fiber/matrix cohesive failures, matrix cracking, fiber breakage, and fiber buckling resulting from static and dynamic loading events. The tests included flexure, short beam shear, drop impact, flexure-after-impact, ballistic impact, and split Hopkinson compression bar (SHCB) and were performed on 20-ply Kevlar/epoxy WFRP laminates. Laminates of three different Kevlar fabric weave styles were fabricated using plain, 2×2 twill, and 4H satin weaves. A fourth laminate was constructed having a mixture of weave styles forming a hybrid crimp gradient construction. The experimental results demonstrated that weave style selection and CGs can positively influence the spatial and temporal distributions of stress resulting from severe loading events and (that the fiber/ matrix cohesive zone stresses that often lead to delamination can be reduced. Accordingly, the dependence of mechanical performance on weave styles, crimp contents, and CGs can be exploited to increase the damage tolerance levels and energy absorption capacities in WFRP composites.

Ullah and Harland (2014) performed dynamic flexure testing of 4-ply woven-glass and woven-carbon laminates using a pendulum fixture. Both laminates were constructed of twill (2×2) fabric architectures and thermoplastic polyurethane (TPU) matrices. Computer tomography (CT) scans were used to examine the damage zones, which revealed that the damage mechanisms consisted of matrix cracking, delamination, yarn debonding, and fiber breakage. Numerical The Finite Element Method (FEM) was performed using cohesive zone elements, quadratic stress criterion for damage initiation, and the Benzeggagh-Kenane criterion for damage evolution. The carbon-fiber-reinforced polymer (CFRP) laminates exhibited lower fracture toughness and higher impact strengths than the glass-fiber-reinforced polymer (GFRP) laminates. The FEM results correlated

to the test results and captured the sequence of failure modes.

Research by Cavallaro and Sadegh (2010) was performed on single-ply woven fabrics subjected to ballistic impact using ABAQUS/Explicit analysis. Their numerical modeling results demonstrated that, compared to crimp-balanced woven fabrics, crimp-imbalanced woven fabrics can achieve greater dynamic energy absorption capacities for normal and oblique impacts. They further showed that crimp imbalance can minimize stress-wave reflections at the crossover region and can positively alter the spatial and temporal behaviors of stress wave propagations within the fabrics.

Another important factor influencing FRP composites' ballistic performance is the polymer matrix type because it is the binder that combines all of the reinforcement. Polybenzoxazines are a novel class of phenolic resin that undergoes polymerization via the ring-opening reaction of cyclic benzoxazine resins under thermal conditions. This process obviates the requirement for a catalyst or curing agent and does not generate any by-products during thermal polymerization (Chung, 2017; Ratna et al., 2004; Hallal et al.,2012; Haim, 2017). Polybenzoxazines exhibit superior characteristics upon polymerization including dimensional stability, near-zero volumetric shrinkage, and low water absorption (Cavallaro et al., 2006). The polymerization reaction of benzoxazine resins also generates phenolic moieties which are highly useful functional groups that facilitate further interaction with other fibers or fillers and enable further modification with other chemicals, resins, or polymers in the network formation of polybenzoxazine (Dipen, 2019; Wahab, 2014). This versatility allows for the tailoring of properties to meet the requirements of numerous applications, including ballistic protection. Gopinath et al., (2012) suggested that the interaction between the polymer matrix and reinforcement was one of the most important factors affecting impact response. They found that the deformation area was decreased with the presence of the appropriated interactions between the stiff matrix and yarns because their excessive interaction and embedded yarns would restrict the movement of yarns, thereby reducing energy absorption and the ballistic performance of the composites.

Okhawilai et al., (2018) investigated the impact performance of the strike panel composite based on glass fiber reinforced polybenzoxazine composites. Experimental panels were manufactured from E-glass and S-glass fiber reinforced polybenzoxazine backed by aramid fiber reinforced composites and subjected to 7.62 × 51 mm rifle projectile at a high velocity of 847 ± 9.1 m/s. Based on the test results, the specimens were able to protect against perforation by the projectile. Comparing the same number of plies, cone deformation on the last panel of S-glass composite was significantly lower than that of the specimen manufactured using E-glass composite. Less damaged area and depth of penetration on backing panels of S-glass composites were significantly observed when compared to that of E-glass specimens under the ballistic test. The authors that the high tensile modulus of the strike panel could result in superior ballistic impact response in terms of both reduction in back face deformation and depth of penetration on the back side of the backing panel. Moreover, the hardness of the strike panel indicated an ability to destroy the projectile into fragments with no failure on the backing panel. This result also revealed a potential use of S-glass fiber reinforced polybenzoxazine composite as a strike panel for hard ballistic armor. Therefore, the important properties i.e. appropriated interaction between matrix-fiber, hardness, and tensile modulus of the strike panel materials are key parameters for reducing back face deformation and depth of penetration on the back side of the backing panel. The authors that the interaction between the polymer matrix and reinforcement was one of the most important factors affecting the impact response. They found that the deformation area was decreased with the presence of the appropriated interactions between the stiff matrix and yarns because their excessive interaction and embedded yarns would restrict the movement of yarns to dissipate the energy absorption and ballistic performance of the composites decreased.

Furthermore, the important issue encountered in the study of penetration mechanics under ballistic impact is the determination of ballistic limit velocity, which refers to a critical velocity below which a projectile could perforate the armor. Many attempts have studied the effect of impact velocity and residual velocity of the projectile on the ballistic limit velocity for a variety of materials (Chocron et al., 2010; Flores-Johnson et al., 2014; Ansari and Chakrabarti, 2017; Sevkat et al., 2009). Due to the complex ballistic penetration process, numerical simulation is used to predict the ballistic performance and study ballistic behavior.

Ansari and Chakrabarti (2017) have studied the experimental and finite element analyses of perforation behavior of unidirectional glass fiber reinforced cross-ply laminate, by considering different projectile nose shapes, impact velocities, impact angles, and laminate thickness. A three-dimensional finite element model was developed using Lagrangian, eight nodded brick elements in ANSYS/AUTODYN. The properties of GFRP laminate were obtained from tensile tests in a Universal Testing Machine. The ballistic limit and damage pattern in the target plate are presented and compared. They revealed that the obtained results from numerical simulation had a good correlation with the corresponding experimental values.

Sevkat et al., (2009) studied the damage in composite beams subject to ballistic impact using a high-speed gas gun by a combination of experimental and 3D dynamic nonlinear finite element (FE) analysis. LS-DYNA with the Chang–Chang linear-orthotropic damage model was used for comparison. They found good agreement between experimental and FE results from the

comparisons of damage patterns. Moreover, FE simulations were conducted to predict the ballistic limit velocity (V_{50}) using either the number of damaged layer approach similar to the classical Lambert–Jonas equation for metals.

Naik et al., (2000) performed 3-D FEM modeling of thin woven and UD cross-ply E-glass/epoxy laminated plates subjected to low-velocity impact. An in-plane failure function based on the Tsai-Hill criterion was used to assess damage initiation during impact (failures occurred when the failure function achieved a magnitude≥1.0). Their results demonstrated that the in-plane failure function magnitudes were greater along the impact surfaces versus the rear surfaces of the woven laminates suggesting that in-plane failures would initiate near the impact surfaces, and greater along the rear surfaces of the UD cross-ply laminate suggesting that in-plane failures would initiate near the rear surfaces. However, the failure function magnitudes reported for the cross-ply laminates were approximately five times greater than those of the woven laminates. Based upon the in-plane failure criterion alone, the woven laminates achieved a five times greater damage initiation threshold for low-velocity impact than that for the UD cross-ply laminates.

Therefore, in this work, a comparative study of the ballistic performance of three different weave patterns of (CFR-poly(BA-a)) composite against the penetration of a 7.62×51 mm projectile by using an energy absorption equation that includes fiber/matrix cohesive failures to predict the appropriate thickness of the composite to protect against penetration. The damage area of the specimen composites is also studied by comparing the experimental and numerical simulations and predicting the penetration depth and damage extent of the perforation observed in the strike panel by numerical simulation. The focus of the present study is to develop CFR-poly(BA-a) composite for use as strike panels that can be impacted by a rigid 7.62×51 mm projectile at an impact velocity of 847±9.1 m/s. It was investigated using numerical simulation to predict the behavior of composites. The predictive capability allows for safe, rapid, and cost-effective design validation and testing by leveraging virtual ballistic impact test models of real-world assets for a person interested in studying them in the future.

2. MATERIALS AND PREPARATION

2.1 Materials

The composite materials studied in this research were manufactured using benzoxazine resin (BA-a) based on bisphenol-A, formaldehyde, and aniline as the polymer matrix reinforced with textiles made of carbon. The bisphenol-A (polycarbonate grade) was kindly supplied by Thai Polycarbonate Co., Ltd. (Rayong, Thailand). Formaldehyde (AR grade) and aniline (AR grade) were purchased from Merck Co., Ltd. and Panreac Quimica, S.A., respectively. Three weave styles were sourced: plain, twill, and unidirectional carbon fabric weaves with area weight densities of 1.507, 1.507, and 1.526 g/cm^3, respectively. These fabrics were used as reinforcing fabrics and were purchased from BRP Composite Limited Partnership (Thailand). All chemicals and the carbon fiber were used as received.

2.2 Resin preparation

BA-a resin was synthesized from bisphenol A, formaldehyde, and aniline at a molar ratio of 1:4:2 based on solvent-less technology (Ishida, 1996). The mixture solution was continuously stirred at 110°C for approximately 40 min. The obtained resin was in a clear homogenous mixture with a yellowish color and solid at room temperature. The solid resin was ground into fine powder and kept in a refrigerator before copolymer preparation.

2.3 Sample preparation

The samples in this study consist of composite panels, also known as strike panels. The strike panels were prepared from 65%wt of CFR-poly(BA-a) composite (Inthakun, 2023). The plain, twill, and unidirectional weave patterns of carbon fabric with approximate dimensions of 150 mm x 150 mm consisting of 4, 8, and 12 plies of carbon fiber were coated with the BA-a resin using a hand lay-up procedure. This procedure was employed to fabricate the laminated composite panels at 120°C to yield the prepregs. The obtained prepregs were stacked and preheated at 180°C for 20 minutes, 200°C for 10 minutes, and fully cured at 200°C for 2 hours in a compression molder using a pressure of 15 MPa. All samples were air-cooled to room temperature in the open mold. The plain, twill, and unidirectional weave patterns of CFR-poly(BA-a) composites consist of 4, 8, and 12 plies as shown in Figure 1.

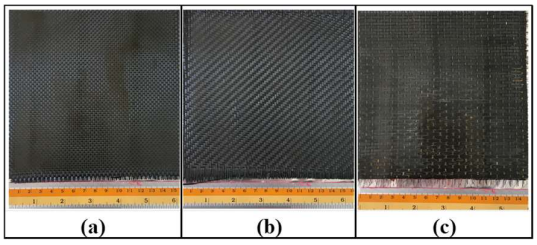

Figure 1 The weave patterns of CFR-poly(BA-a) composites (a) The plain, (b) twill, and (c) unidirectional

2.4 Characterization

2.4.1 Ballistic performance of the samples

The ballistic impact test was performed at the shooting range of Chulachomklao Royal Military Academy, Nakhon Nayok, Thailand. The tests were conducted using cartridges to propel projectiles onto composite specimens which were laminated from three weave patterns of CFR-poly(BA-a) composite containing carbon fiber at 4, 8, and 12 plies. On the impact test of the

projectiles, two sets of chronograph units were placed at 2 m in front and behind the target acquisition unit to record the impact and residual velocities of the projectiles, respectively. The 150×150 mm^2 composite plate was clamped in the target holder and placed on a steel frame at 15 m in line with the gun barrel and subjected to the impact of the projectiles. The tests were conducted using a high-level ballistic impact test based on NIJ standard level III using 7.62×51 mm projectiles at an impact velocity of 847±9.1 m/s at an angle of 90° to the specimen for one shot at the center. The initial impact velocity was measured by placing optical sensors in the field which were connected to a data acquisition system. The 7.62×51 mm projectiles have a diameter of 7.79 mm and a mass of 9.65 g as shown in Figure 2. The experimental setup is shown in Figure 3. The energy absorption of the composite specimen was determined by the difference between the initial kinetic energy and the final kinetic energy according to Equation (1).

$$E_a = 1/2m_p(V_s^2-V_r^2) \quad (1)$$

where E_a is energy absorption of the sample (J), m_p is the mass of a projectile (kg), V_s is impact projectile velocity (m/s) and V_r is residual projectile velocity after penetrating through the sample (m/s), respectively. This equation is under the assumption of the undeformed projectile.

Figure 2 7.62x51 mm FMJ NATO projectiles used.

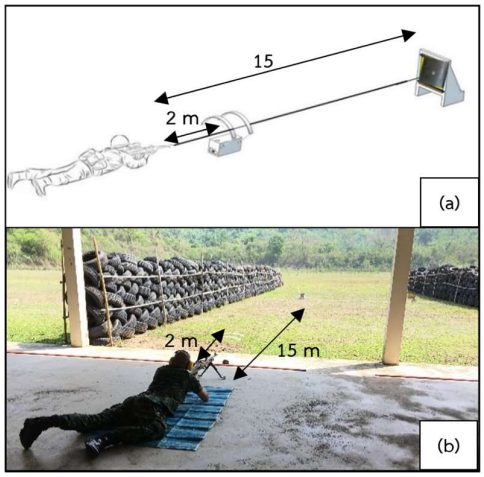

Figure 3 The experimental setup for high-velocity ballistic impact tests. (a) the schematic of the experimental setup and (b) the actual experimental setup.

2.4.2 Morphology of the samples

Sample morphology was studied using a scanning electron microscope (SEM, model JSM-IT300 from JEOL Ltd. (Tokyo, Japan)) using an acceleration voltage of 15 kV. All samples were coated with a thin layer of gold film using a sputter coater to make the surfaces conductive.

2.4.3 Numerical Simulations of ballistic characteristics

Numerical simulations of the experimental ballistics tests were conducted using finite element analysis (FEA) is the process of predicting an object's behavior based on calculations made with the finite element method (FEM). While FEM is a mathematical technique, FEA is the interpretation of the results FEM provides. FEA is insights into complex systems and structures, helping make more informed design decisions. FEA is the application of FEM equations and is the basis of many types of simulation software. It's used to validate and test designs safely, quickly, and economically by creating virtual models of real-world assets (Ferris, 2024).

The numerical modeling approach previously described was used to simulate all configurations of the ballistic impact carried out in the experimental tests. Moreover, the same approach was subsequently used as a virtual test environment to enrich (virtually) the data by obtaining the full ballistic curve for each configuration, allowing the determination of the ballistic limit by best fitting the impact data to the Recht-Ipson curve (Recht and Ipson, 1963) using the nonlinear least square method.

2.4.3.1 Comparison of the experimental and numerical method

The ballistic performance and the damage pattern of twill weave patterns of CFR-poly(BA-a) composite at the thickness of 1, 1.85, and 2.70 mm., respectively were studied using a series of numerical simulations. The impact test on specimens with dimensions of 150 × 150 mm^2 was tested using 7.62 × 51 mm projectiles at various impact velocities. The perforation process and deformation of the specimen were evaluated numerically with a commercial ANSYS AUTODYN system by using the material properties of the composite in parameters of young modulus, Poisson's ratio, strength: shear modulus, failure: tensile failure stress or strain, failure: tensile failure strain, density, and thickness, presented in Table 1 from Inthakun (2023) for the simulation evolution of the projectile penetrating process of composite panels. Then measure the extent of the experimental damage area composite and damaged area predicted from the numerical analysis on both the front and rear view of the specimen. Finally, calculate the percentage of the difference between the experimental and predicted damage area according to Equation (2).

$$\frac{(w_p-w_{exp})\,x\,(l_p-l_{exp})}{A_{d(exp)}} \text{ x } 100 \quad (2)$$

where w_p is the width of the predicted damage area (mm), w_{exp} is the width of the experimental damage area composite (mm), l_p is the length of the predicted damage area (mm), l_{exp} is the length of the experimental damage area composite (mm), $A_{d(exp)}$ is the damage area of the experimental (mm^2), respectively.

2.4.3.2 The ballistic performance predicted the thickness confirmed by numerical simulation

Numerical simulation analysis was used to evaluate the ballistic impact behavior of hard armor prepared from strike panel based on poly(BA-a) composite prepared from the plain, twill, and unidirectional weave of CFR-poly(BA-a) composites at thicknesses of 48.7, 45.2, and 65.7 mm, respectively. The 150 × 150 mm^2 specimens were tested by 7.62 × 51 mm projectiles at an impact velocity in the range of 847±9.1 m/s for one shot. Ballistic testing of the specimen was evaluated numerically with a commercial ANSYS AUTODYN system using the material properties of the composite presented in Table 2 from (Inthakun, 2023) for the simulation evolution of the projectile penetrating process of composite panels.

Table 1 Material properties of twill weave CFR-poly(BA-a) by various thickness (Inthakun, 2023).

Properties		Twill weave pattern of CFR-poly(BA-a) composite		
		4 plies	8 plies	12 plies
Thickness, mm		1.00	1.85	2.70
Density, g/cm³		1.46		
Young modulus, kPa	E_{11}	3.83×10^7		
	E_{22}	3.83×10^7		
	E_{33}	2.60×10^6		
Poisson's ratio	ν_{12}	0.07		
	ν_{23}	0.7		
	ν_{31}	0.075		
Strength: Shear modulus, kPa	G_{12}	5.8×10^5		
	G_{23}	1.7×10^4		
	G_{31}	1.7×10^4		
Failure: Tensile failure stress or strain	σ_{11}	8.3×10^5		
	σ_{22}	7.2×10^5		
	σ_{33}	7×10^4		
Failure: Tensile failure strain	ε_{11}	0.012		
	ε_{22}	0.014		
	ε_{33}	0.02		

Table 2 Material properties of each weave pattern composite panels (Inthakun, 2023).

Properties		Weave patterns of CFR-poly(BA-a) composite		
		Plain	Twill	UD
Thickness, mm		48.7	45.2	65.7
Density, g/cm³		1.43	1.46	1.45
Young modulus, kPa	E_{11}	3.64×10^7	3.83×10^7	3.58×10^7
	E_{22}	3.64×10^7	3.83×10^7	3.58×10^7
	E_{33}	2.48×10^6	2.60×10^6	2.43×10^6
Poisson's ratio	ν_{12}	0.07	0.07	0.07
	ν_{23}	0.7	0.7	0.7
	ν_{31}	0.075	0.075	0.075
Strength: Shear modulus, kPa	G_{12}	5.5×10^5	5.8×10^5	4.8×10^5
	G_{23}	1.7×10^4	1.7×10^4	1.7×10^4
	G_{31}	1.7×10^4	1.7×10^4	1.7×10^4
Failure: Tensile failure stress or strain	σ_{11}	7.2×10^5	8.3×10^5	10.3×10^5
	σ_{22}	7.2×10^5	7.2×10^5	1.7×10^5
	σ_{33}	7×10^4	7×10^4	7×10^4
Failure: Tensile failure strain	ε_{11}	0.013	0.012	0.018
	ε_{22}	0.013	0.014	0.11
	ε_{33}	0.02	0.02	0.02

3. RESULTS AND DISCUSSION

3.1 Effect of thickness on the ballistic performance of CFR-poly(BA-a) composite

The relationship between energy absorption and thickness of three different CFR-poly(BA-a) composite weave patterns. The fabric weaves included the plain pattern interlaced one up and down, the 2x2 twill interlaced two up and down, and unidirectional patterns in all the fibers running in a single, parallel direction. Specimens with various thicknesses as thin as the projectile were tested under impact event using 7.62×51 mm projectiles at an average velocity (V_s) of 847 ± 9.1 m/s according to NIJ at level III. Energy absorption was calculated using Equation (1) and plotted in Figures 4-6. The results demonstrated that the energy absorption value of the composite during the ballistic impact test increased with increasing thickness for all three weave pattern specimens composite. The results indicated an effective stress transfer between plies with thicker composites

because thicker composite layers produce heavier and increased fiber composite areal density to enhance the impact performance under high impact velocity (Colakoglu et al., 2007). Evaluation of the energy absorption E_a values with specimen thickness revealed a relatively nonlinear increase with increasing thickness of the composite. Quadratic fit gives exponents depicting the dependence of E_a of the plain, twill, and unidirectional weave of CFR-poly(BA-a) composite with the exponent values of 0.1277, 0.1451, and 0.0563, respectively (Carrillo J.G. et al, 2012).

The experimental results showed that the highest energy absorption was from the specimen reinforced with a twill weave pattern of CFR-poly(BA-a) composite presented in Figure 7, its high flexural strength and impact resistance properties due to the 2D woven structure were able to transmit load simultaneously in longitudinal and transverse weave directions. Therefore, it resisted stiffness, stress, and stress distribution. As in the weave structure of composite, it could be seen that twill weave had low contact friction, crimp, and binding effect because of its minimum intersection point compared with plain weave and unidirectional fabrics, therefore twill weave is a low level of fiber crimp impart relatively high mechanical properties compared with other weaves (Tong L. et al., 2002; Cavallaro, 2016). The damage figure in the front and rear view of CFR-poly(BA-a) composite specimen after impact with 7.62×51 mm projectiles is shown in Figure 8. The results demonstrated that the estimated residual kinetic energy of the projectile was significantly decreased with increasing thickness of the specimen composite. The estimated residual kinetic energy of the projectile was reduced to lower or equal to zero, exhibiting full ballistic protection from those projectiles.

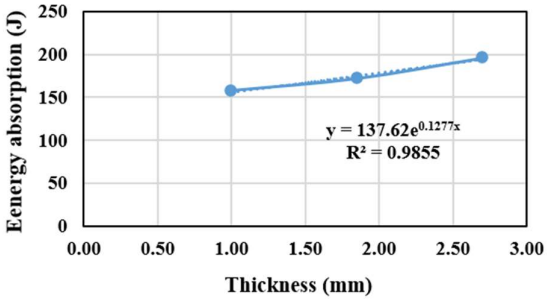

Figure 4 Relationship between energy absorption and thickness of plain weave CFR-poly(BA-a) composite.

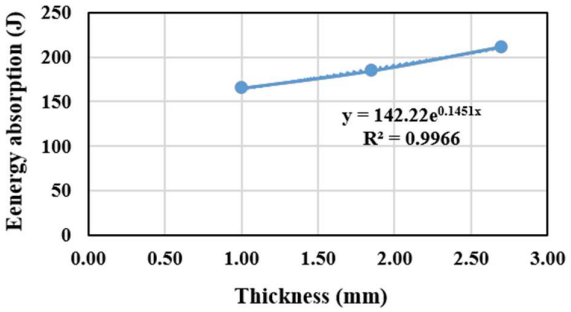

Figure 5 Relationship between energy absorption and thickness of twill weave CFR-poly(BA-a) composite.

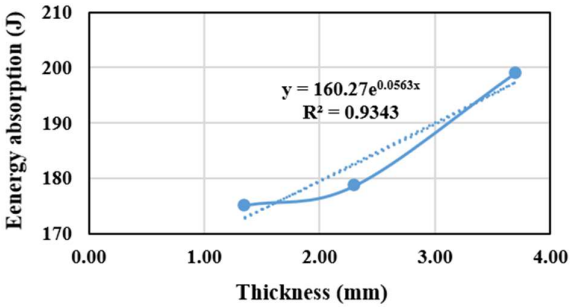

Figure 6 Relationship between energy absorption and thickness of unidirectional weave CFR-poly(BA-a) composite.

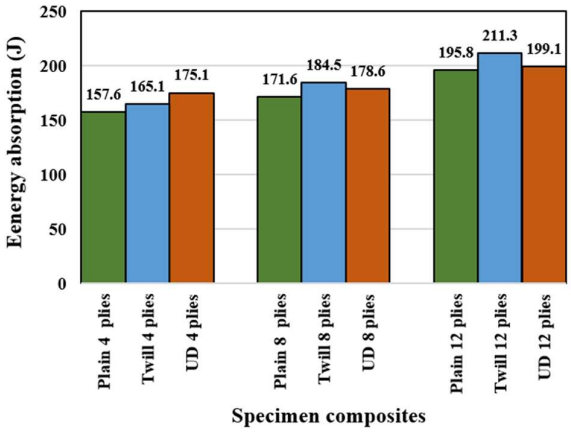

Figure 7 Relationship between energy absorption and the pile of each specimen composite

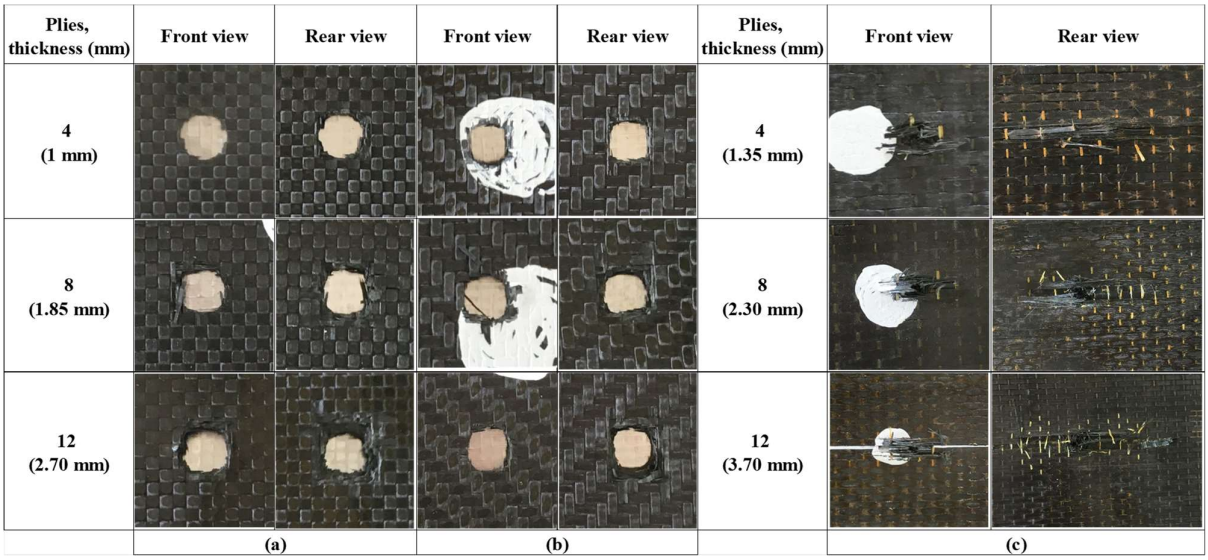

Figure 8 The damage figure in front and rear view of CFR-poly(BA-a) composite
(a) The plain, (b) twill, and (c) unidirectional weave pattern after impact with 7.62×51 mm projectiles

The results suggested that the suitable thickness tested by 7.62×51 mm projectile at an upper impact velocity of the plain, twill, and unidirectional weave of CFR-poly(BA-a) composite was 48.7, 45.2, and 65.7 mm, respectively, and the estimated energy absorption of specimen composites was found to be as high as 3536.28 J as shown in Table 3. The estimated residual kinetic energy was calculated using the nonlinear ballistic equation and Equation (1). However, to produce armor or strike panels for ballistic protection of projectiles of CFR-poly(BA-a) composite, the twill weave pattern of CFR-poly(BA-a) composite was stronger than any other weave pattern of CFR-poly(BA-a) composite because the twill weave pattern of CFR-poly(BA-a) composite has the highest energy absorption and the thinnest thickness for supporting the upper impact velocity of ballistic when compared with other weave patterns of CFR-poly(BA-a) composite.

Table 3 The thickness and energy absorption of three weave patterns of CFR-poly(BA-a) composite

Weave of specimen composite	Calculation of the specimen composite*	
	Thickness (mm)	Energy absorption (J)
Plain	48.7	3536.28
Twill	45.2	
UD	65.7	

* Calculation by use of 7.62×51 mm projectiles at an impact velocity of 847±9.1 m/s

3.2 Morphological Analysis

The fracture surface of CFR-poly(BA-a) composite after impact with 7.62×51 mm projectiles is also studied by Scanning electron microscopy (SEM) micrographs at 1500x magnification were taken of the warp region of the plain, twill, and unidirectional weave patterns of CFR-poly(BA-a) composite, as shown in Figure 9 (a), Figure 9 (b), and Figure 9 (c), respectively.

The SEM micrographs indicate that the carbon fabric of the plain and twill weave patterns was potentially adhered to the poly(BA-a) matrix, as can be observed from the pieces of matrix attached to the fiber, similar to the specimen composite before impact testing with 7.62×51 mm projectiles, as shown in Figure 9 (a) and Figure 9 (b). The CFR-poly(BA-a) composite of unidirectional weave pattern in the warp region shows adhesive and cohesive fracture due to matrix debonding, fibers pulled out, and breakage fibers when compared with the specimen composite before impact testing with 7.62×51 mm projectiles, as shown in Figure 9 (c). Moreover, the fracture surface is extensively embedded with poly(BA-a) matrix to correspond with the damage photo of CFR-poly(BA-a) composite specimen as shown in Figure 8. This implies that cohesive failure occurred in the poly(BA-a) matrix region due to the significant improvement in the interfacial adhesion between the carbon fabric and the poly(BA-a) matrix (Taraghi, 2014).

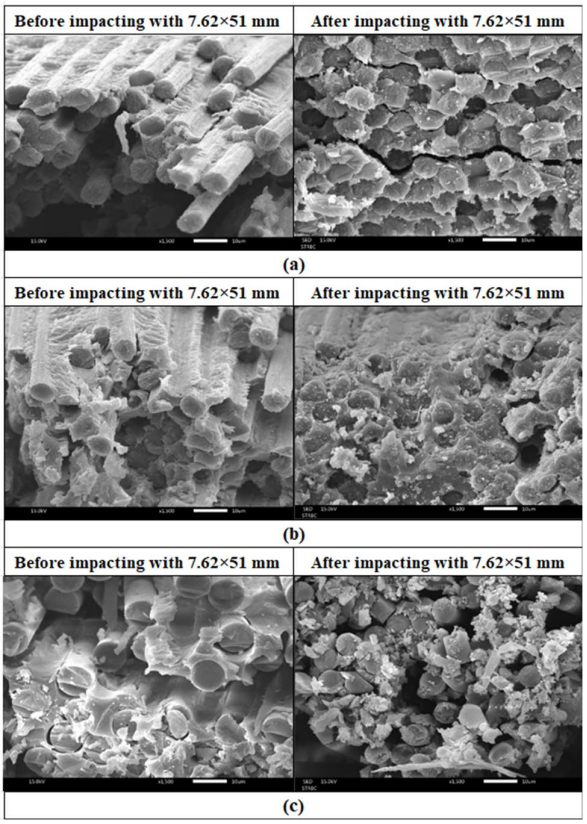

Figure 9 The scanning electron microscope at 1500x of CFR-poly(BA-a) composite in warp region filled before and after impacting with 7.62×51 mm (a) The plain weave pattern, (b) The twill weave pattern (c) The unidirectional weave pattern

3.3 Comparison of the experimental and numerical results

The experimental and numerical results of ballistic impact tests in terms of the damage areas on both the front and rear sides of the composite specimen at various thicknesses, as shown in Figures 10-12. The numerical simulation model qualitatively predicted the extent of damage for the specimen. From Figure 10, the extent of the experimental damage area of the composite was measured to be 8 mm × 7 mm, while the predicted damage extent measured 9 mm × 8 mm. The difference between the experimental and predicted damage area was approximately 2%.

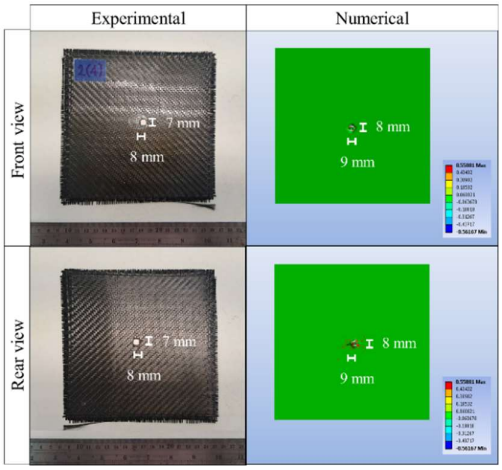

Figure 10 Comparison of the experimental and numerical damage areas of the poly(BA-a) composite at the thickness of 1 mm.

Figure 11, the extent of the experimental damage area of the composite was measured to be 9 mm × 7 mm, while the predicted damage extent measured 11 mm × 8 mm. The difference between the experimental and predicted damage area was approximately 3%.

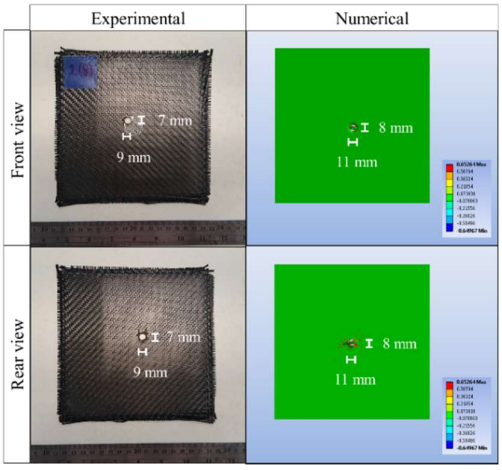

Figure 11 Comparison of the experimental and numerical damage areas of the poly(BA-a) composite at the thickness of 1.85 mm.

Figure 12, the extent of the experimental damage area of the composite was measured to be 10 mm × 10 mm, while the predicted damage extent measured 12 mm × 11 mm. The difference between the experimental and predicted damage area was approximately 2%.

From the results, the experimental results are in good agreement with the numerical simulation model. The numerical simulation model also did a good job of qualitatively predicting the extent of the damage for this specimen (Ansari and Chakrabarti, 2017).

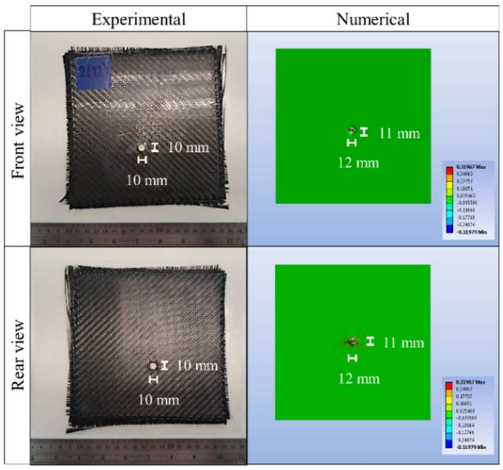

Figure 12 Comparison of the experimental and numerical damage areas of the poly(BA-a) composite at the thickness of 2.70 mm.

3.4 The ballistic performance predicted the thickness confirmed by the numerical simulation result

The results revealed that the plain, twill, and unidirectional weave pattern of CFR-poly(BA-a) composites could protect against projectiles one shot without perforation on the back side of the strike panel. The penetration depth and damage extent of the perforation observed in the strike panel in the side and rare view were in good agreement with the numerical simulation model shown in Figure 11. The result indicated a strike panel for hard armor based on polybenzoxazine composites which was prepared from a strike panel of plain, twill, and UD weave patterns of CRF-poly(BA-a) composite with thicknesses was 48.7, 45.2, and 65.7 mm, respectively, could completely protect against projectiles one shot without the perforation on the rear side of the strike panel tested by 7.62 × 51 mm projectiles at an impact velocity in the range of 847±9.1 m/s.

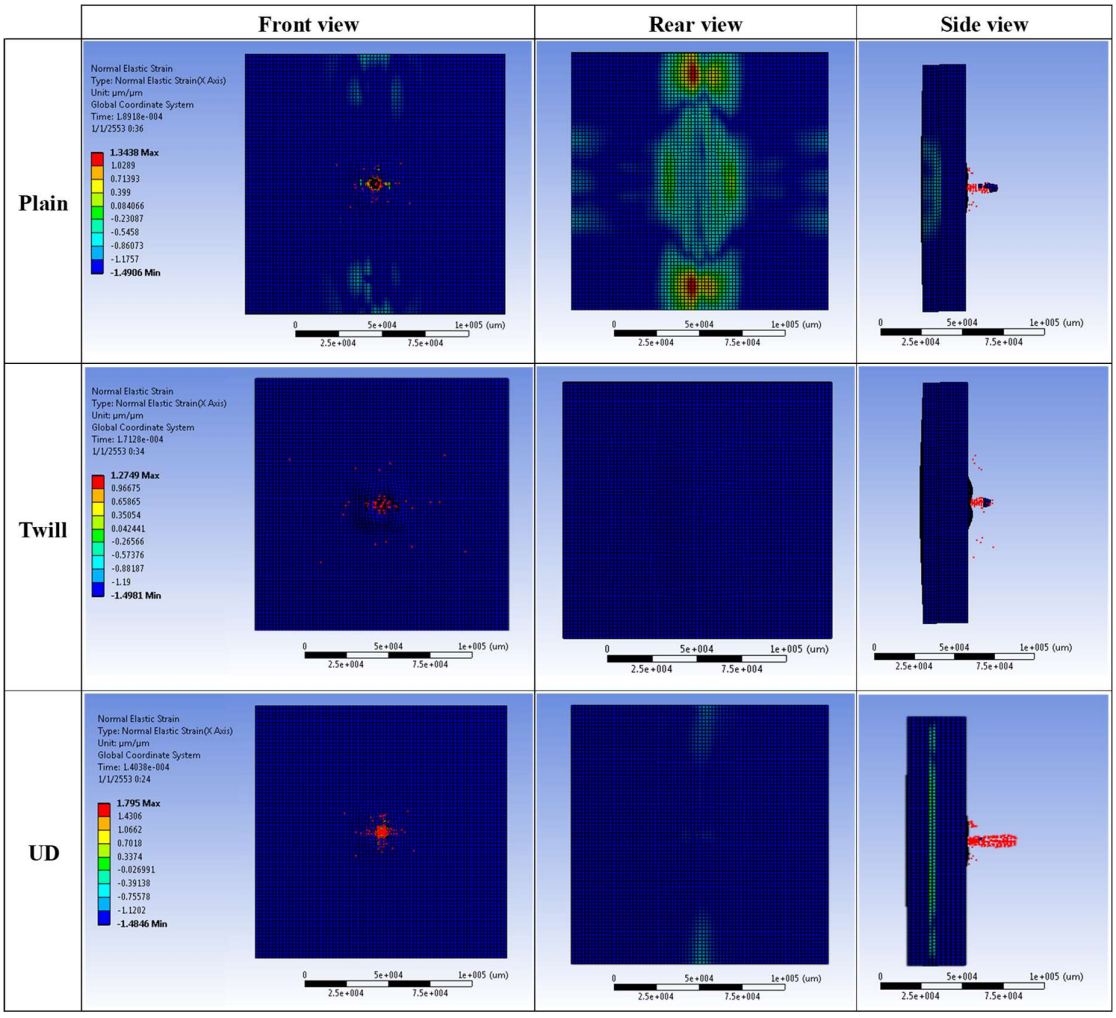

Figure 11 One-shot performance by numerical simulation of a strike panel based on three weave patterns of CFR-poly(BA-a) composite.

4. CONCLUSION

The numerical simulation results obtained were compared with experimental data to verify the suitable thickness for the ballistic protection of 7.62×51 mm projectiles. A satisfactory correlation of the suitable thickness of three weave patterns of CFR-poly(BA-a) composite was achieved with experimental observations. In particular, the error in the prediction of the difference between the experimental and predicted damage area was less than 3%. Moreover, the suitable thickness of the developed composites was predictable using the obtained energy absorption equation. Furthermore, the specimen based on CFR-poly(BA-a) composites at the appropriate thickness can protect against the penetration of 7.62×51 mm projectile at a velocity of 847±9.1 m/s. The results demonstrated that the energy absorption value of the composite during the ballistic impact test increased with increasing thickness for all three weave pattern composites. The results indicated an effective stress transfer between plies with thicker composites because thicker composite layers produce heavier specimens and initiate increased areal density of fiber composite to enhance the impact performance under high impact velocity. The predicted thickness of plain, twill, and unidirectional weave pattern CFR-poly(BA-a) composite was found to be 48.7, 45.2, and 65.7 mm, respectively. The result of the energy absorption of the twill weave pattern CFR-poly(BA-a) composites was the highest because the 2D woven structure could transmit load simultaneously in longitudinal and transverse weave directions. Therefore, it resisted stiffness, stress, and stress distribution. As in the weave structure of composite, it could be seen that twill weave had low contact friction, crimp, and binding effect because of its minimum intersection point compared with plain weave and unidirectional fabrics, therefore twill weave is a low level of fiber crimp impart relatively high mechanical properties compared with other weaves to corresponding with morphological analysis. Moreover, the hardness of three weave pattern CFR-poly(BA-a) composites from experimental conformed to the ballistic performance result by numerical simulation could protect against projectiles one shot without the perforation on the rear side of the strike panel. Results revealed that the CFR-poly(BA-a) composites have high ballistic performance to be utilized as a strike panel for hard armor applications. The findings demonstrate a correlation between numerical simulation outcomes from ballistic impact tests and experimental results, effectively predicting the behavior of CFR-poly(BA-a) composites with relatively low error and good correlation with the experimental data. This predictive capability allows for safe, rapid, and cost-effective design validation and testing by leveraging virtual ballistic impact test models of real-world assets for a person interested in studying them in the future.

5. ACKNOWLEDGMENT

This work was supported by the Chulachomklao Royal Military Academy Development Fund in the year 2019 from Chulachomklao Royal Military Academy. The authors gratefully acknowledge Prof. Sarawut Rimdusit, Ph.D., and Dr. Phattarin Mora for their consulting advice in conducting the research.

6. REFERENCES

Al-Haik, M., Borujeni., A. Y., & Tehrani, M. (2016). 5-Ballistic damage of hybrid composite materials. *In Advanced Fibrous Composite Materials for Ballistic Protection*, 121-143. https://doi.org/10.1016/B978-1-78242-461-1.00005-4

Pach, J., Pyka, D., Jamroziak, K., & Mayer, P. (2017). The experimental and numerical analysis of the ballistic resistance of polymer composites. *Composite. Part B Engineering, 113*, 24-30. https://doi.org/10.1016/ j.compositesb.2017.01.006

Yashas Gowda, T.G., Sanjay, M.R., Subrahmanya Bhat, K., Madhu, P., Senthamaraikannan, P., & Yogesha, B. (2018). Polymer matrix-natural fiber composites: An overview. *In Cogent Engineering, 5(1)*, 1-13. https://doi.org/10.1080/23311916.2018.1446667

Sherif, G., Chukov D., Tcherdyntsev V., & Torokhov V. (2019). Effect of Formation Route on the Mechanical Properties of the Polyethersulfone Composites Reinforced with Glass Fibers. *Polymers, 11(8)*, 1364. https://doi.org/10.3390/polym11081364

Chukov, I. D., Nematulloev, S., Zadorozhnyy, M., Tcherdyntsev, V., Stepashkin, A., & Zherebtsov, D. (2019). Structure, mechanical and thermal properties of polyphenylene sulfide and polysulfone impregnated carbon fiber composites. *Polymers, 11(4)*, 684. https://doi.org/10.3390/polym11040684

Linul, E., Lell, D., Movahedi, N., Codrean, C., & Fiedler, T. (2019). Compressive properties of zinc syntactic foams at elevated temperatures. *Composites Part B: Engineering, 167*, 122-134. https://doi.org/10.1016/ j.compositesb.2018.12.019

Buehler, F.U., & Seferis, J.C. (2000). Effect of reinforcement and solvent content on moisture absorption in epoxy composite materials. *Composites Part A: Applied Science and Manufacturing, 31(7),* 741-748. https://doi.org/ 10.1016/S1359-835X(00)00036-1

Ishida, H., & Chaisuwan, T. (2003). Mechanical property improvement of carbon fiber reinforced polybenzoxazine by rubber interlayer, *Polymer Composites, 24(5)*, 597-607. https://doi.org/10.1002/ pc.10056

Li, W., Yao, S.Y., Ma, K.M., & Chen, P. (2013). Effect of plasma modification on the mechanical properties of carbon fiber/phenolphthalein polyaryletherketone composites. *Polymer Composites, 34(3)*, 368-375. https://doi.org/10.1002/pc.22385

Delmonte, J. (1981). *Technology of Carbon and Graphite Fiber Composites*. Van Nostrand Reinhold.

Shalin, R.E. (1995). *Polymer Matrix Composites* (1st ed). Chapman and Hall. https://books.google.com.cy/books?id=ubw_zEgOhr4C&lpg=PA2&pg=PA2#v=onepage&q&f=false

Shen, S., & Ishida, H. (1996). Development and characterization of high-performance polybenzoxazine composites., *Polymer Composites, 17,* 710-719. https://doi.org/ 10.1002/pc.10663

Rajak, D. K. (2019). Fiber-Reinforced Polymer Composites: Manufacturing. *Properties, and Applications., Polymers (Basel), 11(10)*, 1667. https://doi.org/ 10.3390/polym11101 667

Al-Haik, M., Borujeni, A.Y., & Tehrani, M. (2016). Ballistic damage of hybrid composite materials. *Advanced Fibrous Composite Materials for Ballistic Protection*, 121-143. https://doi.org/10.1016/B978-1-78242-461-1.00005-4

Rebouillat S. (2016). 2 - ARAMIDS: 'Disruptive', open and continuous innovation. *Advanced Fibrous Composite Materials for Ballistic Protection*, 11-70. https://doi.org/10.1016/B978-1-78242-461-1.00002-9

Okhawilai, M., & Rimdusit, S. (2017). Chapter 35 - Hard Armor Composites From Ballistic Fiber-Reinforced Polybenzoxazine Alloys A2. *Advanced and Emerging Polybenzoxazine Science and Technology, Elsevier*, Amsterdam, 699-723. https://doi.org/10.1016/B978-0-12-804170-3.00035-4

Che, D., Saxena, I., Han, P., & Guo P., (2014). Machining of carbon fiber reinforced plastics/polymers: A Literature Review. *Journal of Manufacturing Science and Engineering, 136(3).* https://doi.org/ 10.1115/1.4026526

Wang, X. M., & Zhang, L. C. (2003). An experimental investigation into the orthogonal cutting of unidirectional fibre reinforced plastics. *International Journal of Machine Tools and Manufacture, 43(10)*, 1015-1022. https://doi.org/10.1016/S0890-6955(03)00090-7

Dandekar, C. R., & Shin, Y. C. (2012). Modeling of Machining of Composite Materials: A Review. *International Journal of Machine Tools and Manufacture, 57*, 102–121. https://doi.org/10.1016/j.ijmachtools.2012.01.006

Ratna, D., Chongdar, T.K., & Chacraborty, B.C. (2004), Mechanical Characterization of New Glass Fiber Reinforced Epoxy Composite. *Polymer Composites, 25(2)*, 165-171. https://doi.org/10.1002 /pc.20013

Hallal, A., Younes, R., Fardoun, F., & Nehme, S. (2012). Improved analytical model to predict the effective elastic Dyna 176, 2012 123 properties of 2.5D interlock woven fabrics composite. *Composite Structures, 94(10)*, 3009-3028. https://doi.org/10.1016/j.compstruct.2012.03.019

Haim, A. (2017). 9 - Stability of composite stringer-stiffened panels. *Stability and vibrations of thin walled composite structures*, 461–507. https://doi.org/10.1016/B978-0-08-100410-4.00009-0

Colorado, H. A. Chaves Roldán, C., & Vélez, J. M., (2006). Internal Friction and Anaelstic Behavior in Solids. *Dyna (Medellin, Colombia), 73(148)*, 39-49. https://www.researchgate.net/publication/262666032

Wahab, Md.S., Rejab, M.N., & Saiman, M.P. (2014) Analysis of mechanical properties for 2D woven kenaf composite. Applied Mechanics and Materials, 660, 125-129. https://doi.org/10.4028/www.scientific.net/AMM.660.125

Cavallaro, P.V. (2016). Effects of Weave Styles and Crimp Gradients in Woven Kevlar/Epoxy Composites. *Experimental Mechanics, 56*, 617-635. https://doi.org/10.1007/s11340-015-0075-4

Ullah, H., Harland, A., & Silberschmidt V. (2014). Evolution and interaction of damage modes in fabric-reinforced composites under dynamic flexural loading. *Composites Science and Technology, 92*, 55–63. https://doi.org/10.1016/j.compscitech.2013.12.007

Cavallaro, P.V., & Sadegh, A.M., (2010). Crimp-Imbalanced Protective (Crimp) Fabrics. IMECE2010-40610, *Mechanics of Solids, Structures and Fluids, 9*, 331-349. https://doi.org/10.1115 /IMECE2010-40610

Gopinath, G., Zheng, J.Q., & Batra, R.C. (2012). Effect of matrix on ballistic performance of soft body armor. *Composite Structures, 94(9)*, 2690-2696. https://doi.org/10.1016/j.compstruct.2012.03.038

Okhawilai, M., Hiziroglu S., & Rimdusit S. (2018). Measurement of ballistic impact performance of fiber reinforced polybenzoxazine/polyurethane composites. *Measurement, 130*, 198-210. https:// doi.org/10.1016/j.measurement.2018.08.006

Chocron, S., Figueroa, E., King, N., Kirchdoerfer, T., Nicholls, A.E., Sagebiel, E., Weiss, C., & Freitas, C.J. (2010). Modeling and validation of full fabric targets under ballistic impact. *Composites Science and Technology, 70(13)*, 2012-2022. https:// doi.org/10.1016/j.compscitech.2010.07.025

Flores-Johnson, E.A., Shen, L., Guiamatsia, I., & Nguyen, G.D. (2014). Numerical investigation of the impact behavior of bioinspired nacre-like aluminum composite plates. *Composites Science and Technology,* 96, 13-22. https://doi.org/10.1016/ j.compscitech.2014.03.001

Ansari, M.M., & Chakrabarti, A. (2017). Influence of projectile nose shape and incidence angle on the ballistic perforation of laminated glass fiber composite plate, *Composites Science and Technology, 142*, 107-116. https://doi.org/ 10.1016/j.compscitech.2016.12.033

Sevkat, E., Liaw, B., Delale, F., & Raju, B.B. (2009). A combined experimental and numerical approach to study ballistic impact response of S2-glass fiber/toughened epoxy composite beams. *Composites Science and Technology, 69(7-8)*, 965-982. https://doi.org/10.1016/j.compscitech.2009.01.001

Naik, N., Sekher, YC., & Meduri, S., (2000). Damage in woven-fabric composites subjected to low-velocity impact. *Composites Science and Technology, 60(5)*, 731-744. https://doi.org/10.1016/S0266-3538(99) 00183-9

Ishida, H. (1996). Process for preparation of benzoxazine compounds in solventless systems. *United States Patents, 5,* 516. https://patentimages. storage.googleapis.com/f0/58/d7/88aa918889bd08/U S5543516.pdf

Inthakun, K. (2023). "Effects of Weave Structure on Mechanical Behavior of Carbon Fiber Fabric Reinforced Polybenzoxazine Composites. *CRMA Journal, 21*, 94-109. https://ph01.tci-thaijo.org/ index.php/crma-journal/issue/view/ 17392/4236

Tong, L., Mouritz, A.P., & Bannister, M.K. (2002). *3D Fiber Reinforced Polmer Composites* (1st ed.), Elsevier Science Ltd,. https://doi.org/10.1016/B978-0-08-043938-9.X5012-1

Ferris, T. (2024). Finite Element Analysis (FEA). Retrieved from https://www.ansys.com/simulation-topics/what-is-finite-element-analysis

Recht, R. F., & Ipson, T. W. (1963). Ballistic Perforation Dynamics. *In Journal of Applied Mechanics., 30(3),* 384-390. https://doi.org/10.1115/ 1.3636566

Colakoglu, M., Soykasap, O., & Özek, T. (2007). Experimental and numerical investigations on the ballistic performance of polymer matrix composites used in armor design, *Applied Composite Materials 14(1)*, 47-58. https://doi.org/10.1007/s10443-006-9030-y

Taraghi, I., Fereidoon, A., & Mohyeddin, A. (2014). The effect of MWCNTs on the mechanical properties of woven Kevlar/epoxy composites, *Steel and Composite Structures, 17(6)*, 825-834. https://doi.org/10.12989/scs.2014.17.6.825

Carrillo, J.G., Gamboa, R.A., Flores-Johnson, E.A., & Gonzalez-Chi, P.I. (2012). Ballistic performance of thermoplastic composite laminates made from aramid woven fabric and polypropylene matrix. *Polymer Testing. 31(4)*, 512-519. https://doi.org/10.1016/j. polymertesting.2012.02.010